Wissenschaftszentrum Weihenstephan für Ernährung, Landnutzung und Umwelt

Lehrstuhl für Experimentelle Genetik

Implications of mitochondrial dysfunction in neurologic Wilson disease

Sabine Borchard

Vollständiger Abdruck der von der Fakultät Wissenschaftszentrum Weihenstephan für Ernährung, Landnutzung und Umwelt der Technischen Universität München zur Erlangung des akademischen Grades eines

Doktors der Naturwissenschaften

genehmigten Dissertation.

Vorsitzender:	Prof. Dr. med. Heiko Witt
Prüfer der Dissertation:	1. apl. Prof. Dr. Dr. Jerzy Adamski
	2. Prof. Dr. Martin Klingenspor

Die Dissertation wurde am 28.11.2019 bei der Technischen Universität München eingereicht und durch die Fakultät Wissenschaftszentrum Weihenstephan für Ernährung, Landnutzung und Umwelt am 20.05.2020 angenommen.

Table of contents

SUMMARY

Wilson disease (WD), an autosomal-recessive inherited disorder, is characterized by an impaired copper metabolism caused by mutations in the copper-transporting ATPase ATP7B. These mutations cause a partial or complete loss of ATP7B function leading to an impaired biliary copper excretion. Hence, copper accumulates in the liver, leading to mitochondrial dysfunction and subsequent cell death. Thereby, copper is released into the systemic circulation favoring the accumulation of copper in peripheral organs, *e.g.*, the brain, kidneys and heart. Besides the liver disease, neurological disturbances are the most common symptoms in Wilson disease patients.

Whereas mitochondrial impairments are an established and early feature of the hepatic phenotype of Wilson disease, their role in the neurological subtype of the disease is rather unclear. Therefore, isolated mitochondria from rat liver, kidney, heart and brain were analyzed regarding their sensitivity to copper with respect to mitochondrial function and structure. Here, brain mitochondria present with profound copper-induced structural alterations that are paralleled by a decreased stability of the mitochondrial membrane potential and a reduced ATP production capacity. In contrast, equal copper challenges do not affect heart mitochondria and only induce slight alterations in organelles from liver and kidney. The observed impairments of brain mitochondria are linked to the copper-induced modification of mitochondrial protein thiols. In contrast, massive production of reactive oxygen species, a previously thought prime mode of copper toxicity, presents as a late feature of copper-induced mitochondrial dysfunction that is only detectable when the organelles are readily destroyed. As brain mitochondria represent an inhomogeneous population of organelles from different cell types, the impact of copper on SH-SY5Y (neuroblastoma) and U-87MG (astrocytoma) cells was further evaluated. SH-SY5Y mitochondria are more sensitive to copper challenges compared to U-87MG mitochondria. This higher susceptibility may be plausibly caused by their limited cellular defense mechanisms, *i.e.*, the lack of copper-detoxifying metallothionein and lower cellular glutathione levels, that provoke mitochondrial dysfunction although SH-SY5Y cells accumulate significantly less copper compared to U-87MG cells.

Previous reports suggested an impairment of the blood-brain barrier in neurologic Wilson disease patients, but up to date no further studies followed this line of evidence. Therefore, the impact of copper on blood-brain barrier forming cells was evaluated. U-87MG (astrocytoma) and EA.hy926 (endothelium) are shown to be highly sensitive to copper regarding their mitochondrial structure and function and the presence of the high-affinity chelator WTX101 prevents copper-induced mitochondrial damage. This is partially linked to the reduced cellular copper content upon co-treatment with WTX101. Additionally,

the consequences of copper treatment on blood-brain barrier integrity were investigated in an *in vitro* Transwell® setting. Primary porcine brain capillary endothelial cells are shown to be sensitive to copper challenges that induce the opening of the barrier already in the absence of cellular toxicity. This model was further used to determine the transport of copper through the endothelial cell layer as well as the immunocytochemical and electron microscopic evaluation of tight junction proteins. The presence of the high-affinity chelator WTX101 leads to a decreased transport of copper through the monolayer and preserves the intactness of the tight junctions.

As rat brain mitochondria were shown to be highly susceptible to copper and mitochondrial protein thiols to be sensitive targets of modification by copper, substrate-specific respiration of U-87MG mitochondria was evaluated either after irreversible modification of thiols by N-ethylmaleimide or copper. NADH-linked respiration is shown to be highly sensitive to thiol modification, whereas succinate-linked respiration is unchanged. Furthermore, copper-treated U-87MG display with a comparable impairment of NADH-linked respiration and unaltered succinate-linked respiration. This suggests the involvement of complex I in copper-induced mitochondrial dysfunction and subsequent cell death what, however, remains to be validated in future studies.

ZUSAMMENFASSUNG

Der Morbus Wilson ist eine autosomal-rezessiv vererbte Erkrankung, die sich durch eine gestörte Kupferhomöostase äußert. Zurückzuführen ist dies auf Mutationen im *ATP7B* Gen, welches für die gleichnamige kupfertransportierende ATPase kodiert. Folglich ist die biliäre Exkretion von überschüssigem Kupfer gestört und das Metall akkumuliert in der Leber. Diese massive Kupferansammlung bewirkt eine Dysfunktion der Mitochondrien und führt schlussendlich zum Untergang der Hepatozyten. Dabei kann es zur Freisetzung von Kupfer in den Blutkreislauf und damit einhergehend zu einer Ansammlung des Metalls in peripheren Organen, z.B. dem Gehirn, den Nieren oder dem Herzen, kommen. Neben einer Beeinträchtigung der Leberfunktion zählen neurologische Störungen zu den häufigsten Symptomen des Morbus Wilson.

Eine mitochondriale Dysfunktion gilt als frühes und etabliertes Merkmal der Pathogenese des hepatischen Phänotyps des Morbus Wilson. Im Gegensatz dazu ist die Rolle dieser Organellen im neurologischen Subtyp der Erkrankung bislang wenig untersucht. Daher wurden isolierte Mitochondrien aus Rattenleber, -niere, -herz und -gehirn hinsichtlich ihrer Kupfersensitivität untersucht und dabei sowohl strukturelle als auch funktionelle Aspekte beleuchtet. Hierbei zeigen Gehirnmitochondrien massive Kupfer-induzierte strukturelle Veränderungen, die von einer verminderten Stabilität des mitochondrialen Membranpotentials sowie einer reduzierten ATP Produktionskapazität begleitet sind. Im Gegensatz hierzu beeinträchtigt die gleiche Kupferdosis Herzmitochondrien nicht und induziert nur geringe Veränderungen in Leber- und Nierenmitochondrien. Die beobachteten Beeinträchtigungen in Gehirnmitochondrien können mit einer Kupfer-bedingten Modifikation mitochondrialer Proteinthiole in Verbindung gebracht werden. Die massive Produktion reaktiver Sauerstoffspezies ist hingegen ein spätes Merkmal der Kupfer-induzierten mitochondrialen Dysfunktion und tritt erst bei einer Zerstörung der Organellen auf. Sie ist daher eher als Konsequenz mitochondrialen Schäden zu betrachten, nicht als deren Ursache. Da Gehirnmitochondrien eine inhomogene Population von Organellen aus verschiedensten Zelltypen darstellen, wurden nachfolgend die Auswirkungen von Kupfer auf die Zelllinien SH-SY5Y (Neuroblastom) und U-87MG (Astrozytom) untersucht. Mitochondrien aus SH-SY5Y Zellen zeigen hierbei eine erhöhte Sensitivität gegenüber dem Metall im Vergleich zu U-87MG Mitochondrien. Dies kann auf verminderte zelluläre Abwehrmechanismen, z.B. das Fehlen des Kupfer-bindenden Proteins Metallothionein, zurückgeführt werden. Daher tritt eine Kupfer-induzierte mitochondriale Dysfunktion in SH-SY5Y Zellen auf, obwohl dieser Zelltyp signifikant weniger Kupfer akkumuliert als U-87MG Zellen.

In einer früheren Studie wurde eine Beeinträchtigung der Blut-Hirn-Schranke in Morbus Wilson Patienten mit vornehmlich neurologischen Symptomen beschrieben, jedoch fehlen bislang Studien, die diesen Pathomechanismus weiter untersuchen. Daher wurde der Einfluss von Kupfer auf Zellen, die am Aufbau der Bluthirnschranke beteiligt sind, untersucht. U-87MG (Astrozytom) und EA.hy926 (Endothel) Zellen zeigen eine hohe Kupfersensitivität hinsichtlich der Struktur und Funktion ihrer Mitochondrien. Diese kann durch die Anwesenheit des hochaffinen Kupferchelators WTX101 und dem damit einhergehenden verminderten intrazellulären Kupferlevel verhindert werden. Zudem wurde der Einfluss von Kupfer auf die Blut-Hirn-Schranke in einem *in vitro* Transwell®-System untersucht. Primäre Schweinhirn-Kapillarendothelzellen reagieren hierbei sensitiv auf Kupfer, welches eine Öffnung der Barriere bereits vor dem Auftreten von Zelltod induziert. Dieses Modell wurde genutzt, um den Kupfertransport durch die Endothelzellschicht zu untersuchen und Veränderungen der Tight Junctions mittels Immunozytochemie und Elektronenmikroskopie sichtbar zu machen. Die Anwesenheit des hochaffinen Chelators WTX101 führt hierbei zu einem verminderten Transport von Kupfer durch die Endothelzellschicht und zu einem Erhalt der Barrierenintegrität.

In den genannten Versuchen reagierten Gehirnmitochondrien sehr sensitiv auf Kupfer und mitochondriale Proteinthiole wurden als empfindliche Ziele für die Modifikation durch Kupfer identifiziert. Daher wurde die Substrat-spezifische Atmung von Mitochondrien aus U-87MG Zellen nach irreversibler Thiolmodifikation durch N-Ethylmaleinimid (NEM) oder Kupfer untersucht. Die Atmung in Anwesenheit von Komplex I-assoziierten Substraten zeigt dabei eine hohe Sensitivität gegenüber einer Thiolmodifikation durch NEM, während die mitochondriale Atmung mittels Komplex II-assoziierten Substraten unverändert ist. Kupfer-behandelte U-87MG Zellen zeigen eine ähnliche beeinträchtigte Atmung via Komplex I und eine unveränderte Atmung via Komplex II des Elektronentransportsystems. Diese Ergebnisse legen eine Beteiligung von Komplex I in der Kupfer-induzierten mitochondrialen Dysfunktion und dem damit einhergehenden Zelltod nahe, die in der Zukunft noch detaillierter untersucht werden sollte.

1 INTRODUCTION

1.1 Copper – an essential trace element

1.1.1 Copper uptake, distribution and excretion

Copper is an essential co-factor of numerous vital enzymes including the mitochondrial cytochrome *c* oxidase [1], superoxide dismutase 1 [2] and dopamine beta-hydroxylase [3]. Hence, an adequate copper supply is crucial and requires the daily uptake of approximately 2 mg of the metal from the diet [4-6]. Nutritional copper is taken up in the intestine by enterocytes and transported via the portal circulation to the liver. Extracellularly, copper is present in its cupric form (Cu^{2+}) associated to albumin or amino acids, *e.g.*, histidine [7, 8]. Cupric copper needs to be reduced to cuprous copper (Cu^{1+}) prior to its uptake by the copper transporter 1 (CTR1) [9, 10]. This reduction is most probably performed by a group of metalloreductases, so-called Steap proteins [11].

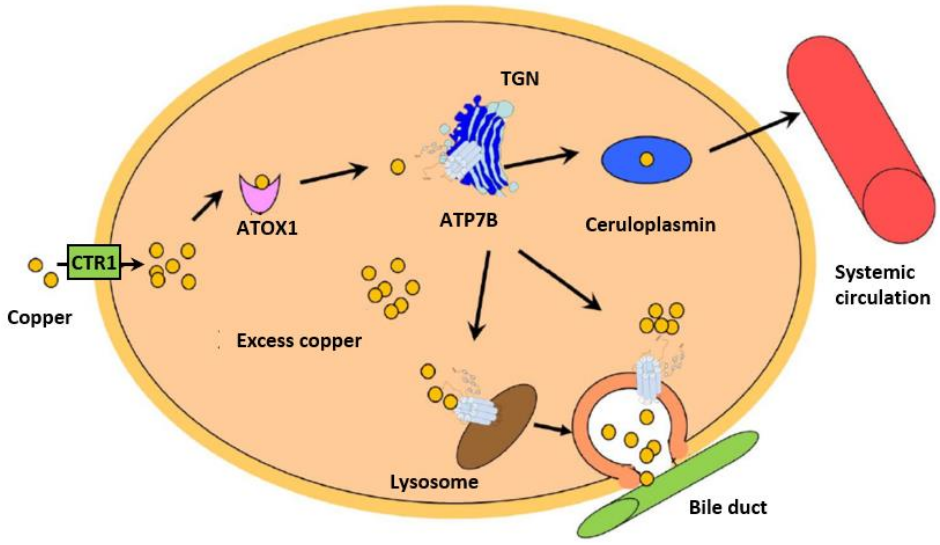

Figure 1. Schematic representation of the intracellular delivery of copper within hepatocytes under physiological conditions. Dietary copper is transported via the portal circulation to the liver. Here, copper enters the hepatocytes via the CTR1 and directly binds to chaperones, *e.g.*, ATOX1, in the cytosol. Under physiological conditions, these chaperones transfer copper to the trans Golgi network (TGN). Here, copper is incorporated into ceruloplasmin, followed by its secretion into the systemic circulation. Additionally, excess copper leads to the trafficking of ATP7B from the TGN to lysosomes and subsequent excretion into the bile. Adapted from Wu et al., 2015 [12] with permission.

After its CTR1-mediated uptake (**Figure 1**), copper is intracellularly bound to the metal-detoxifying protein metallothionein [13], low-molecular weight ligands like glutathione (GSH) [14] or to copper chaperones that facilitate the transport of copper into its final destinations [15], *e.g.*, the mitochondria.

The copper chaperone ATOX1 transfers copper to the trans Golgi network (TGN), where it directly interacts with the copper-transporting ATPase ATP7B that fulfills two functions depending on the intracellular copper load [16]. Here, copper is either incorporated into ceruloplasmin at low intracellular copper levels [17] or the redistribution of ATP7B to lysosomes leads to the biliary excretion of excess copper at high intracellular copper levels [18]. Besides ATOX1, the copper chaperone for SOD1 (CCS) facilitates SOD1 metalation in the cytosol [19] and a low-molecular weight ligand of unknown entity is hypothesized to transport copper to the mitochondria [20] where additional copper chaperones (COX17, SCO1 and COX11) facilitate the incorporation of the metal into cytochrome *c* oxidase [21].

	$Fe^{3+}/\mathbf{Cu^{2+}} + O_2^{\bullet-}$	$\leftrightarrow$	$Fe^{2+}/\mathbf{Cu^{1+}} + O_2$
Fenton reaction	$Fe^{2+}/\mathbf{Cu^{1+}} + H_2O_2$	$\rightarrow$	$Fe^{3+}/\mathbf{Cu^{2+}} + OH^{\bullet} + OH^{-}$
Haber-Weiss reaction	$O_2^{\bullet-} + H_2O_2$	$\leftrightarrow$	$O_2 + OH^{\bullet} + OH^{-}$

Figure 2. Fenton chemistry-based reactions catalyzed by copper.

Copper can participate in Fenton chemistry-based reactions and thereby can catalyze the production of reactive oxygen species similarly to iron. Taken from Giorgi et al., 2018 [22] with permission.

Due to these various proteins and ligands that coordinate intracellular copper, no free copper is detectable within cells [23]. This is of major importance as copper can shift between the oxidized state (Cu^{2+}) and the reduced state (Cu^{1+}) [24] and aqueous free copper ions could otherwise participate in Fenton chemistry-based reactions (**Figure 2**) leading to the production of highly reactive hydroxyl radicals ($OH^{\bullet}$) and subsequent substantial damage to DNA, proteins and lipids [25]. Nevertheless, the shift between oxidized and reduced state is the prerequisite for copper's participation as a co-factor in critical enzymes of cellular metabolism. Here, the cytochrome *c* oxidase as part of the mitochondrial electron transport systems (ETS) is of major interest.

1.1.2 Mitochondria and copper

Mitochondria are central organelles of cellular energy production [26, 27]. They vary in form, number, functional properties and their organ-specific molecular composition [28, 29], but their basic structure is similar. Mitochondria are defined from the cytoplasm by the outer mitochondrial membrane (OMM) which is widely permeable to ions and larger molecules [30]. In contrast, the inner mitochondrial membrane (IMM) is nearly impermeable and forms a great number of cristae which extend into the matrix and thereby implicate an enormous surface enlargement [27]. Furthermore, the IMM separates

the protein-rich mitochondrial matrix from the intermembrane space that is restricted from the cytosol by the OMM [31, 32].

The IMM harbors the five protein complexes of the oxidative phosphorylation (**Figure 3**). The impermeability of the IMM is an essential prerequisite for the establishment of an electrochemical proton gradient across the membrane. This gradient is generated by three of the four complexes of the mitochondrial electron transport system including complex I (NADH:ubiquinone oxidoreductase), complex III (ubiquinol:cytochrome *c* oxidoreductase) and complex IV (cytochrome *c* oxidase).

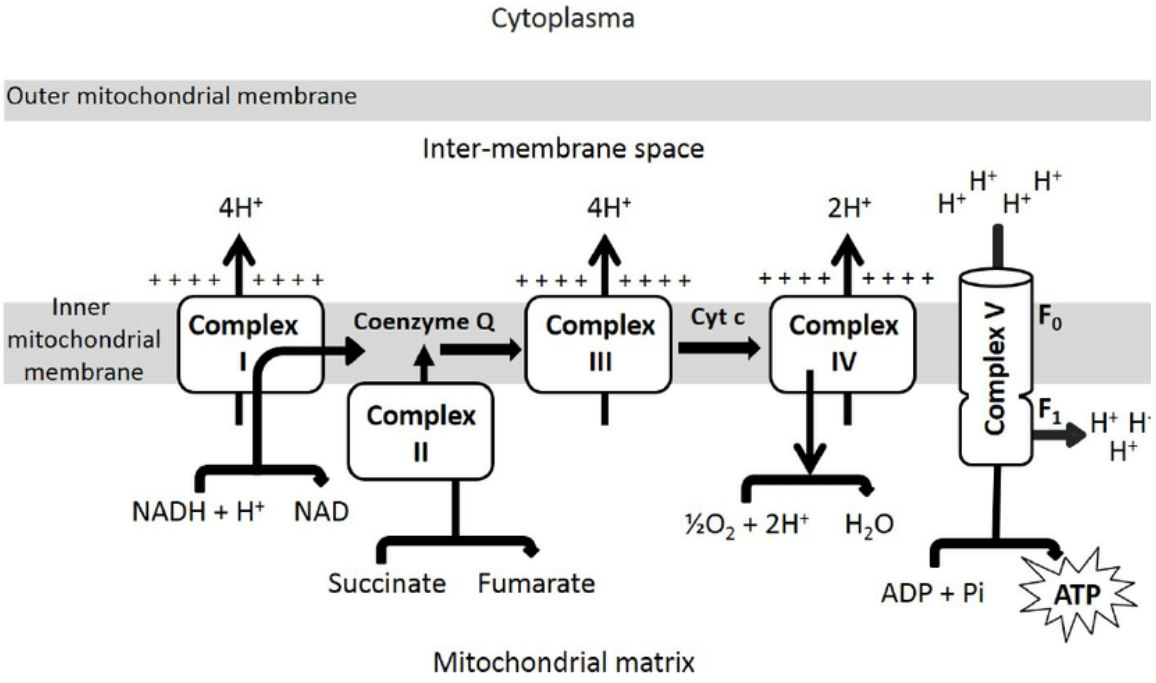

Figure 3. The five protein complexes of the oxidative phosphorylation.

The electron transport system (ETS) is located in the inner mitochondrial membrane and consists of the complexes I to IV. The ETS generates an electrochemical proton gradient (mitochondrial membrane potential, ΔΨ) by pumping protons from the matrix into the mitochondrial intermembrane space. This gradient is used by complex V to produce ATP. Taken from Correa et al., 2017 [33] with permission.

Here, proton pumping is coupled to the transport of electrons arising from $NADH/H^+$ oxidation at complex I [34-36] via complex III to complex IV where the electrons are finally transferred to molecular oxygen [37, 38]. In contrast, complex II (succinate dehydrogenase) is not able to pump protons from the matrix into the IMS [39] but also feeds electrons into the electron transport system. Subsequently, these protons are re-translocated from the IMM into the matrix by the fifth and final complex, the F_OF_1 ATP synthase (complex V), thereby generating ATP from ADP and inorganic phosphate [40]. The indirect coupling of electron transfer and synthesis of ATP via an electrochemical gradient is called the

chemiosmotic theory and was established by Mitchell in 1961 [41]. Among others, the amount of ATP production is controlled by the availability of ADP and thereby, the cellular energy demand. In the absence of ADP, the substrate turnover is low, whereas in presence of ADP oxidative phosphorylation reaches the maximum speed. The coupling of substrate oxidation and ATP production is termed respiratory control [42].

Mitochondrial energy production via oxidative phosphorylation is highly dependent on adequate copper supply. The metal is a critical co-factor of the cytochrome *c* oxidase that harbors three copper ions [43] present in two copper centers, Cu_A (subunit II) and Cu_B (subunit I). Whereas the Cu_A site forms the entrance for electrons from cytochrome *c* into the protein complex [44], the Cu_B site participates in the transfer of electrons to oxygen during oxidative phosphorylation [45]. Due to a permanent mitochondrial turnover [46], a constant supply of the organelles with copper is necessary. However, overload of the mitochondrial compartment with copper can be detrimental as well, highlighting the need for a tight regulation of copper transport to mitochondria as ensured by the relay of copper chaperones.

1.2 Wilson disease – a copper overload disorder

1.2.1 The pathophysiology of Wilson disease

In 1912, Samuel Alexander Kinnier Wilson described a neurological disease associated with liver cirrhosis [47] thereafter termed “Wilson disease” (WD). WD is an autosomal-recessive inherited disorder of copper metabolism [48, 49] characterized by an enormous accumulation of the metal in various organs, mainly the liver and the brain [49-51]. This copper accumulation is the result of one or several mutations in a gene on chromosome 13 [52] coding for the copper-transporting ATPase ATP7B [53-55]. These mutations cause partial or complete loss of function of ATP7B and thereby, a lack of copper incorporation into ceruloplasmin (**Figure 4**). Hence, WD patients display significantly lower ceruloplasmin levels in the blood compared to healthy controls [56, 57]. Additionally, impaired or lost ATP7B function leads to a severely reduced or complete lack of biliary excretion of excess copper. Consequently, copper accumulates in the liver up to 15-fold [49, 58] causing hepatocyte death and subsequent acute or chronic hepatitis, progressive liver cirrhosis and liver failure [47, 59, 60]. Furthermore, hepatocyte death leads to the release of copper into the blood, thereby increasing the blood level of non-ceruloplasmin bound copper (NCBC) [57] and favoring the accumulation of the metal in peripheral organs, *e.g.*, the brain, kidneys or heart. However, renal and cardiac disturbances are

rather rare in WD patients, often overlooked due to mild manifestations and mainly present as a late, end-stage clinical event [61-65].

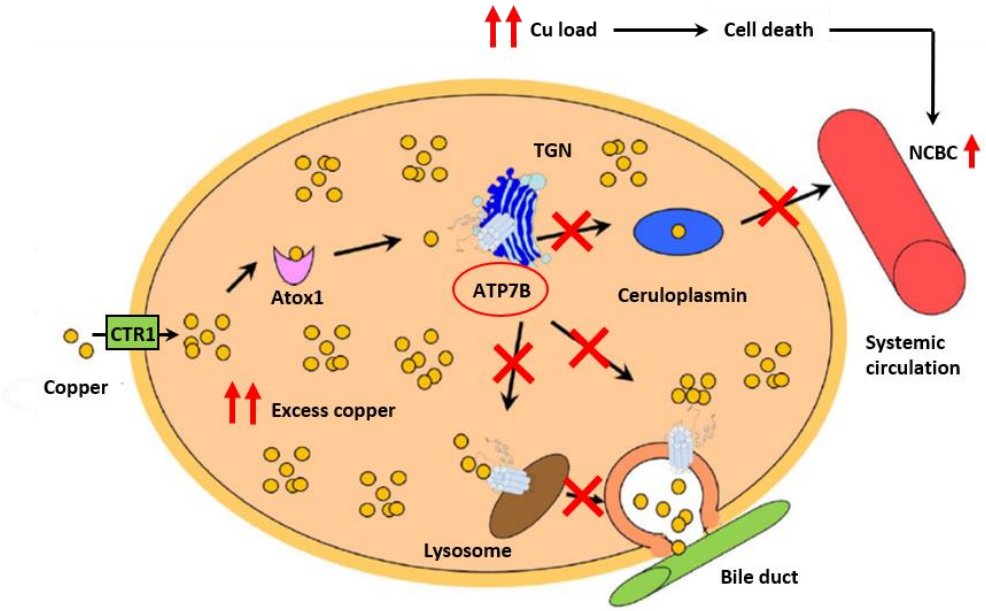

Figure 4. Schematic representation of the intracellular delivery of copper within hepatocytes in Wilson disease.
In Wilson disease, an impaired ATP7B function results in strongly increased intracellular copper levels by a reduced excretion of excess copper into the bile. Subsequent cell death leads to an increased level of non-ceruloplasmin bound copper (NCBC) in the systemic circulation. Furthermore, incorporation of the metal into ceruloplasmin fails. Adapted from Wu et al., 2015 [12] with permission.

Hence, based on the organ mainly affected, WD patients are divided into two major groups: 1) patients predominantly displaying hepatic disturbances and 2) patients mainly suffering from neurological and/or psychiatric symptoms [66].

1.2.2 The hepatic phenotype

Approximately 40 - 50 % of WD patients present with a symptomatic liver disease [67]. Usually, these patients have initial symptoms starting at an average age between 10 and 13 years of age [68]. Liver disease in WD can range from mild disease to liver failure and can progress from cirrhosis to hepatocellular carcinoma in rare cases [60]. The most common hepatic signs include jaundice, anorexia and vomiting, ascites/edema and hepatomegaly/splenomegaly [66, 68, 69]. As the liver is the first place to sequester copper after its intestinal uptake, WD patients display a strongly increased hepatic copper load above 250 µg/g dry weight, whereas normal liver copper levels range from 15 to 55 µg/g dry weight [49, 58, 70, 71].

Due to copper's redox activity, the hepatic copper overload in WD patients was hypothesized to cause the formation of ROS (**Figure 2**) and subsequent damage to lipids, proteins, DNA and RNA [72, 73]. In accordance, several studies showed a reduced level of GSH, increased lipid peroxidation and enhanced DNA damage in livers of WD patients that underwent liver transplantation [74-76]. However, the role of oxidative stress due to copper overload was more extensively studied in animal models of WD, *e.g.*, the LEC rat, that harbors a deletion in the *Atp7b* gene [77]. Here, oxidative stress was absent in still healthy WD animals but was an unambiguous feature at the stage of liver damage and jaundice [78-80]. Hence, copper-induced formation of ROS seems to be a late stage event rather than the causative factor of liver damage in WD. Therefore, alternative mechanisms of hepatocyte damage and death in the context of Wilson disease were investigated. Here, a direct binding of the metal to thiol and amino residues of proteins was hypothesized as potential mechanism of copper toxicity thereby causing either crosslinking of proteins or functional disturbances [81-84]. Furthermore, copper was described to directly impair protein folding [14].

Additionally, mitochondria as main utilizers of copper within the cell, were described to be highly susceptible to the metal in the context of WD. Liver mitochondria were shown to accumulate dramatic amounts of copper [84-86] that lead to severe alterations of the organelles already in the early stages of the disease. Hence, mitochondrial damage was identified as initial event of hepatic injury in the context of WD [74, 84, 85].

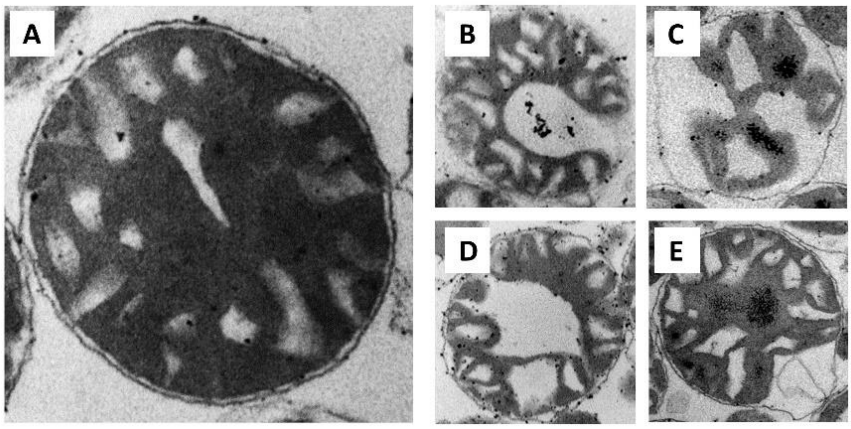

Figure 5. Isolated *Atp7b*$^{-/-}$ rat liver mitochondria display structural alterations typical for Wilson disease.

(A) Electron micrographs of liver mitochondria isolated from wild-type *Atp7b*$^{+/-}$ rats display well-defined cristae and a distinct matrix space. In contrast, liver mitochondria isolated from *Atp7b*$^{-/-}$ rats present with electron-dense inclusions (B), separated inner and outer membrane (C), abnormal cristae structure (D) and membranous inclusions (D). Adapted from Zischka and Borchard, 2018 [87] with permission.

Liver mitochondria from WD animals [74, 84, 85, 88-90] and patients [91, 92] display massive structural alterations characterized by, *e.g.*, enlarged cristae, membranous inclusion, an increased IMS and electron-dense inclusions (**Figure 5**). Besides these structural abnormalities, functional disturbances occur in copper-loaded mitochondria including reduced activities of respiratory chain enzymes [88, 93-95] and accordingly, a reduced ATP production capacity and a decreased stability of the mitochondrial membrane potential [85].

1.2.3 The neurologic phenotype

Besides the liver, ATP7B is also present in the basal ganglia, cerebellum and cortex [96]. Additionally, the endothelial cells of the blood-brain barrier (BBB) and the choroid plexus express the copper-transporting ATPase on their apical membrane [97]. Accordingly, ATP7B dysfunction also leads to neurological disturbances in Wilson disease patients. Most neurologic WD patients also display liver disturbances. This can be attributed to the limited copper storage capacity of the liver. Once this capacity is exceeded, copper is transferred to the systemic circulation leading to the accumulation of the metal in peripheral organs, especially the brain [98]. In neurologic WD patients, brain copper levels can rise to 450 µg/g dry weight, whereas control patients display 7 - 60 µg/g dry weight [49, 70, 99, 100]). Consequently, these copper deposits result in brain lesions [101] causing psychiatric symptoms (cognitive and behavioral changes) in 20 – 70 % of the neurologic WD patients [98, 102, 103] and/or a progressive movement disorder in 40 – 60 % of the patients. The latter can present as mild tremor, dysarthria, dysphagia or dysgraphia [98, 102, 104-106]. In contrast to the hepatic phenotype of WD, the initial symptoms of neurologic WD patients appear in their mid-teens or twenties [107] and much less is known about the pathophysiology of the neurologic phenotype. However, brain copper levels were correlated with the severity of the disturbances [108] as well as the level of NCBC in the blood [109]. Additionally, Stuerenburg suggested an involvement of the blood-brain barrier and its partial disruption by copper [110].

Since approximately 95 % of the brain's ATP are produced by mitochondria [111], their efficiency is essential for a proper brain function and a copper-induced impairment of these organelles would have profound consequences. Studies by Vogel and colleagues revealed a severe neurotoxicity of copper in cats [112] and structural as well as functional impairments of brain mitochondria upon copper treatment [113, 114]. However, due to the lack of adequate animal models for the neurologic phenotype of WD further insights into the role of mitochondria in the pathogenesis of the disease are rare. Whereas WD rats show neurological involvement only in very rare cases [115], mouse models of WD of display higher

brain copper levels compared to controls paralleled by slight neurological impairments [116-118]. However, no information about an involvement of mitochondria is available so far.

1.2.4 Treatment options in Wilson disease

In WD patients, the impaired function of ATP7B leads to the accumulation of copper in various organs, most prominently the liver and the brain. To reduce their daily dietary copper intake, WD patients are obliged to avoid copper-rich food, *e.g.*, nuts, seafood and mushrooms [119, 120]. Additionally, maintenance therapy can be achieved by the application of zinc salts to decrease the uptake of the metal from the diet. Here, large oral doses of zinc induce the expression of metallothioneins in the enterocytes [121-123]. As metallothioneins exhibit a higher affinity for copper than zinc, the former cannot be transferred into the portal circulation [120]. Hence, the shedding of enterocytes in their normal turnover [124] leads to the excretion of copper via the feces. However, this mode-of-action also accounts for the most abundant side effect of zinc application, gastritis [125]. Additionally, zinc is maybe preferable in asymptomatic WD patients and patients suffering from neurological symptoms [126], but acute manifestations of the disease need to be treated with highly effective copper chelators.

The main goal of copper chelators is to substantially reduce the hepatic copper burden and thereby, reverse mitochondrial impairments. Here, the most frequently used drug worldwide is D-penicillamine (DPA) [119, 125, 127, 128]. First described by Walshe in 1956 [129], its effectiveness was proven in several studies showing a reduction of liver copper and an improvement of clinical symptoms in WD patients [127, 130]. However, life-long administration of DPA (1000 to 1500 mg/day) is necessary [119]. DPA mainly binds non-ceruloplasmin bound copper in the blood and forms water-soluble penicillamine-metal complexes, that are readily excreted via the urine [61, 119, 120, 129]. This urinal excretion bears the risk of dramatic side effects. Besides renal impairment [68, 131-133], neurological deterioration is the most frequent and severe complication during DPA administration leading to treatment discontinuation. It occurs shortly after treatment initiation in 22 to 50 % of WD patients suffering from neurological symptoms and is only partially reversible [134-136]. Here, the increased availability of non-ceruloplasmin bound copper in the blood [137] is supposed to further increase the cerebral copper burden and thereby, copper-induced neuronal damage. This neurological worsening occurs in a comparable extent in WD patients treated with trientine [128, 138]. First described in 1969 [139], trientine is the second-line therapy for WD [119]. It decreases intestinal copper absorption by 80 % [140] and enhances the elimination of the metal by forming a highly stable complex with non-ceruloplasmin bound copper in the blood. Subsequently, these trientine-copper complexes are excreted via the urine

[140-142]. In summary, copper chelators used in the clinical context can stabilize and improve the hepatic phenotype of WD but display a severe risk of neurological deterioration in symptomatic neurologic WD patients. Therefore, new chelators are required to fulfill the unmet needs of neurologic WD patients. Here, tetrathiomolybdate (TTM), first described by Walshe in 1986 [143], appears to be a promising agent. In the blood, TTM forms an inert complex with copper in the presence of albumin [144]. In contrast to DPA and trientine, no neurological deterioration was recorded in a phase 2 clinical study with WTX101 (bis-choline TTM) and blood levels of non-ceruloplasmin bound copper were significantly reduced. Furthermore, WTX101 was proven to be effective by once-daily oral administration, thereby increasing patient compliance compared to DPA treatment [145, 146]. However, further studies are needed to evaluate potential short- and long-term risks of WTX101 in the treatment of WD. Here, previous studies reported dose-dependent elevation of liver transaminases and blood count reductions [138, 145], that were reversible after lowering the dosage or temporary discontinuation of the treatment [145]. Therefore, the efficacy and safety of TTM in the treatment of WD is under further investigation in an ongoing phase 3 clinical trial [103].

In the case of life-threatening complications (*e.g.*, acute liver failure or treatment failure), liver transplantation is indicated in WD patients [119, 120]. Several studies showed the excellent long-term outcomes of liver transplantation in hepatic WD patients [147-151]. The correction of the metabolic defect of WD leads to the restoration of normal biliary copper excretion. Thereby, disease recurrence is prevented and copper removal from extrahepatic sites is promoted. However, liver transplantation in WD patients suffering from neurological symptoms is controversial [152-155]. Mostly, an improvement can be achieved in patients with mild neurologic deficits whereas only a minimal improvement is seen in patients with severe neurologic impairments [156, 157]. Additionally, although liver transplantation is a lifesaving therapy and WD medication is redundant, lifelong immunosuppression is needed [156, 158].

1.3 Aim of the thesis

Wilson disease is an autosomal-recessive inherited disease of copper metabolism that is characterized by a dramatic accumulation of the metal in various organs. Whereas the liver and the brain are massively affected in WD patients, kidney and heart problems are rather rare. Furthermore, previous studies revealed an important role of liver mitochondria in the pathogenesis of the disease. Therefore, the first

aim of this thesis is to compare the vulnerability of mitochondria from rat liver, brain, heart and kidney towards copper overload to gain further insight into the differential effect of the metal on these organs.

In contrast to the pathophysiology of hepatic WD that is extensively described in the literature, the neurologic phenotype of the disease is largely unexplored. This is mainly due to the lack of adequate animal models of neurologic WD. Therefore, the second aim of the thesis is to investigate the impact of copper on the brain using *in vitro* methods. Thus, the sensitivity of mitochondria from the astrocytoma cell line U-87MG and the neuroblastoma cell line SH-SY5Y is compared upon copper challenge. Furthermore, the impact of the metal on mitochondrial structure and function is evaluated to unravel potential molecular mechanisms that cause neurodegeneration in the context of WD.

Neurological worsening of symptoms is a common and early feature upon treatment of neurologic WD patients with D-penicillamine (DPA). In contrast, this phenomenon is not observed upon treatment with bis-choline tetrathiomolybdate (WTX101). Therefore, the third aim of this thesis is to evaluate the ability of DPA and WTX101 to rescue copper-induced cell death in the four cell lines HepG2 (hepatocellular carcinoma), EA.hy926 (endothelial cell line), U-87MG and SH-SY5Y. Furthermore, the impact of the chelators on copper-induced mitochondrial alterations is investigated.

The fourth aim of this thesis is to gain further insight into the mechanism of mitochondrial copper toxicity. To this end, the influence of thiol modification on mitochondrial respiration is investigated by measuring NADH-linked and succinate-linked respiration of U-87MG cells upon copper exposure.

2 MATERIALS & METHODS

2.1 Reagents and technical equipment

Table 1. Chemicals and dyes

Name	Producer
ADP (adenosine-5'-diphosphate)	Sigma-Aldrich, Taufkirchen, Germany
Albumin Fraction V (BSA, fatty acid free)	Carl Roth, Karlsruhe, Germany
Amplex™ Red	Molecular Probes, Invitrogen, Karlsruhe, Germany
Antimycin A	Sigma-Aldrich, Taufkirchen, Germany
Antibiotic-antimycotic solution	Life Technologies, Darmstadt, Germany
Aqua Poly/Mount	Polysciences, Washington, USA
ATP (adenosine-5'-triphosphate disodium salt)	Roche Diagnostics, Mannheim, Germany
ATP Bioluminescence Assay Kit	Roche Diagnostics, Mannheim, Germany
ATRA (all-trans retinoic acid)	Sigma-Aldrich, Taufkirchen, Germany
BDNF (brain-derived neurotrophic factor)	Biomol, Hamburg, Germany
BODIPY-FL	Thermo Fisher Scientific, Waltham, USA
$CaCl_2$	Carl Roth, Karlsruhe, Germany
CCCP (carbonyl cyanide m-chloro-phenyl-hydrazone)	Sigma-Aldrich, Taufkirchen, Germany
CellTiter-Glo® Luminescent Cell Viability Assay	Promega, Fitchburg, USA
Collagen Type I	Merck, Darmstadt, Germany
$CuCl_2$ * 2 H_2O (copper (II)-chloride dihydrate)	Sigma-Aldrich, Taufkirchen, Germany
Digitonin	Calbiochem, Sigma-Aldrich, Taufkirchen, Germany
DiOC6 (3,3'-dihexyloxacarbocyanine iodide)	Molecular Probes, Invitrogen, Karlsruhe, Germany
DMSO (dimethylsulfoxide)	Sigma-Aldrich, Taufkirchen, Germany
DPA (D-penicillamine)	Laborchemie Apolda, Apolda, Germany
DPBS (Dulbecco's phosphate buffered saline)	Biochrom, Berlin, Germany
DTNB (5,5'-dithiobis-2-nitrobenzoic acid)	Sigma-Aldrich, Taufkirchen, Germany
EGTA (ethylene glycol-bis(2-amino-ethylether)-tetraacetic acid)	Fluka, Sigma-Aldrich, Taufkirchen, Germany
Ethanol	Merck, Darmstadt, Germany
FCCP (carbonyl cynanide-p-trifluoromethoxy-phenylhydrazone)	Sigma-Aldrich, Taufkirchen, Germany
FCS (fetal calf serum)	Biochrom, Berlin, Germany
FGF-2 (fibroblast growth factor 2)	Merck, Darmstadt, Germany
Glutathione	Sigma-Aldrich, Taufkirchen, Germany
Glutathione reductase	Roche Diagnostics, Mannheim, Germany
Glycine	Sigma-Aldrich, Taufkirchen, Germany

Name	Producer
HEPES (4-(2-hydroxyethyl)piperazine-1-ethansulfonic acid)	Sigma-Aldrich, Taufkirchen, Germany
Hoechst 33258	Merck, Darmstadt, Germany
KCl (potassium chloride)	Merck, Darmstadt, Germany
KCN (potassium cyanide)	Sigma-Aldrich, Taufkirchen, Germany
KOH (potassium hydroxide)	Merck, Darmstadt, Germany
20x LumiGlo® reagent and 20x peroxide	Cell Signaling, Frankfurt a.M., Germany
L-Histidine	Sigma-Aldrich, Taufkirchen, Germany
$MgCl_2$ (magnesium chloride)	Sigma-Aldrich, Taufkirchen, Germany
Malate (disodium salt)	Merck, Darmstadt, Germany
Metaphosphoric acid	Merck, Darmstadt, Germany
Methanol	VWR, Ismaning, Germany
MitoSOX™ Red	Molecular Probes, Invitrogen, Karlsruhe, Germany
MOPS (4-morpholinepropanesulfonic acid)	Fluka, Sigma-Aldrich, Taufkirchen, Germany
NaCl (sodium chloride)	Sigma-Aldrich, Taufkirchen, Germany
Na_2CO_3 (sodium carbonate)	Merck, Darmstadt, Germany
NADPH	Roche Diagnostics, Mannheim, Germany
NaOH (sodium hydroxide)	Fluka, Sigma-Aldrich, Taufkirchen, Germany
NEAA (non-essential amino acids)	Life Technologies, Darmstadt, Germany
Neutral red	Sigma-Aldrich, Taufkirchen, Germany
Nitric acid 65 %	Merck, Darmstadt, Germany
NQS (1,2-naphthoquinone-4-sulfonate)	Sigma-Aldrich, Taufkirchen, Germany
Oligomycin	Sigma-Aldrich, Taufkirchen, Germany
Percoll®	GE Healthcare, Munich, Germany
H_3PO_4 (phosphoric acid)	Sigma-Aldrich, Taufkirchen, Germany
Rh123 (rhodamine 123)	Invitrogen, Karlsruhe, Germany
Roti®-Nanoquant (Bradford reagent)	Carl Roth, Karlsruhe, Germany
SDS (sodium dodecyl sulfate)	Serva Electrophoresis GmbH, Heidelberg, Germany
Sodium pyruvate	Life Technologies, Darmstadt, Germany
Succinate (sodium salt)	Sigma-Aldrich, Taufkirchen, Germany
TEMED	Sigma-Aldrich, Taufkirchen, Germany
TES	Sigma-Aldrich, Taufkirchen, Germany
Triethanolamine	Fluka, Sigma-Aldrich, Taufkirchen, Germany
TRIS	VWR, Ismaning, Germany
Triton X-100	Sigma-Aldrich, Taufkirchen, Germany
Trypan blue	Sigma-Aldrich, Taufkirchen, Germany
Vinylpyridine	Sigma-Aldrich, Taufkirchen, Germany
WTX101 (bis-choline tetrathiomolybdate)	Wilson Therapeutics AB, Stockholm, Sweden

Table 2. Technical equipment

Name	Application	Producer
BioPhotometer	Protein determination	Eppendorf, Hamburg, Germany
Cell Homogenizer	Mitochondria isolation from cells	Isobiotec, Heidelberg, Germany
CellZscope	TEER and capacitance measurements	nanoAnalytics, Münster, Germany
Centro LB 960 luminometer	Luminescence measurements	BD Bioscience, Heidelberg, Germany
ClarioStar plate reader	Fluorescence, absorbance, luminescence measurements	BMG Labtech, Ortenberg, Germany
DM6B microscope	Fluorescence microscopy	Leica Microsystems, Wetzlar, Germany
FUSION FX7 detection system	Chemiluminescence (Western Blot), Fluorescence (SDS gels, Western Blot)	Vilber Lourmat, Germany
ICP-QQQ 8800 (ICP-MS/MS)	Metal determination	Agilent, Waldbronn, Germany
LUNA-II™ Automated Cell Counter	Determination of cell number, size and viabiltiy	Logos biosystems, Anyang, South Korea
Oxygraph-2k	Respiration measurements	Oroboros Instruments, Innsbruck, Austria
Synergy 2 plate reader	Fluorescence and absorbance measurements	BioTek Instruments, Bad Friedrichshall, Germany
Transwell® inserts	TEER measurements, transport studies	Corning, New York, USA
96-well plates (white, flat bottom)	ATP assays	ThermoFisher Scientific GmbH, Dreieich, Germany
96-well plates (black, clear flat-bottom)	mitochondrial membrane potential, swelling, H_2O_2 production	Greiner Bio-One, Frickenhausen, Germany
96-well plates (clear flat-bottom)	Neutral red, CCK-8,	Falcon, VWR, Ismaning, Germany

Table 3. Primary antibodies

Name	Application	Dilution	Cat. number	Producer
4-Hydroxynonenal	WB	1:1000	ab46545	Abcam, Cambridge, UK
Citrate synthase	WB	1:1000	16131-1-AP	Proteintech, Rosemont, USA
Claudin 5	ICC	1:250	203-1557	Zytomed Systems, Berlin, Germany
Hsp60	WB	1:5000	611562	BD Bioscience, Heidelberg, Germany
Metallothionein	WB	1:1000	ab12228	Abcam, Cambridge, UK
Zonula occludens-1	ICC	1:250	226-0031	Zytomed Systems, Berlin, Germany

Table 4. Secondary antibodies

Name	Application	Dilution	Cat. number	Producer
goat anti-Biotin (HRP)	WB	1:2000	7075	Cell Signaling, Frankfurt a.M., Germany
donkey anti-goat (IgG, HRP)	WB	1:1000	sc-2020	Santa Cruz, Dallas, USA
goat anti-mouse (IgG, HRP)	WB	1:2000	7076	Cell Signaling, Frankfurt a.M., Germany
goat anti-mouse (IgG, Alexa Fluor® 488)	ICC	1:1000	A11001	Invitrogen, Karlsruhe, Germany
goat anti-rabbit (IgG, HRP)	WB	1:2000	7074	Cell Signaling, Frankfurt a.M., Germany

2.2 Animals

2.2.1 Housing

The *Atp7b*$^{-/-}$ rat was provided by Jimo Borjigin, University of Michigan, Ann Arbor, Michigan, USA. The *Atp7b*$^{-/-}$ rat is a crossbreed between LEC rats, carrying a deletion in the *Atp7b* gene, and PVG rats [159]. Rats had access to an ad libitum Altromin 1314 diet (Altromin Spezialfutter GmbH, Lage, Germany) and tap water [84]. All rats were housed under the guidelines for the care and use of laboratory animals of the Helmholtz Center Munich, Neuherberg, Germany. In this study, heterozygous *Atp7b*$^{+/-}$ rats served as controls and were compared with homozygous *Atp7b*$^{-/-}$ rats.

2.2.2 Treatment and sample acquisition

At treatment start, all animals were healthy and presented no signs of acute liver damage (serum AST < 200 U/l and serum bilirubin < 0.5). *Atp7b*$^{-/-}$ rats (age: 79 - 96 days) were treated intraperitoneal for four consecutive days with 2.5 mg/kg bw. WTX101 once daily or 100 mg/kg bw. DPA once daily. Untreated *Atp7b*$^{+/-}$ and *Atp7b*$^{-/-}$ rats served as controls. For urine and feces collection, rats were housed individually in metabolic cages for four days. After a two-day resting period off treatment in normal cages and group housing, rats were sacrificed for serum collection. Copper levels in urine, serum and feces were analyzed by ICP-OES (see 2.13). Animal experiments were done by Dr. Claudia Einer, Tamara Rieder and Josef Lichtmannegger (Institute of Molecular Toxicology and Pharmacology, Helmholtz Center Munich, Germany).

2.3 Cell culture

HepG2 cells were purchased from ATCC (ATCC® HB-8065™) and represent a human hepatocellular carcinoma cell line derived from a 15-year-old male Caucasian [160]. U-87MG cells were purchased from ATCC (ATCC® HTB-14™) and represent a glioblastoma derived from a male patient of uncertain age [161]. SH-SY5Y cells were purchased from ATCC (ATCC® CRL-2266™) and represent a neuroblastoma derived from the bone marrow of a 4-year-old female [162]. EA.hy926 cells were purchased from ATCC (ATCC® CRL-2922™) and represent a human intraspecies hybrid derived by fusing umbilical vein endothelial cells with the permanent cell line A549 [163]. All stated cell lines were cultured in Dulbecco's Modified Eagle Medium (DMEM) supplemented with 10 % fetal calf serum (FCS) and 1 % penicillin/streptomycin. Additionally, U-87MG and SH-SY5Y cells were cultured in minimum essential medium (MEM) with 1.9 mM GlutaMAX™ containing 5.5 mM glucose supplemented with 10 % FCS, 1 % non-essential amino acids, 1 % sodium pyruvate and 1 % antibiotic-antimycotic.

U-87MG and SH-SY5Y were differentiated as previously described [164, 165]. Briefly, U-87MG cells were treated for six consecutive days with 1 µM all-trans retinoic acid (ATRA) in MEM supplemented with 1.9 mM GlutaMAX™ containing 5.5 mM glucose supplemented with 10 % FCS, 1 % non-essential amino acids, 1 % sodium pyruvate and 1 % antibiotic-antimycotic. The differentiation of SH-SY5Y cells was achieved by incubation with 10 µM ATRA for five days, followed by incubation with 5 ng/ml brain-derived neurotrophic factor (BDNF) for one day.

All cells were maintained at 37 °C in a humidified atmosphere with 5 % CO_2.

2.4 Treatment solutions

Typically, intracellular copper exists in the monovalent state ("cuprous" Cu^{1+}). In contrast, extracellular copper is in the bivalent state ("cupric" Cu^{2+}) [24, 166]. To mimic intracellular copper exposure, isolated mitochondria were challenged with pre-mixed solutions of Cu^{2+} and glutathione (GSH), the major intracellular reductant. Here, Cu^{2+} causes stoichiometric oxidation of GSH to GSSG [167]. The resulting Cu^{1+} forms a complex with the remaining GSH to give Cu^{1+}-$[GSH]_2$ complexes [168, 169]:

$$2\ Cu^{2+} + 6\ GSH \rightarrow 2\ Cu^{1+} - [GSH]_2 + GSSG$$

Thus, at ratios of copper/GSH below 3:10 (corresponding to 300 µM copper and 1 mM GSH), cuprous copper largely predominates, with cupric well below 1 % as determined by EPR spectroscopy [167]. As

GSH is also a physiological copper binding molecule [15], the setting mimics intracellularly increased but GSH-bound Cu^{1+} levels. At strongly elevated copper, *e.g.*, at a copper/GSH ratio of 5:10, GSH becomes limiting, causing incomplete Cu^{2+} reduction and incomplete GSH complexation. Therefore, such a setting mimics conditions of severe copper overload.

For cellular copper challenge experiments, U-87MG and SH-SY5Y cells were incubated for 48 h with 2.5 µmol (corresponds to 500 µM) or 6.7 µmol (corresponds to 1340 µM) copper histidine (CuHis)/1×10^6 cells. These values are comparable to copper concentrations found in brains of Wilson disease patients (ranging from 297 µM to 1092 µM) [170]. The copper histidine solution was prepared as previously described [171].

Additionally, HepG2, U-87MG, EA.hy926 and SH-SY5Y cells were treated for 24 h with 250 µM BSA and increasing copper concentrations (0 to 2500 µM) in the absence or presence of 250 µM or 750 µM WTX101 or DPA in DMEM containing 2 % FCS.

2.5 Cell viability assays

2.5.1 CellTiterGlo® assay

For analyzing cell viability, 2 x 10^4 cells were seeded into each well of a white, flat bottom 96-well plate and incubated for 24 h at 37 °C and 5 % CO_2. Afterwards, cells were treated with the respective treatment solutions for 24 h and subsequently analyzed by CellTiterGlo® assay according to manufactural instructions with minor modifications. Briefly, cells were washed twice with PBS after the respective treatment and 100 µl PBS were added to each well. After addition of 30 µl CellTiterGlo® reagent to each well and shaking for 5 min at 400 rpm, luminescence was measured using a plate reader for the determination of cellular ATP content.

2.5.2 Neutral red uptake assay

2 x 10^4 cells were seeded into each well of a clear, flat-bottom 96-well plate and incubated for 24 h at 37 °C and 5 % CO_2. After treatment with the respective treatment solutions for 24 h, cell viability was assessed by neutral red as previously described [172]. Briefly, the medium was discarded and 150 µl 40 µg/ml neutral red (in DMEM containing 2 % FCS) were added to each well. Cells were incubated for 2 h at 37 °C and 5 % CO_2. Afterwards, cells were washed twice with PBS and de-stained using 100 µl de-stain solution (1 % acetic acid, 50 % ethanol, 49 % H_2O) by shaking for 10 min at 400 rpm. Fluorescence (λ_{Ex} 520/25 nm, λ_{Em} 620/40 nm) was detected using a plate reader.

2.5.3 Trypan blue exclusion test

Cell viability measurements for cellular copper determinations and high-resolution respirometry were performed by Trypan blue exclusion test [173]. Briefly, cells were washed once with PBS followed by trypsinization at 37 °C and 5 % CO_2. Trypsinization was stopped by the addition of DMEM containing 2 % FCS and cells were centrifuged for 5 min at 200 xg. After resuspending cells in medium, cell viability was determined by the addition of Trypan blue and using a Neubauer hemocytometer.

2.6 Cellular copper content

2.5 x 10^6 cells were incubated for 24 h with the respective treatment solution medium containing 2 % FCS. Afterwards, cells were trypsinized, washed once by centrifugation and counted by an automated cell counter for determination of cell viability (by Trypan blue), cell number and cell size. Subsequently, a defined cell number was wet ashed with 65 % nitric acid and copper and molybdenum levels were determined as described in 2.13.

2.7 Mitochondrial preparation

2.7.1 Mitochondrial isolation from U-87MG and SH-SY5Y cells

Mitochondria from cells were isolated by a pump-controlled cell rupture system as previously described [174]. In brief, 5 x 10^6 U-87MG or SH-SY5Y cells/ml were pumped 3 times (clearance: 6 µm, flow rate: 1400 µl/min) through the cell homogenizer. Mitochondria were collected by differential centrifugation at 800 xg and 9000 xg. Mitochondrial pellets were pooled and stored on ice until usage or flesh frozen in liquid nitrogen followed by storage at -80°C for enzyme activity assays.

2.7.2 Mitochondrial isolation from rat tissues

Mitochondria from heterozygous *Atp7b*$^{+/-}$ rat liver, kidney, heart and brain were isolated as recently reported [175]. Briefly, rat organs were rinsed with ice-cold 0.9 % NaCl, placed in ice-cold isolation buffer containing BSA (0.3 M sucrose, 5 mM TES, 0.2 mM EGTA, 0.1 % BSA (w/v), pH 7.2), and cleared from surrounding tissue and blood. Liver, kidney and brain were homogenized using a Teflonglass homogenizer with 5 - 10 strokes at 800 rpm. Rat heart was minced and manually homogenized in a rough glass-in-glass homogenizer with 5 strokes. All tissue homogenates were centrifuged twice at 800 xg for clearance of cell debris and nuclei. From the supernatant, liver, kidney and heart mitochondria

were pelleted at 9,000 xg, but brain mitochondria at 20,000 xg, as they are mostly contaminated with low density myelin. The resulting crude mitochondrial fractions were further purified by density gradient centrifugation at 9000 xg using an 18/30/60 % Percoll™ gradient system for rat liver and kidney mitochondria. Brain and heart mitochondria were resuspended in the 18 % Percoll™ solution and placed over a 30/60 % gradient followed by centrifugation at 29,000 xg. The purified organelles were washed, resuspended in isolation buffer without BSA and stored on ice until usage or flesh frozen in liquid nitrogen followed by storage at -80 °C for enzyme activity assays.

2.8 Functional analyses of mitochondria

2.8.1 ATP production of isolated mitochondria

According to the manufactural instructions, ATP production of isolated mitochondria was determined by the ATP Bioluminescence Assay Kit. Briefly, 10 µg of freshly isolated mitochondria were preincubated with the respective treatment solutions for 10 min prior to incubation for 30 min at RT in the presence of 160 µM ADP, 5 mM succinate and 2 µM rotenone in a buffer containing 0.2 M sucrose, 10 mM MOPS, 1 mM P_i and 10 µM EGTA (pH 7.4). For background correction, 2 mM KCN was added to block complex IV of the mitochondrial electron transport system. Using an ATP standard curve ranging from 0 to 1.65 µM ATP, the obtained luminescence values were converted into the rate of ATP production per minute and normalized to the protein content.

2.8.2 Mitochondrial ROS production

Mitochondrial hydrogen peroxide production was analyzed by horseradish peroxidase-catalyzed oxidation of Amplex™ red to fluorescent resorufin (λ_{Ex} 540/20 nm, λ_{Em} 620/40 nm) in a black 96-well plate (clear flat-bottom) as described previously [176]. Briefly, 75 µg of freshly isolated mitochondria were assayed in the presence of the reaction buffer (125 mM KCl, 10 mM HEPES, 5 mM $MgCl_2$, 2 mM K_2HPO_4, 5 µM $MnCl_2$) and the substrates 10 mM succinate and 2 µM rotenone. After addition of 50 µl of a mixture containing 320 µM Amplex™ Red, 2 units/ml HRP and 60 units/ml SOD, production of hydrogen peroxide was observed for one hour. Subsequently, fluorescence values were converted into the rate of H_2O_2 production per minute and normalized to protein content using a H_2O_2 standard curve (0 - 20 µM H_2O_2).

Production of mitochondrial reactive oxygen species (ROS) on the cellular level was evaluated by MitoSOX™ staining. Therefore, 1 x 10^5 cells were stained with 5 µM MitoSOX™ in PBS for 15 min at 37 °C. Subsequently, fluorescence (λ_{Em} 580 nm) was detected using a plate reader.

2.8.3 Mitochondrial membrane potential and permeability transition

Mitochondrial membrane potential (MMP, Δψm) and permeability transition (MPT, "swelling") were determined simultaneously in a black 96-well plate (clear flat-bottom) as previously described [177-179]. MMP was monitored by Rhodamine 123 (Rh123) fluorescence (λ_{Ex} 485/20 nm, λ_{Em} 528/20 nm), whereas MPT was analyzed by light scattering at 540 nm. Briefly, 75 µg of freshly isolated mitochondria were assayed in the presence of the reaction buffer (125 mM KCl, 10 mM HEPES, 5 mM $MgCl_2$, 2 mM K_2HPO_4, 5 µM $MnCl_2$) for 100 min in the presence of 10 mM succinate and 2 µM rotenone. Addition of 1 µM FCCP after 90 min served as internal control for MMP measurements. Quantitative analyses of MMP loss were done as recently described. Presence of 100 µM calcium served as positive control for mitochondrial swelling experiments.

Membrane potential of mitochondria on the cellular level was analyzed by $DiOC_6$. Therefore, 1 x 10^5 cells were stained with 20 nM $DiOC_6$ in PBS for 15 min at 37 °C. Subsequently, fluorescence (λ_{Em} 530 nm) was detected using a plate reader.

2.8.4 GSH content and thiol status of mitochondria

GSH/GSSG levels were determined according to Rahman et al. [180] with slight modifications. Mitochondrial suspensions were mixed with equal volumes of 10 % metaphosphoric acid to precipitate proteins and subsequently neutralized by triethanolamine. Total GSH content was assayed without further processing. For GSSG determination, samples were further processed by masking GSH with 9 % 2-vinylpyridine. Samples were assayed in the presence of the reaction buffer (0.1 M potassium phosphate, 0.3 mM NADPH, 20 units of glutathione reductase, pH 7.4) and 0.2 mM 5,5'-dithiobis-(2-nitrobenzoic acid) (DTNB). The formation of TNB was quantified at 412 nm.

Mitochondrial thiol levels were measured as previously described [181]. Briefly, mitochondrial suspensions were incubated with the respective treatment solutions. Subsequently, samples were washed twice, and accessible free thiols were quantified by DTNB at 412 nm.

Oxidation of mitochondrial protein thiols was examined by absence of fluorescent labeling using BODIPY-FL. Freshly isolated mitochondria were treated with the respective treatment solution for 30 min. Proteins were labeled with 0.3 nmol BODIPY-FL/µg mitochondrial protein and separated by

SDS-PAGE without thiol-reducing agents [84]. Fluorescence was detected using a FUSION FX7 detection system.

2.8.5 High-Resolution (Fluo)Respirometry

Oxygen consumption was assessed by high-resolution respirometry (HRR) using the Oxygraph-2k as described previously [182]. Per chamber, 1.5 - 2 x 10^6 living cells were supplied in 2 ml of MiR05 buffer (0.5 mM EGTA, 3 mM $MgCl_2$, 60 mM lactobionic acid, 20 mM taurine, 10 mM KH_2PO4, 20 mM HEPES, 110 mM sucrose, 1 g/l BSA, pH 7.1) and routine respiration was measured (**Figure 6**). Addition of 2.5 µM oligomycin (inhibitor of the F_OF_1-ATPase) enabled the measurement of leak respiration and stepwise addition of CCCP (1 µl steps from 1 mM stock solution) allowed the determination of the maximum oxygen flux and thereby the capacity of the electron transport system (ETS). The oxygen flux was baseline-corrected for non-mitochondrial oxygen consuming processes (ROX) by the addition of 2.5 µM of the complex III - inhibitor antimycin A.

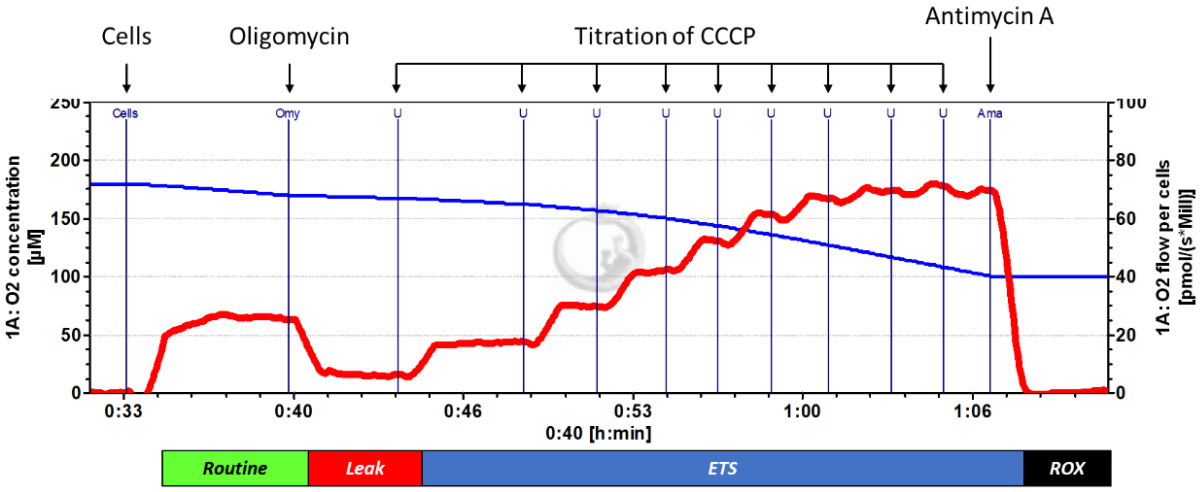

Figure 6. Schematic representation of high-resolution respirometry using intact cells.

After addition of intact cells, the oxygen flux (red line) increases until it reaches a plateau (routine respiration). Upon addition of oligomycin, oxygen flux decreases (leak state), appears maximal after CCCP titration (ETS) and drops if the respiratory chain complex III is blocked by antimycin A. Therefore, the O_2 concentration in the chamber (blue line) decreases at routine state and much more pronounced during ETS but displays almost no reduction at leak state or if CIII is blocked.

Additionally, untreated or CuBSA-treated (ratio of 1:3 for 24 h) U-87MG cells were exposed to digitonin for permeabilization of the cell membrane. Subsequently, oxygen consumption was assessed by HRR. First, leak respiration was determined by the addition of 5 mM pyruvate and 2 mM malate ($N(PM)_L$). After the addition of 2.5 mM ADP, NADH-linked OXPHOS capacity ($N(PM)_P$) was determined. Further addition of 10 mM succinate enabled the determination of the NS-linked OXPHOS capacity ($NS(PMS)_P$)

with convergent electron flow through complex I and complex II. Furthermore, addition of 2 µM of the complex I - inhibitor rotenone resulted in the determination of the succinate-linked OXPHOS capacity ($S(SR)_P$). Afterwards, titration of the uncoupling compound CCCP enabled the determination of the succinate-linked capacity of the electron transport system ($S(SR)_{ETS}$). Finally, addition of 2.5 µM antimycin A resulted in the determination of the residual oxygen consumption ($S(SR)_{ROX}$).

Furthermore, freshly isolated mitochondria from U-87MG cells (see 2.7.1) were used for the parallel determination of oxygen consumption and the mitochondrial membrane potential. First, fluorescence was calibrated by the stepwise addition of Rhodamine 123 (Rh123) to a final concentration of 1 µM (**Figure 7**). After addition of approximately 100 µg mitochondrial protein into each chamber of the Oxygraph-2k, either 1 µl 20 µM N-ethylmaleimide (NEM) or 1 µl H_2O were added.

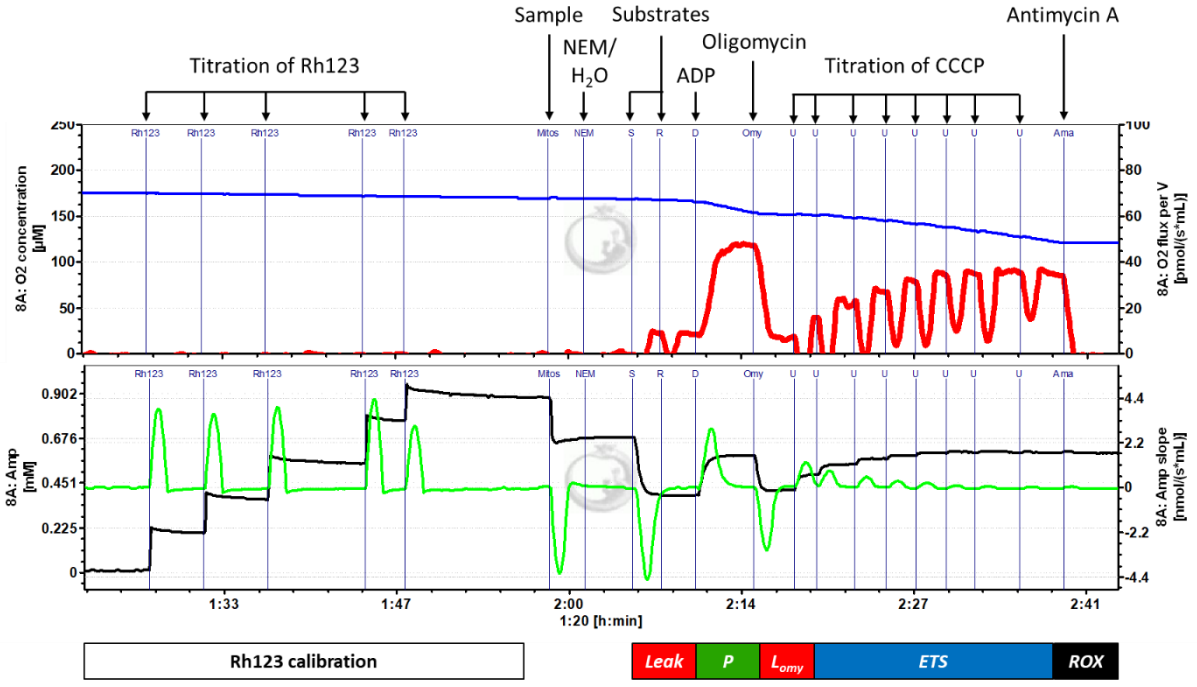

Figure 7. Schematic representation of high-resolution fluorespirometry using freshly isolated mitochondria.

First, Rh123 was titrated to a final concentration of 1 µM for calibration. After sample addition, mitochondria were treated with NEM or H_2O, respectively. Addition of substrates leads to an increase in oxygen flux (upper panel) and a decrease in the fluorescent signal (lower panel) due to quenching of the Rh123 fluorescence by uptake into the mitochondrial matrix. Addition of ADP leads to a dramatic increase in respiration but also to an increase of Rh123 fluorescence as the mitochondrial membrane potential is partially used up for ATP production. After addition of oligomycin, the membrane potential builds up again as shown by a decrease in Rh123 fluorescence paralleled by a decrease in oxygen flux. Titration of CCCP leads to a stepwise increase in respiration and a loss of membrane potential as shown by an increase in Rh123 fluorescence.

Besides measurements at tissue hyperoxia (180 µM O_2), mitochondria were exposed to 30 µM oxygen (tissue normoxia) achieved by the addition of nitrogen shortly before sample addition. Treatment with NEM or H_2O was performed at this lower oxygen concentration and was followed by reoxygenation to 180 µM O_2 prior to substrate addition. The leak state was achieved by the addition of the substrates 10 mM succinate and 2 µM rotenone for Succinate-linked respiration ($S(SR)_L$) or 5 mM pyruvate and 2 mM malate for NADH-linked respiration ($N(PM)_L$). Addition of 2.5 mM ADP allowed the determination of the OXPHOS capacity ($S(SR)_P$ or $N(PM)_P$) and subsequent addition of 2.5 µM oligomycin and stepwise addition of CCCP enabled the determination of the ETS state ($S(SR)_E$ or $N(PM)_E$). Finally, the oxygen flux was baseline-corrected for non-mitochondrial oxygen consuming processes (ROX) by the addition of antimycin A.

2.8.6 Mitochondrial enzyme activities

Activity of mitochondrial complex IV (cytochrome *c* oxidase) was measured according to Spinazzi et al. [183] with minor modifications. Approximately 2.5 x 10^6 cells were lysed by the addition of 20 mM hypotonic potassium phosphate buffer and three times freeze/thawing. Complex IV activity was measured by adding 10 µl of the sample to 90 µl of potassium phosphate buffer (pH 7.0) containing 50 µM reduced cytochrome *c* with or without 0.3 mM KCN. Absorbance was measured at 550 nm for 10 min in a plate reader and complex IV activities were calculated from the linear slopes of the initial rates corrected for unspecific activity (in the presence of KCN). Complex IV activity was normalized to protein content (see 2.13).

Aconitase activity was measured as previously described [184]. Briefly, freeze/thawed mitochondrial suspensions were assayed in the presence of reaction buffer (50 mM Tris-HCl, 60 mM sodium citrate, 1 mM $MnCl_2$, 0.2 mM $NADP^+$, 4 units of $NADP^+$ isocitrate dehydrogenase, pH 7.5) and NADPH formation was monitored at 340 nm for 60 min at 37 °C. Aconitase activity was normalized to protein content and time.

2.8.7 Structural analysis of mitochondria by electron microscopy

Fixation, prestaining with osmium tetroxide, dehydration with ethanol and propylene oxide as well as embedding and staining of samples was performed by Carola Eberhagen. Electron microscopy of isolated embedded samples was done as previously described [84, 179] on a 1200EX electron microscope (JEOL, Japan) at 80 kv. Pictures were taken with a KeenView II digital camera (Olympus, Germany) in a blinded way and processed by the iTEM software package (analysis FIVE, Olympus, Germany). Data acquisition was done either by Carola Eberhagen (Institute of Molecular Toxicology and

Pharmacology, Helmholtz Center Munich, Germany) or Dr. Bastian Popper (Department of Anatomy and Cell Biology, Biomedical Center, Ludwig-Maximilians-University Munich, Germany).

Mitochondrial shape and structure were analyzed identically for all samples using ImageJ. Mitochondria were considered "roundish", when the ratio maximum vs. minimum diameter was < 1.5; otherwise, mitochondria were deemed "elliptical".

2.9 The *in vitro* blood-brain-barrier model

2.9.1 Cell preparation

Primary porcine brain capillary endothelial cells (PBCECs) were kindly provided by Prof. Tanja Schwerdtle. PBCECs were isolated as previously described [185] and frozen in liquid nitrogen until usage. All experiments where done under the guidance of Prof. Dr. Tanja Schwerdtle and Stefanie Raschke (Department of Food Chemistry, University of Potsdam, Germany).

2.9.2 Transepithelial electrical resistance

For barrier integrity studies, transepithelial electrical resistance (TEER) experiments were carried out as previously described [103]. Briefly, cryopreserved cells were thawed and cultivated in Earle's Medium 199 supplemented with 10 % FCS, 50 U penicillin/ml, 50 µg/ml streptomycin, 100 µg/ml gentamycin and 0.7 mM l-glutamine. Cells were either seeded on rat tail collagen-coated 96-well plates (clear flat-bottom) for cytotoxicity testing or on rat tail collagen-coated Transwell® membrane inserts (area: 1.12 cm^2, pore size: 0.4 µm) for barrier integrity studies in a humidified atmosphere at 37 °C and 5 % CO_2. After 48 h, the medium was changed to serum-free DMEM/Ham's F12 (1:1) containing 50 U penicillin/ml, 50 µg/ml streptomycin, 100 µg/ml gentamycin, 4.1 mM L-glutamine and 550 nM hydrocortisone. PBCECs were incubated for further 48 h and the medium in the apical chamber was changed to the respective treatment solution. PBCECs were treated with 83.3 µM BSA and 250 µM $CuCl_2$ in the absence or presence of 250 µM WTX101 or DPA for 48 h. During exposure measurements, the transendothelial electrical resistance (TEER) as well as the capacitance was determined continuously using a CellZscope® device (**Figure 8**). The TEER is proportional to the tightness of a barrier, whereas the capacitance is proportional to the plasma membrane surface area. Only PBCEC monolayers with TEER values > 600 Ω cm^2 and capacitance values between 0.45 and 0.6 µF/cm^2were used for permeability studies [186]. TEER and capacitance were measured automatically every 90 min. The barrier integrity was calculated by normalizing the TEER values to the respective start values.

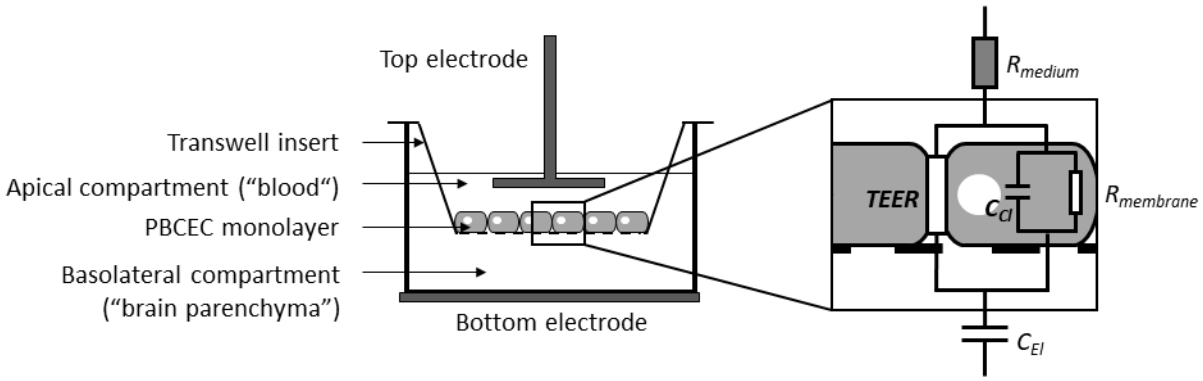

Figure 8. Schematic representation of the Transwell® system and the measured parameters in the CellZscope® device.

Primary porcine brain capillary endothelial cells (PBCECs) were seeded on Transwell® inserts for monolayer formation. Treatment solutions were added to the apical chamber representing the blood compartment. The close-up represents a circuit model of the PBCEC monolayer and the contribution of the trans- and paracellular pathway to the total impedance. The ohmic resistance of the cell membrane ($R_{membrane}$) and the capacitance of the cell layer (C_{Cl}) represent the paracellular pathway, whereas the transepithelial electrical resistance (TEER) represents the transcellular pathway. Additionally, the capacitance of the electrodes (C_{El}) and the ohmic resistance of the medium (R_{medium}) are determined.

2.9.3 Immunocytochemistry

Following the TEER measurements, PBCECs on Transwell® inserts were used for immunocytochemical staining of the tight junction proteins Claudin-5 and Zona occludens-1 (ZO-1). Immunocytochemistry was performed as previously described [103]. Briefly, PBCECs were fixed with 4 % (v/v) formaldehyde for 20 min at 4 °C and permeabilized using 0.2 % (v/v) Triton X-100 for 10 min at RT. Subsequently, unspecific binding sites were blocked by incubation with 3 % BSA in PBS for 20 min and the cells were incubated with the respective primary antibody (diluted in 0.5 % BSA in PBS) for 30 min at 37 °C. Afterwards, a second blocking step was performed, and the cells were incubated for 30 min at 37 °C with the secondary antibody. For staining of nuclei, cells were treated for 30 sec with Hoechst 33258 in methanol. Membranes were cut out of the inserts and carefully mounted in Aqua/Poly Mount. Samples were evaluated using a fluorescence microscope.

2.9.4 ICP-MS/MS analysis

After 0, 24 and 48 h of exposure to the test substances, 20 µl of the apical medium as well as 40 µl of the basolateral medium was collected for subsequent copper determination by ICP-MS/MS. Therefore, samples underwent an acidic (20 % HNO_3) digestion as described previously [187]. Rhodium (0.5 µg/L) served as internal standard. Total copper was determined by a validated inductively coupled plasma mass spectrometer-based method and external calibration as described before [188].

2.10 Immunoblotting

Immunoblot analyses of proteins were performed according to Towbin et al. [189] with slight modifications. 10 µg of mitochondrial protein or 0.5 - 1 x 10^5 lysed cells were subjected to SDS-PAGE and separated proteins were transferred onto a polyvinyldifluoride (PVDF) membrane. Ponceau S staining was used to control protein transfer. Unspecific binding sites were blocked with 5 % milk in TBS-T for 30 min at RT. Afterwards, membranes were incubated with the primary antibody (overnight at 4 °C or 2 h at RT) followed by incubation with the secondary antibody (1 h at RT). Finally, chemiluminescence signals were detected using a FUSION FX7 detection system.

Detection of metallothioneins 1 and 2 (MT 1/2) was performed with minor modifications of the immunoblot protocol according to Mizzen et al. [190]. Briefly, transfer to PVDF membranes was carried out in transfer buffer containing 20 mM $CaCl_2$. Furthermore, membranes were fixed with glutaraldehyde prior to the blocking step with 5 % milk in TBS-T. Incubation with the first and second antibody were performed as described.

For staining of free protein thiols, samples were incubated with 0.3 nmol BODIPY-FL per µg mitochondrial protein for 3 h at RT prior to separation by SDS-PAGE without thiol-reducing agents [84]. Fluorescence was detected using a FUSION FX7 detection system.

2.11 Gel filtration chromatography

10 mg of fatty-acid free bovine serum albumin (BSA) were resuspended in 10 mM Tris-HCl buffer (pH 7.4) and mixed with 45 µl of 10 mM copper chloride. Where indicated, 45 µl of 10 mM WTX101 or DPA were added to the BSA/copper complex before loading the samples onto a Superdex 75 10/300 GL column (GE Healthcare, Chicago, USA). Experiments were done in collaboration with Elisabeth Weber (Institute of Molecular Toxicology and Pharmacology, Helmholtz Center Munich, Germany).

Fractions were analyzed for protein content (see 2.13), molybdenum and copper levels by ICP-OES (see 2.13) and DPA content (fractions 13 – 30) using 1,2-naphthoquinone-4-sulfonate (NQS) as previously described with minor modifications [191]. Briefly, 50 µl of each fraction were mixed with 10 µl 0.2 % NQS, 10 µl of 0.2 M sodium phosphate buffer (pH 12.0) and 30 µl H_2O in a clear 96-well plate. The samples were incubated for 20 min and absorbance was measured at 452 nm. Absolute levels of DPA were calculated using a DPA standard solutions (25 µM to 250 µM) treated the same way as the samples.

2.12 X-ray crystallography

For X-ray crystallography of the tripartite complex (albumin-copper-WTX101), 100 mg of BSA were resuspended in buffer containing 50 mM potassium phosphate and 150 mM sodium chloride (pH 7.5). Copper chloride and WTX101 were added in 200 % molar excess and the mixture was incubated for 30 min at 37°C. The albumin-copper-WTX101 complex (tripartite complex, TPC) was loaded onto a S200 gel filtration column equilibrated with PBS (pH 7.4). Fractions corresponding to the protein in the monomeric state were pooled and protein was concentrated to 100 mg/ml. Screening for crystallization conditions was performed using commercially available buffer sets in a sitting-drop vapor diffusion setup by mixing 0.2 µl of protein complex solution and 0.2 µl of buffer solution. Crystals were obtained at room temperature from a solution containing 0.1 M SPG buffer (pH 7.0) and 0.25 % PEG 1500 and were cryo-protected in 30 % glycerol in the mother liquor and flash-cooled in liquid nitrogen. The diffraction data were collected at the ID23-2 beamline at ESRF (Grenoble, France). The data were indexed and integrated using XDS [192, 193], scaled and merged using Scala [194]. The initial phases were obtained by molecular replacement calculated using Phaser [195] and BSA structure as a search model (PDB 4F5S and [196]). The initial model was manually rebuilt due to the resulting electron density maps using Coot [197]. Due to the low resolution of data, the refined structure did not reach acceptable R_{free} values below 0.40. Nevertheless, analysis was possible regarding the presence of WTX101 due to the high scattering factor of the molybdenum complex resulting in a strong signal detectable despite low resolution of the dataset. Crystallization of the complex, data acquisition and analyses were done by Dr. Krzysztof M. Zak and Dr. Grzegorz M. Popowicz (Institute of Structural Biology, Helmholtz Centre Munich, Germany).

2.13 Miscellaneous

Copper and molybdenum levels were analyzed by ICP-OES (Ciros Vision, SPECTRO Analytical Instruments, Kleve, Germany) as described previously [84, 89]. All measurements were done by Peter Grill (Research Unit Analytical BioGeoChemistry, Helmholtz Centre Munich, Germany).

For electron paramagnetic resonance (EPR) measurements, complexes of BSA/copper (1 mM/2 mM), BSA/copper/WTX101 (1 mM/2 mM/1 mM) and BSA/WTX101 (1 mM/1 mM) were prepared in 10 mM Tris/HCl (pH 7.4) buffer and reduced with an excess of sodium dithionite shortly prior to measurements where indicated. EPR spectra were recorded at 77 K using an EMX spectrometer (ER073, Brucker BioSpin, Karlsruhe, Germany) operating in X-band at about 9.5 GHz. Measurements were done in

collaboration with Dr. Albrecht Wieser (Institute of Radiation Medicine, Helmholtz Centre Munich, Germany).

Protein concentrations were determined by the Bradford assay [198].

Data are presented as mean and standard deviation (SD). Statistical analysis was performed using Student's t test and data were tested unpaired and tow-tailed. For multiple comparisons, two-way ANOVA and Dunnett's test was done with GraphPad Prism 7 (GraphPad Software). Differences were considered statistically significant if * $p < 0.05$, ** $p < 0.01$, *** $p < 0.001$.

3 RESULTS

3.1 Brain mitochondria are severely affected by copper challenges

3.1.1 Brain mitochondria reveal structural peculiarities and a distinct sensitivity to calcium

Mitochondria differ in their structure and functional properties as well as their organ-specific molecular composition [28, 29]. These differences result in a tissue-dependent sensitivity to potentially damaging insults [199]. To demonstrate such tissue-specific mitochondrial sensitivity, organelles from rat liver, kidney, heart and brain were isolated in parallel from the same animals and comparatively tested for their calcium sensitivity.

Electron microscopy revealed the comparable structural integrity and purity of the isolated mitochondrial populations (**Figure 9**A, upper panel) characterized by well-defined cristae, an intact inner and outer mitochondrial membrane and electron-dense matrices. However, isolated rat mitochondria displayed organ-specific structural features. Here, liver mitochondria presented with a prominent electron-dense matrix and sparse cristae, whereas kidney mitochondria showed abundant rounded cristae. Heart mitochondria were characterized by a high number of regular and parallel-oriented cristae and brain mitochondria displayed a comparatively slightly reduced size.

To validate the different sensitivity of these diverse mitochondrial populations to toxic insults, isolated rat liver, kidney, heart and brain mitochondria were exposed to calcium, an inducer of the mitochondrial permeability transition that is known to cause massive mitochondrial “swelling” [200]. Mitoplast formation was observable in liver, kidney and heart mitochondria (**Figure 9**A, lower panel), a process that is characterized by enlarged inner membrane vesicles, electron-transmissive matrices, disrupted outer membranes and a (complete) loss of cristae structure. In contrast, brain mitochondria treated with calcium did not show this typical mitochondrial “swelling” but displayed heterogeneous mixtures of mitochondria with electron-transmissive matrices and rather organized cristae, or with a uniform greyish color and numerous small intramitochondrial structures.

To quantify this ultrastructural finding, the influence of a 100 µM calcium challenge was followed by optical density measurements at 540 nm ($OD_{540\,nm}$). Exemplary curves of isolated rat liver and brain mitochondria in the absence or presence of calcium already indicated differential responses of these mitochondrial populations (**Figure 9**B).

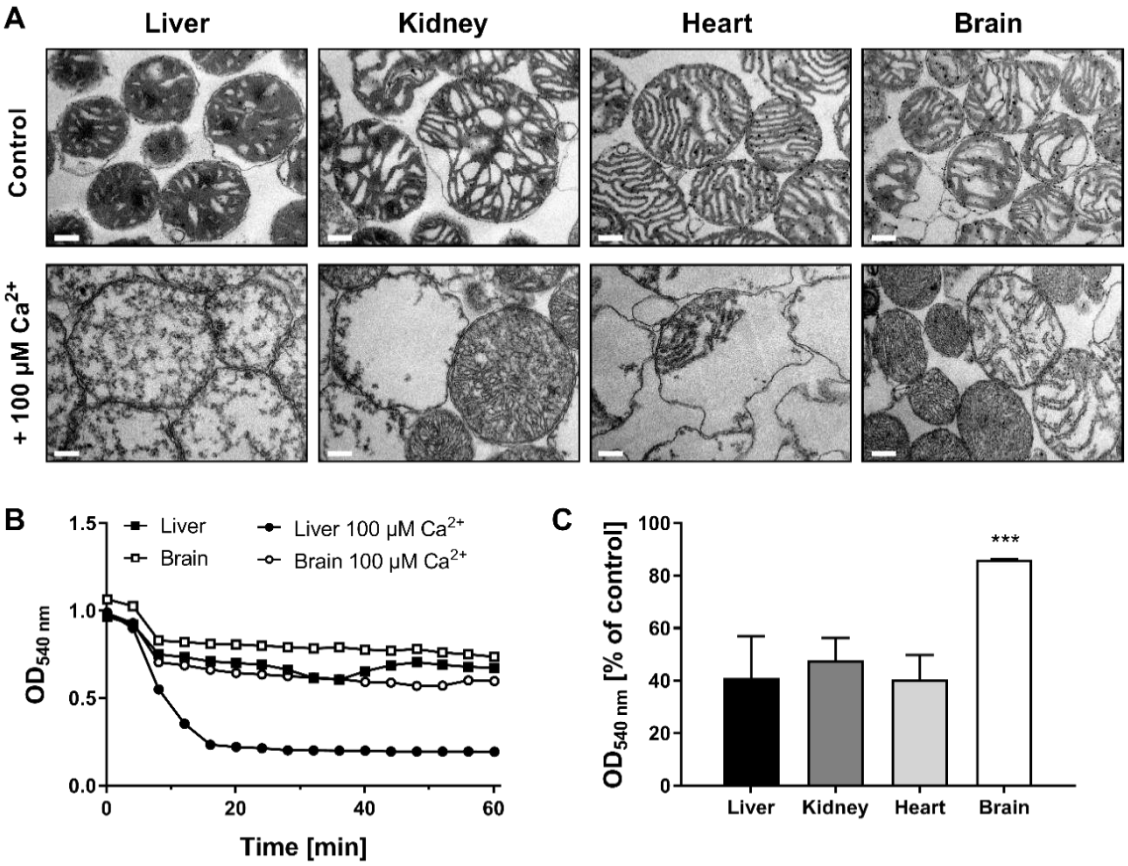

Figure 9. Isolated mitochondria from rat liver, kidney, heart and brain reveal organ-specific features in response to calcium. (A) Electron micrographs of mitochondria isolated in parallel from rat liver, kidney, heart and brain tissues show comparable high purities and intact inner and outer membranes but organ-specific structural features. A 100 µM Ca^{2+} challenge for 90 min results in mitoplast formation in liver, kidney and heart mitochondria, *i.e.*, enlarged inner membrane vesicles with electron-transmissive matrices and disrupted or depleted outer membranes. Such mitoplast formation is mostly absent in equally treated brain mitochondria. Scale bars equal 500 nm. (B) Exemplary curves of optical density measurements at 540 nm of isolated rat liver and brain mitochondria in the absence or presence of 100 µM calcium. (C) Extent of swelling under calcium challenge is similar between liver, kidney and heart mitochondria, but significantly reduced in brain mitochondria (N = 3, n = 3). Adapted from Borchard et al., 2018 [201] with permission**.**

In accordance with the ultrastructural findings, liver mitochondria displayed a strong decrease in optical density in the presence of calcium, whereas brain mitochondria displayed only a slight decrease in $OD_{540\,nm}$. Furthermore, calcium-dependent changes in optical density were quantitatively analyzed for rat liver, kidney, heart and brain mitochondria (**Figure 9**C). Here, brain mitochondria showed a significantly less pronounced $OD_{540\,nm}$ decrease in the presence of calcium compared to mitochondria from other organs.

3.1.2 Copper exposure impairs brain mitochondrial structure and function

Wilson disease is characterized by massive copper accumulation in various organs, mainly the liver and the brain [49, 51, 202, 203]. Mitochondria, although being the prime site of copper utilization within cells, are highly susceptible to copper overload, as described for the hepatic subtype of WD [84, 85, 92, 204]. To assess the organ-specific copper susceptibility of mitochondria, organelles isolated from rat liver, kidney, heart and brain were analyzed.

The mitochondrial membrane potential (MMP, $\Delta\psi_m$), as the driving force of mitochondrial ATP synthesis, is an essential feature of intact mitochondria and thereby one suitable marker of their functionality. Hence, the effect of increasing copper challenges on the mitochondrial membrane potential of diverse mitochondrial populations was assessed (**Table 5**). Increasing copper/GSH ratios were used to mirror an increasing mitochondrial copper burden. This system allows the application of glutathione-bound Cu^{1+} at low copper/GSH ratios, whereas high copper/GSH ratios lead to the presence of Cu^{2+} (see 2.4), that is highly detrimental to mitochondria per se. Whereas cupric copper (Cu^{2+}) is nearly absent within cells under physiological conditions [167], Cu^{2+} dominates extracellularly [24, 205]. The mitochondrial membrane potential of all investigated mitochondrial populations was stable over 90 min under control conditions, demonstrating their functional integrity. At low doses of cuprous copper (Cu^{1+}; copper/GSH ratio of 1:10 and 2:10), isolated rat liver, kidney and heart mitochondria were not affected. In contrast, brain mitochondria already reacted by an MMP loss at around 80 min at a copper/GSH ratio of 2:10. Additionally, the MMP was dissipated within minutes in liver, kidney, heart and brain mitochondria in the presence of cupric copper (copper/GSH ratio of 5:10).

Table 5. Membrane potential loss (Δψm) [min] of rat liver, kidney, heart and brain mitochondria at increasing copper/GSH ratios (taken from Borchard et al., 2018 [201] with permission).

	Control	copper/GSH ratio				
		0:10	1:10	2:10	3:10	5:10
Liver	> 90	> 90	> 90	> 90	59.46 ± 11.45 ***	6.79 ± 4.79 ***
Kidney	> 90	> 90	> 90	> 90	44.13 ± 31.23 *	9.54 ± 0.86 **
Heart	> 90	> 90	> 90	> 90	41.46 ± 35.78 *	6.12 ± 1.64 **
Brain	> 90	> 90	> 90	79.35 ± 16.52	32.12 ± 15.56 ***	6.79 ± 0.88 ***

Additionally, the optical density ($OD_{540\,nm}$) of mitochondrial suspensions in the absence or presence of copper was evaluated (**Figure 10**). Here, brain mitochondria displayed a strong decrease in $OD_{540\,nm}$

already at lowest copper/GSH ratio (1:10). In contrast, liver, kidney and heart mitochondria showed no loss of optical density at this low copper challenge. Liver and kidney mitochondria presented with a decrease of $OD_{540\,nm}$ at copper/GSH ratios of 3:10 and 5:10. Heart mitochondria were highly copper resistant and only the highest dose of copper (copper/GSH ratio of 5:10) led to a distinct loss of optical density.

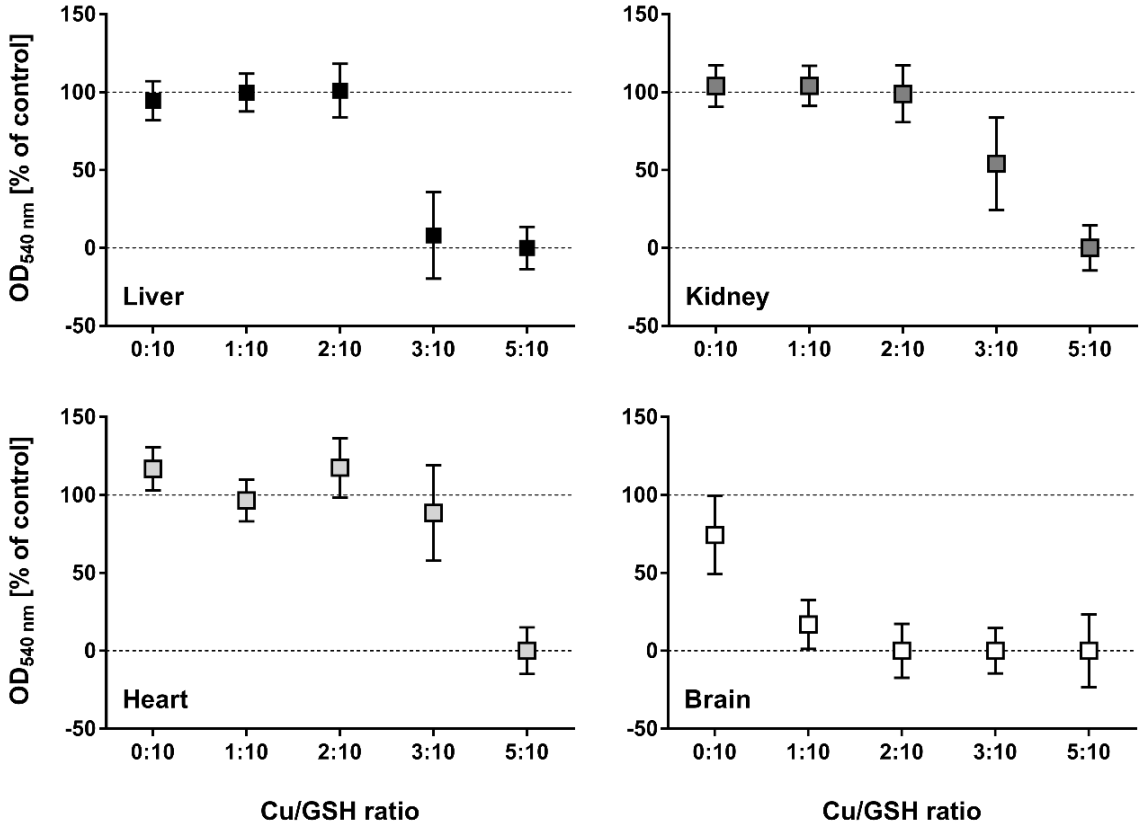

Figure 10. Assessment of mitochondrial swelling reveals high susceptibility of brain mitochondria to copper.

At copper/GSH ratios up to 2:10, liver, kidney and heart mitochondria show no $OD_{540\,nm}$ loss within 90 min. In contrast, brain mitochondria reveal a higher sensitivity to copper as shown by $OD_{540\,nm}$ loss at a copper/GSH ratio of 1:10 (N = 3, n = 3). For the sake of comparability, 100 % OD values are the respective maxima of the mitochondrial suspension, whereas 0 % values were set as the lowest $OD_{540\,nm}$ values derived from 100 µM Ca^{2+} treatments. Taken from Borchard et al., 2018 [201] with permission.

These optical density measurements suggest prominent structural changes in all mitochondrial populations depending on the applied copper dose. To visualize the impact of copper challenges on ultrastructural features of isolated rat liver, kidney, heart and brain mitochondria, electron micrographs were taken from either glutathione-treated mitochondria as control or Cu^{1+}-treated samples after 30 or 90 min of incubation (**Figure 11**).

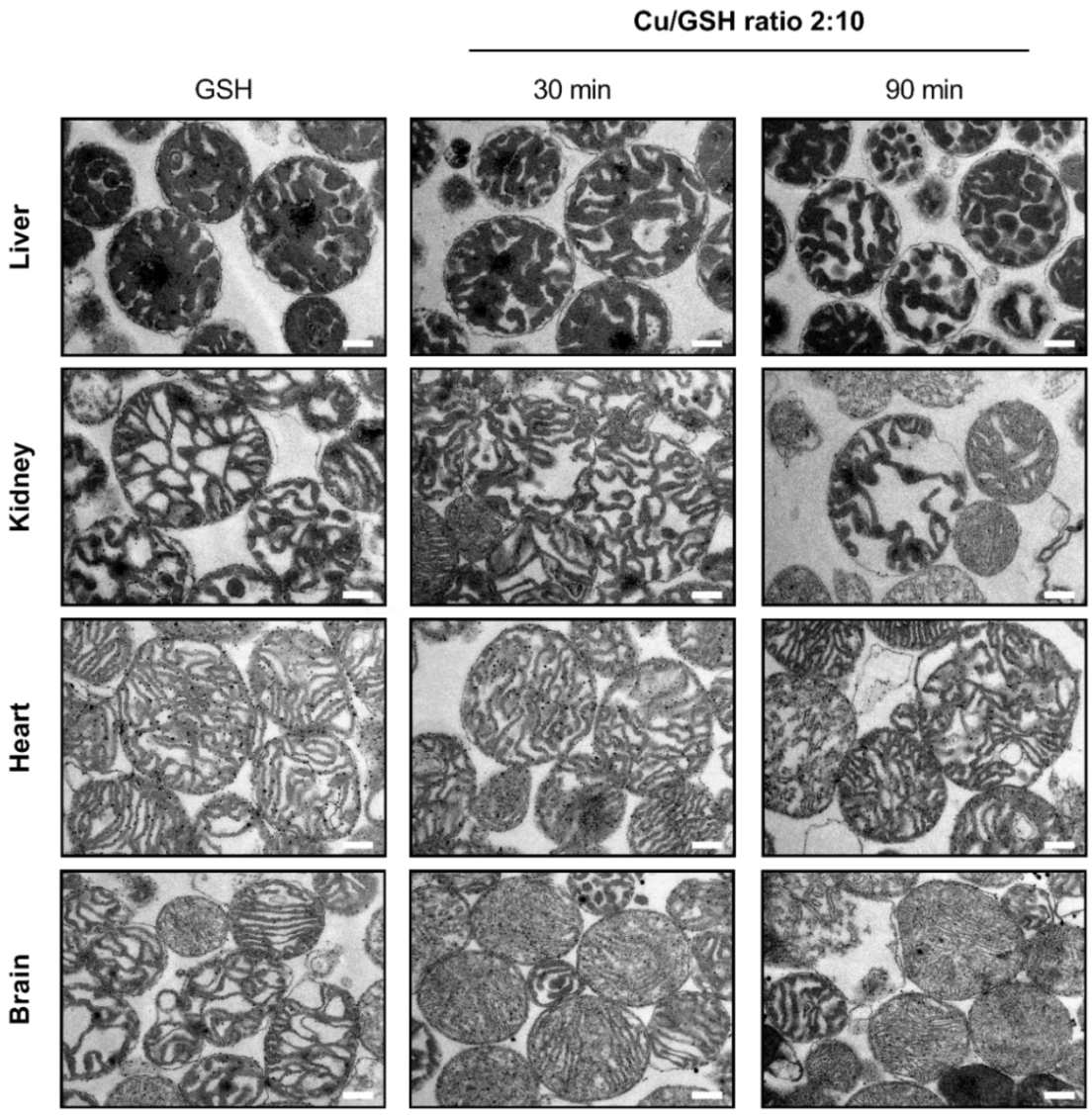

Figure 11. Time-dependent mitochondrial structure changes by copper.

Cuprous Cu^{1+} induces structural alterations in liver mitochondria reminiscent of observations in liver mitochondria in WD patients and WD animal models. Kidney mitochondria appear with heterogeneous structural alterations, but heart mitochondria remain rather unchanged. The most prominent structural alterations appear in brain mitochondria upon copper challenge. Scale bars equal 500 nm. Taken from Borchard et al., 2018 [201] with permission.

Here, liver and kidney mitochondria demonstrated time-dependent structural alterations, mostly characterized by an increase in matrix density and cristae dilatation. This effect was most prominently upon a 90 min copper challenge. As already stated for MMP and $OD_{540\,nm}$ measurements, heart mitochondria were highly copper resistant and appeared largely unaltered even after 90 min of copper exposure. In contrast, brain mitochondria displayed severe structural alterations already after 30 min of Cu^{1+} challenge appearing greyish with strongly thinned cristae compared to mitochondria treated with glutathione only. No further worsening of the mitochondrial phenotype was observable after 90 min.

Hence, Cu^{1+}-induced brain organelle damage occurred fast compared to the other investigated mitochondrial populations.

3.1.3 Fenton chemistry-based toxicity is rather a consequence than the cause of mitochondrial impairments by copper

The trace metal copper is characterized by its redox-activity as it can shift between the oxidized form (Cu^{2+}, cupric copper) and the reduced state (Cu^{1+}, cuprous copper). Therefore, the copper-induced death of hepatocytes occurring in the progression of Wilson disease was previously attributed to the formation of reactive oxygen species [76, 206]. Here, aqueous free copper ions could participate in the production of highly detrimental hydroxyl radicals via Fenton- and Haber-Weiss-based reactions. However, this view contrasts with calculations demonstrating the lack of free copper within cells [23].

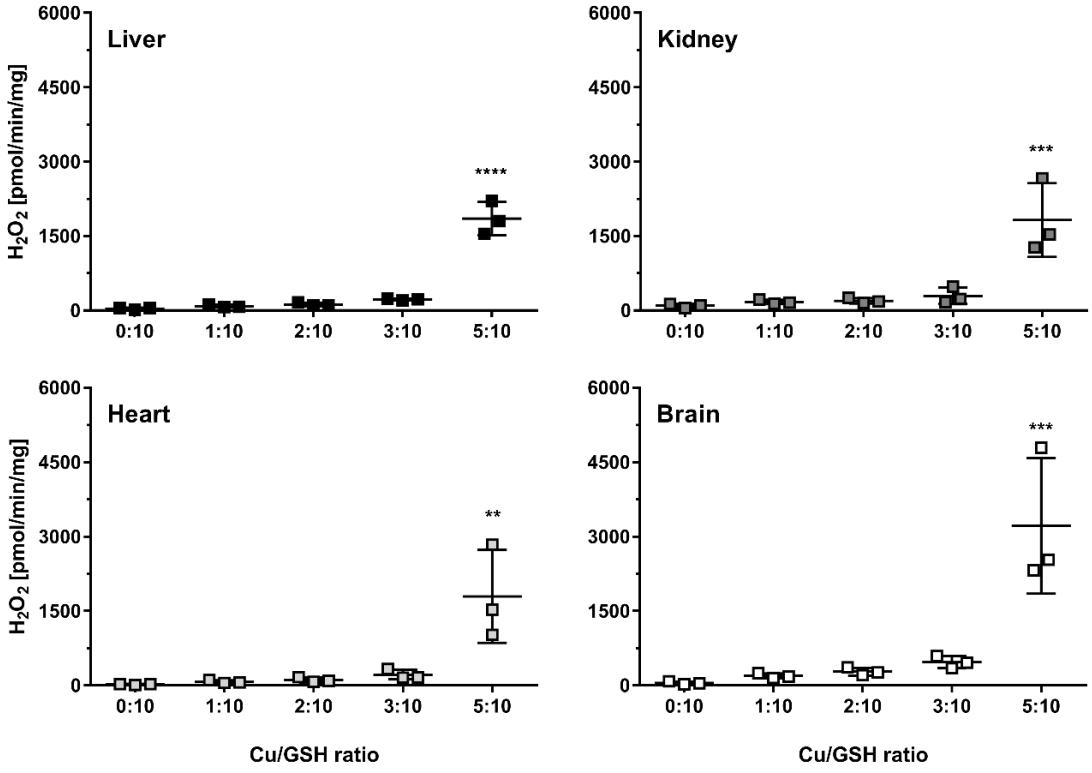

Figure 12. Hydrogen peroxide production in rat mitochondria upon copper challenges.

The rate of hydrogen peroxide (H_2O_2) production in mitochondria from rat liver, kidney, heart and brain is significantly increased upon challenge with a high copper/GSH ratio of 5:10, a condition that readily destroys mitochondria. Brain mitochondria display the highest H_2O_2 production compared to isolated mitochondria from liver, kidney and heart (N = 3, n = 6). Adapted from Borchard et al., 2018 [201] with permission.

Therefore, the production of hydrogen peroxide (H_2O_2) of isolated rat liver, kidney, heart and brain mitochondria under copper challenges was investigated (**Figure 12**). Here, all investigated mitochondrial

populations revealed an only slight, non-significant increase in hydrogen peroxide production in the presence of copper/GSH ratios of 1:10 to 3:10 (*i.e.*, the presence of Cu^{1+}). A significant and massive H_2O_2 production was only apparent at the highest copper/GSH ratio of 5:10, thus in the presence of cupric copper (Cu^{2+}). Additionally, brain mitochondria revealed the highest ROS production in comparison to liver, kidney and heart mitochondria.

For the sake of conciseness, all subsequent analyses were performed with isolated rat liver and brain mitochondria only, as liver and brain are primarily affected by copper overload in the context of Wilson disease. Isolated liver and brain mitochondria were subjected to copper challenges and analyzed for markers of oxidative damage, *e.g.*, aconitase activity and formation of 4-hydroxynonenal (4-HNE) adducts (**Figure 13**). Here, a reduced mitochondrial aconitase activity serves as surrogate marker of oxidative protein damage, whereas the presence of 4-HNE adducts indicates ROS-dependent lipid peroxidation.

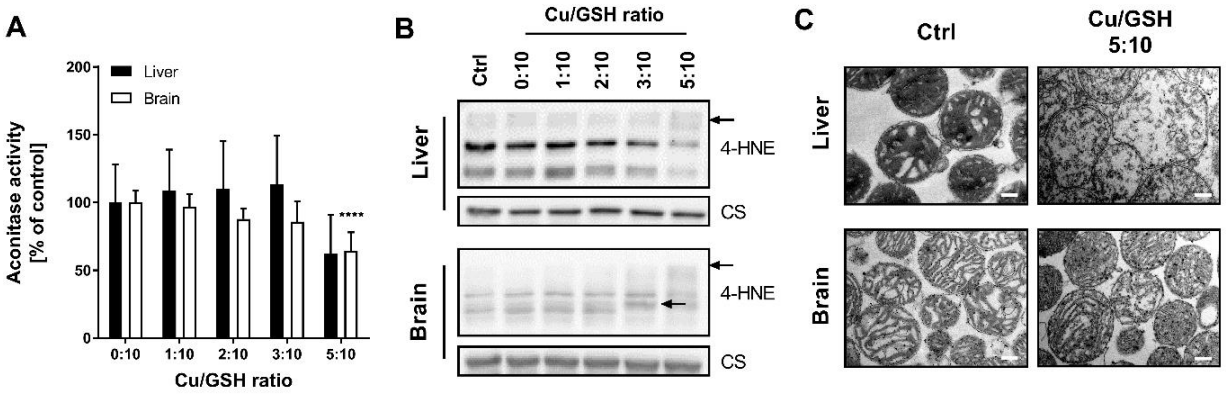

Figure 13. Massive oxidative stress occurs upon copper induced mitochondrial destruction.

(A) The mitochondrial aconitase activity is not affected in both, rat liver and brain mitochondria, by copper/GSH ratios up to 3:10 but significantly decreased at the highest copper/GSH ratio in brain organelles (N = 3 - 4, n = 6 - 8). (B) Lipid peroxidation, determined by 4-hydroxynonenal (4-HNE) adduct formation, was increased at the highest copper/GSH ratio but stable at lower ratios in both, liver and brain mitochondria (N = 3). Citrate synthase (CS) was used as loading control. (C) The highest copper/GSH ratio (5:10) leads to a massive destruction of liver and brain mitochondria compared to control conditions. Scale bars equal 500 nm. Adapted from Borchard et al., 2018 [201] with permission.

The determination of aconitase activity in copper-challenged rat liver and brain mitochondria revealed no reduced activity in both mitochondrial populations at copper/GSH ratios of 1:10 to 3:10 (**Figure 13**A). Only the highest copper/GSH ratio of 5:10, *i.e.*, in the presence of Cu^{2+} led to a significantly reduced aconitase activity in brain mitochondria. Accordingly, 4-HNE protein adducts were only slightly increased in brain mitochondria exposed to copper/GSH ratios of 3:10 and 5:10 (**Figure 13**B), whereas the protein

pattern of liver mitochondria was unambiguously changed only at the highest copper/GSH ratio. Furthermore, liver and brain mitochondria incubated with the highest copper/GSH ratio (5:10) were analyzed by electron microscopy (**Figure 13**C). The presence of cupric copper led to a massive organelle destruction in both mitochondrial populations that was characterized by a loss of cristae structure and a disrupted outer mitochondrial membrane. Additionally, the matrix density of liver mitochondria exposed to a copper/GSH ratio of 5:10 was decreased and the organelles "swelled" as already described in the presence of 100 µM calcium (see 3.1.1). In summary, all applied measurements demonstrated the occurrence of pronounced reactive oxygen species only at the highest copper/GSH ratio of 5:10. This high ROS production was paralleled by a complete destruction of liver and brain mitochondria.

3.1.4 Mitochondrial thiols are primary targets of copper toxicity

As previously described [84], mitochondrial protein thiols are crucial targets of copper toxicity in liver mitochondria leading to their oxidation, crosslinking and finally, impairments of mitochondrial structure and function. Therefore, isolated rat liver and brain mitochondria were treated with increasing copper concentrations for 30 min and the amount of accessible free thiols was determined by DTNB (**Figure *14***A). Here, mitochondrial free thiols were dose-dependently depleted in liver and brain mitochondria. 200 µM copper in the presence of 1 mM glutathione (copper/GSH ratio of 2:10) caused a significant reduction of accessible free thiols in both mitochondrial populations. This reduction was even more prominent when rat liver and brain mitochondria were treated with 400 µM copper in the presence of 2 mM glutathione (copper/GSH ratio of 4:20). Additionally, free protein thiols of liver and brain mitochondria were labeled with BODIPY-FL (**Figure 14**C) to further validate the observed effect. Here, isolated liver and brain mitochondria showed a strongly decreased overall fluorescence intensity after treatment of the organelles with the highest copper/GSH ratio (5:10), whereas lower copper/GSH ratios resulted in a band-specific decrease in fluorescence. Glutathione treatment alone (copper/GSH ratio of 0:10) resulted in a higher fluorescence of specific bands, suggesting a reduction of protein thiols of certain proteins. In summary, mitochondrial protein thiols are prominent targets in organelles isolated from rat liver and brain. However, the question arises, why brain mitochondria are more susceptible to copper than liver mitochondria. Approximately 10 – 15 % of the intracellular glutathione is found within mitochondria [207], thereby representing the main defense mechanism against oxidative protein damage. Therefore, mitochondrial GSH levels were determined (**Figure 14**B).

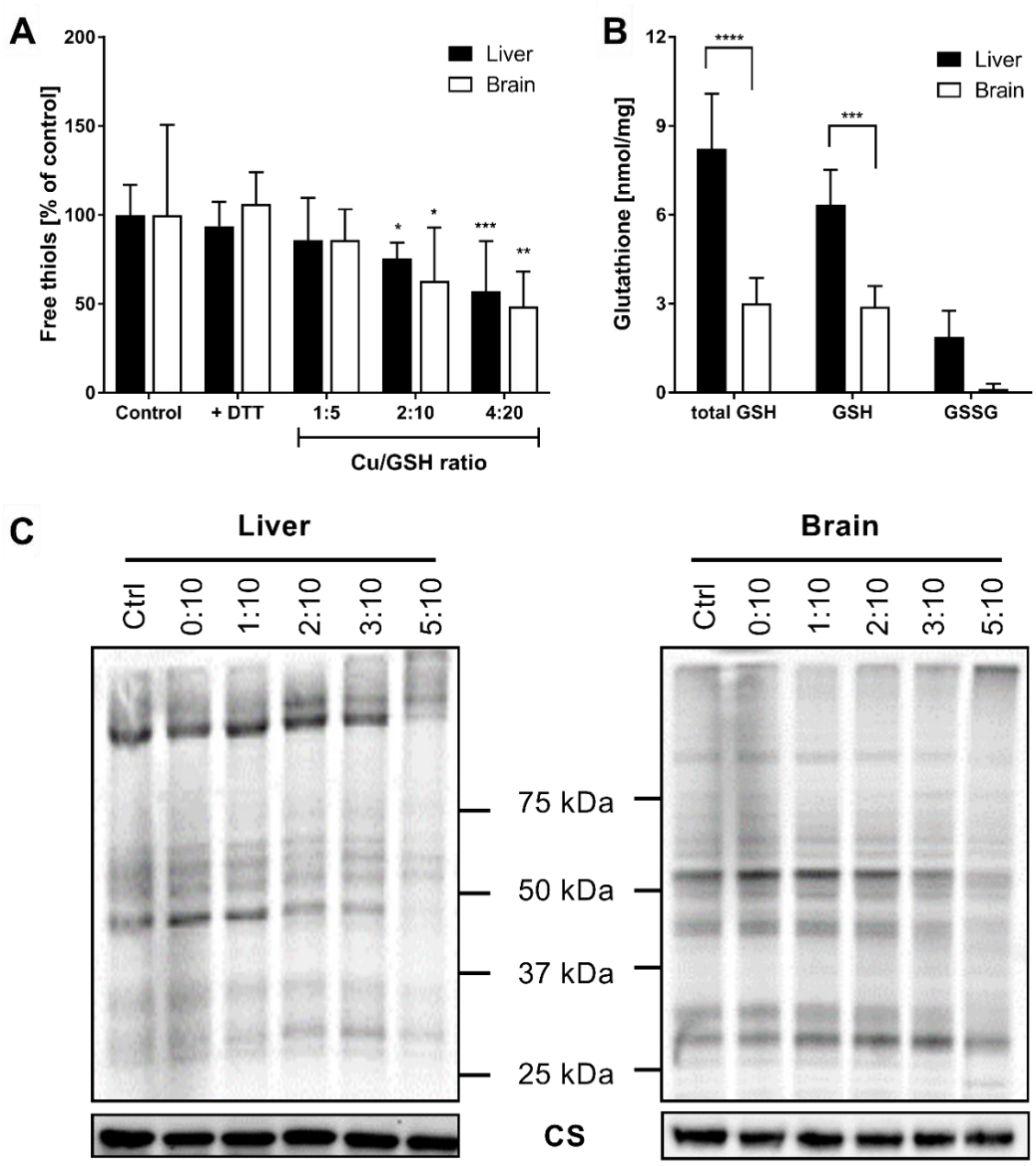

Figure 14. Free protein thiols are primary targets of copper toxicity in rat liver and brain mitochondria.

(A) Free thiols from liver and brain mitochondria are attacked by copper/GSH in a dose-dependent fashion as evidenced by DTNB (N = 5 - 6). (B) Rat brain mitochondria reveal a significantly lower total GSH content compared to rat liver mitochondria (N = 5, n = 10). (C) Fluorescent labeling of free protein thiols with BODIPY-FL reveals decreased fluorescence intensity of distinct bands with increasing copper/GSH ratios in both, liver and brain mitochondria. Citrate synthase (CS) served as loading control (N = 3). Taken from Borchard et al., 2018 [201] with permission.

Here, brain mitochondria revealed a significantly reduced level of total glutathione compared to liver mitochondria, and the amount of reduced GSH was significantly lower in brain compared to liver

mitochondria. However, the percentage of oxidized glutathione was higher in liver (21.95 ± 7.85 %) compared to brain (3.12 ± 3.94 %) mitochondria.

To determine the functional consequences of the direct attack of copper on mitochondrial proteins, the ATP production capacity of isolated rat liver and brain mitochondria in the presence of succinate and rotenone as substrates was investigated (**Figure 15**A). Here, liver mitochondria treated with a copper/GSH ratio of 1:10 revealed an ATP production capacity as high as untreated liver mitochondria. However, the presence of higher copper/GSH ratios resulted in significantly lower ATP production capacities. In contrast, the lowest copper/GSH ratio already significantly reduced the ATP production of isolated brain mitochondria compared to untreated organelles.

The here investigated brain mitochondria originated from total brain homogenates. Hence, they represent a heterogeneous population of organelles arising from different cell types including, *e.g.*, astrocytes and neurons. To gain further insight into cell type specific copper toxicity, the neuroblastoma cell line SH-SY5Y and the astrocytoma cell line U-87MG were used as surrogates for neurons and astroglial cells, respectively. Isolated mitochondria from both cell lines were subjected to the determination of their ATP production capacity in the presence of succinate and rotenone as substrates and a copper/GSH ratio of 1:10 at different concentrations (**Figure 15**B). Here, SH-SY5Y mitochondria revealed a dose-dependent decrease in ATP production capacity, that was significantly lowered at the highest copper concentration tested (100 µM copper / 1 mM glutathione). In contrast, the ATP production capacity of mitochondria isolated from U-87MG cells was unaffected by the applied copper challenges. To further investigate the differential response of organelles from SH-SY5Y and U-87MG cells to copper, isolated mitochondria from both cell types were treated with copper/GSH concentrations comparable to the assessment of ATP production capacity and mitochondrial free protein thiols were labeled with BODIPY-FL (**Figure 15**C). Here, SH-SY5Y mitochondria treated with copper/GSH revealed a dose-dependent overall decrease in BODIPY-FL fluorescence. However, only the highest copper concentration led to a decrease in fluorescence in copper-treated U-87MG mitochondria. Hence, SH-SY5Y mitochondria are remarkably more susceptible to copper toxicity regarding ATP production and protein thiol oxidation than U-87MG mitochondria.

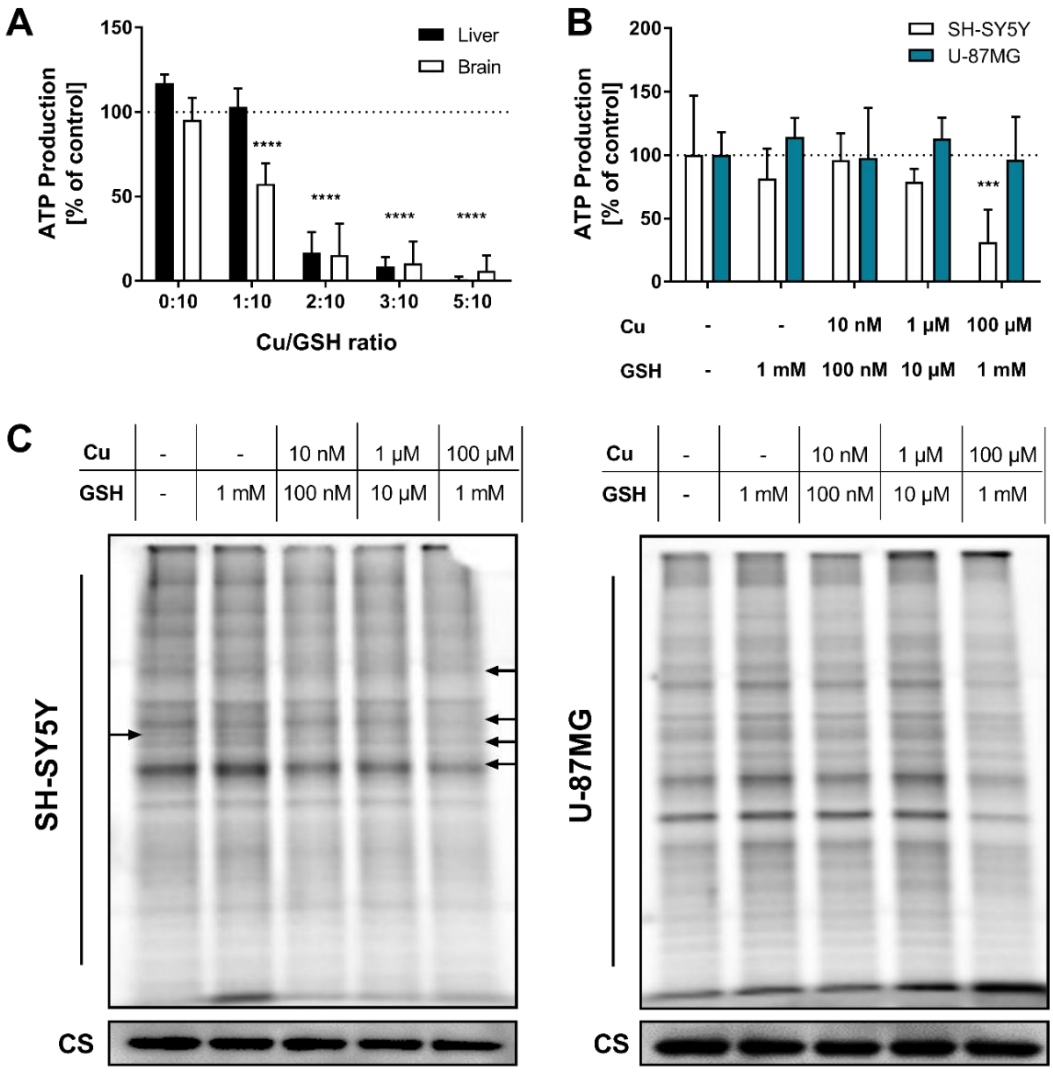

Figure 15. Copper exposure significantly lowers mitochondrial ATP production capacity.

(A) In rat liver mitochondria, ATP production capacity is unchanged at a copper/GSH ratio of 1:10, but significantly decreased at copper/GSH ratios ranging from 2:10 up to 5:10 compared to GSH alone. In comparison, brain mitochondria reveal a significantly decreased ATP production capacity even at the lowest copper/GSH ratio of 1:10 (N = 3, n = 6). (B) Treatment of isolated mitochondria from SH-SY5Y (neuroblastoma) cells with copper/GSH leads to a dose-dependent decrease in ATP production, whereas ATP production of U-87MG (glioblastoma) mitochondria is not affected by copper treatment (N = 3 - 4; n = 6 - 8). (C) Protein thiols of isolated mitochondria from SH-SY5Y and U-87MG cells were labeled with BODIPY-FL. SH-SY5Y mitochondria reveal a dose-dependent decrease of overall fluorescence, whereas U-87MG mitochondria show a loss of fluorescence signal only at the highest copper concentration. Citrate synthase (CS) served as loading control (N = 3). Taken from Borchard et al., 2018 [201] with permission.

3.1.5 Copper causes structural alterations of mitochondria in SH-SY5Y cells

Isolated mitochondria from SH-SY5Y cells were highly sensitive to copper compared to U-87MG cells. Therefore, the copper sensitivity of both cell lines was further analyzed in a cellular context. First, cellular

copper toxicity was assessed by incubation of SH-SY5Y and U-87MG cells with copper histidine for 24 h or 48 h, respectively (**Figure 16**). Here, no cell toxicity was observed up to 5 µmol CuHis/1x10^6 cells for both, SH-SY5Y and U-87MG cells after 24 h or 48 h of incubation. Additionally, 48 h incubation with a CuHis dose of 12.5 µmol CuHis/1x10^6 cells caused a significant reduction of cell viability in both cell lines. Furthermore, the highest tested dose of CuHis (25 µmol CuHis/1x10^6 cells) led to a pronounced cell death in SH-SY5Y and U-87MG cells. However, no difference between the two cell types was observable.

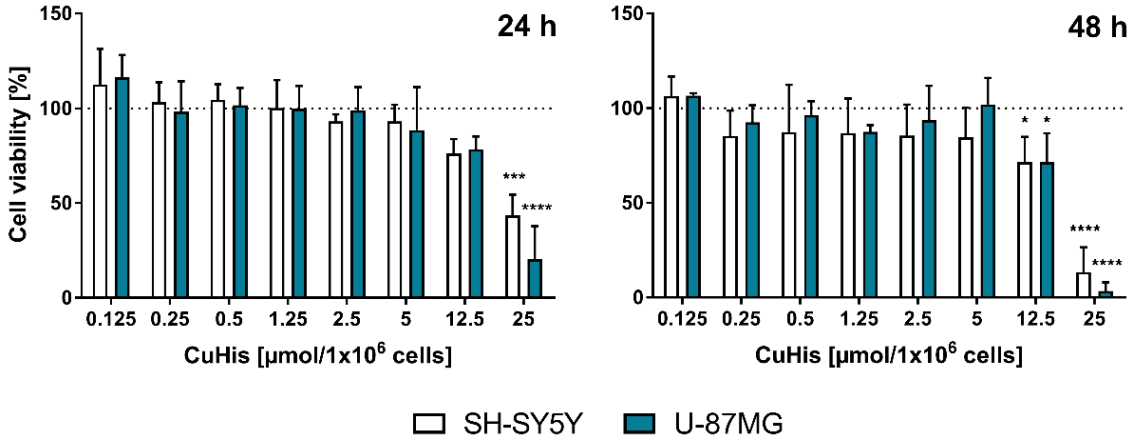

Figure 16. Copper toxicity does not differ in SH-SY5Y and U-87MG cells.

SH-SY5Y and U-87MG were exposed to increasing concentrations of copper histidine (CuHis) for 24 h (left panel) or 48 h (right panel) (N = 3, n = 9) and cell viability was assessed by the CellTiterGlo® assay. No significant differences are detectable in the sensitivity of SH-SY5Y compared to U-87MG cells to copper. Only the highest CuHis concentrations (12.5 µmol/1x10^6 cell and 25 µmol/1x10^6 cells) lead to a highly significant decrease in cell viability.

For subsequent analysis, both cell lines were treated either with 2.5 or 6.7 µmol CuHis/1x10^6 cells for 48 h and analyzed by electron microscopy for mitochondrial area, number and shape (**Figure 17**). Electron micrographs of SH-SY5Y and U-87MG cells already gave insights into mitochondrial structural changes in the presence of copper (**Figure 17**A). These effects were mainly present in SH-SY5Y cells and were mostly characterized by a loss of cristae structure and a disrupted outer mitochondrial membrane in a subset of mitochondria. Therefore, these mitochondrial structural alterations were further quantified by means of mitochondrial number, area and shape. Mitochondrial area and number were not influenced by copper exposure in both SH-SY5Y and U-87MG cells (**Figure 17**B). Additionally, mitochondria were categorized as “roundish” or “elliptical” for further characterization of their shape (**Figure 17**C and D). Again, no significant differences were detected in mitochondrial shape alterations due to copper challenges in either SH-SY5Y or U-87MG cells. To further analyze the impact of copper on mitochondria from both cell lines, four distinct categories of mitochondrial structure were defined

(**Figure 18**A). Stage I mitochondria are characterized by an intact inner and outer mitochondrial membrane and a distinct cristae structure, whereas stage II mitochondria display shortened cristae.

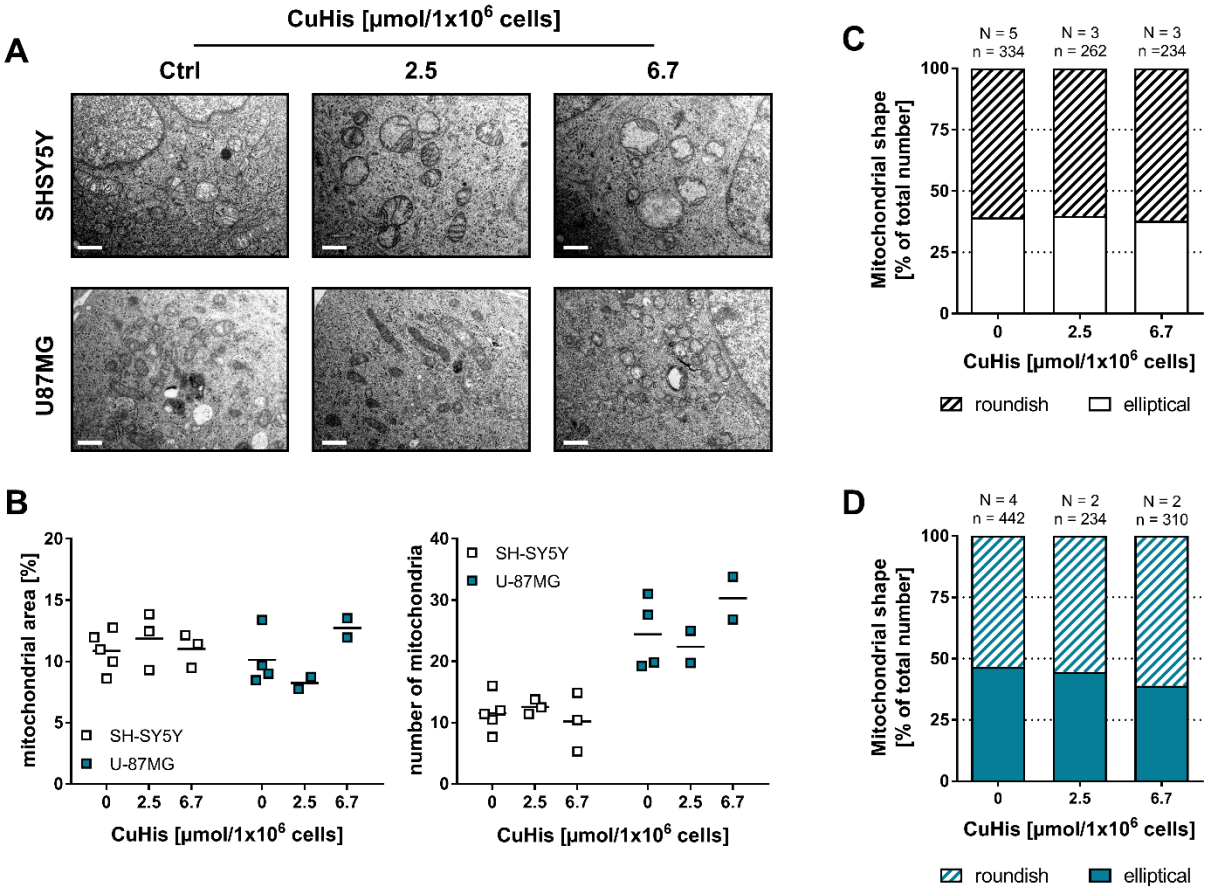

Figure 17. Mitochondrial area, number and shape are unaltered in copper-treated SH-SY5Y and U-87MG cells.

(A) Exemplary electron micrographs of SH-SY5Y and U-87MG cells cultured under control conditions or in presence of 2.5 or 6.7 µmol/1 x 10^6 cells for 48 h, respectively. Scale bars equal 1 µm. (B) Mitochondrial area (left panel) and number (right panel) per image are unchanged in both cell lines in the presence of copper compared to control conditions. Additionally, the mitochondrial shape is not affected by copper histidine (CuHis) in both cell lines, SH-SY5Y (C) and U-87MG (D). "N" represents the number of biological replicates. "n" represents the number of analyzed images. Adapted from Borchard et al., 2018 [201] with permission.

Stage III mitochondria have more dissipated cristae and membranous deposits. In contrast, stage IV mitochondria are characterized by a destroyed outer membrane and a complete loss of cristae structure. Quantification of mitochondrial subtypes in copper-treated SH-SY5Y and U-87MG compared to untreated cells is shown in **Figure 18**B, C and **Table 6**. Copper-histidine treatment of SH-SY5Y resulted in massively altered mitochondria as demonstrated by a dose-dependently decreased amount of stage I mitochondria. Contrary, the percentage of stage II mitochondria was unchanged at the lower CuHis dose

(2.5 µmol CuHis/1x10^6 cells), whereas the presence of 6.7 µmol CuHis/1x10^6 cells resulted in a significantly decreased amount of stage II mitochondria in SH-SY5Y cells compared to control conditions.

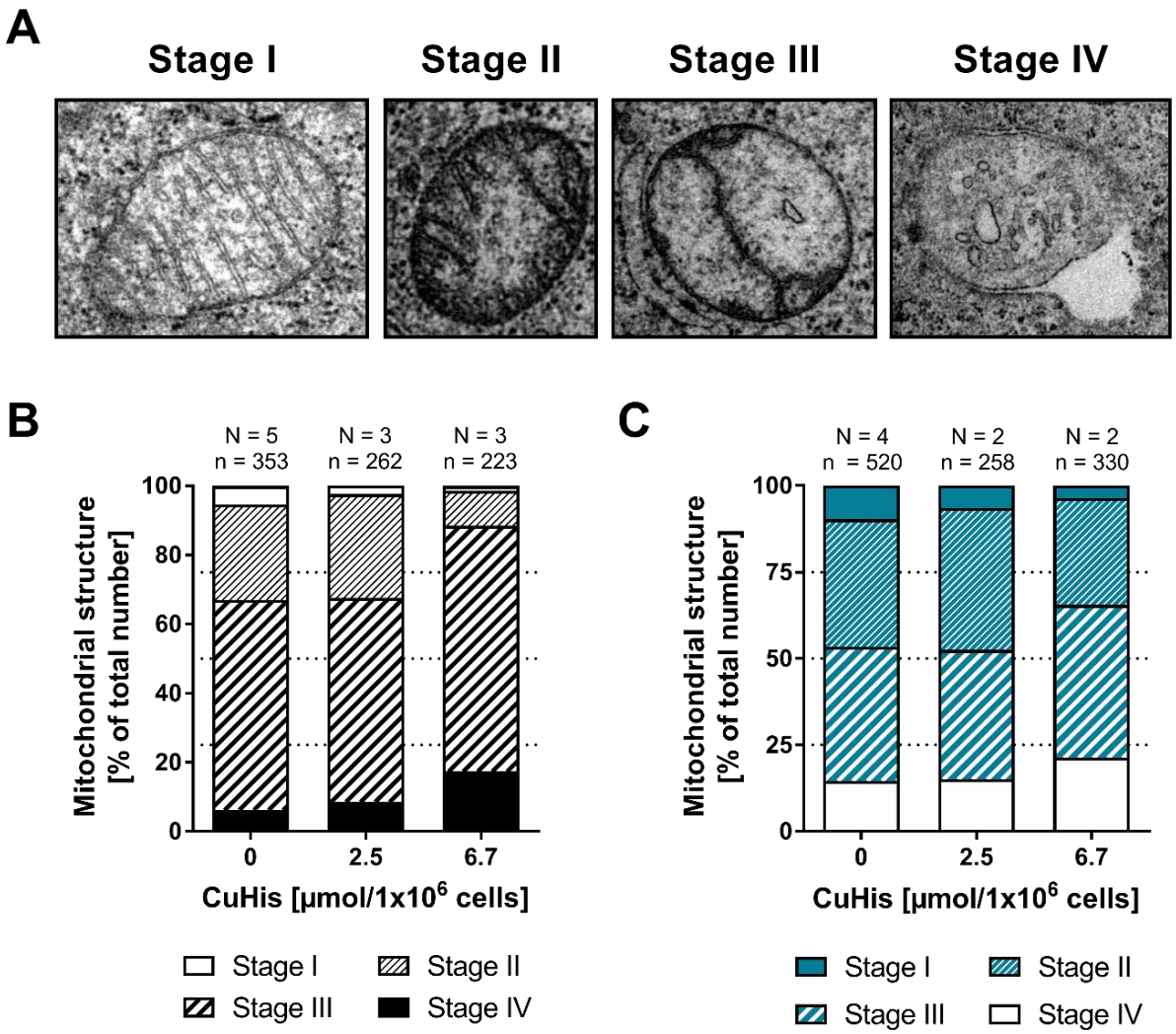

Figure 18. Mitochondria from SH-SY5Y cells are highly susceptible to copper.

(A) Mitochondria were divided into four stages defined by cristae structure, membrane integrity and matrix density. (B) SH-SY5Y cells display a dose-dependent increase in stage III and IV mitochondria when incubated for 48 h with CuHis. (C) In U-87MG cells, an increase of stage IV mitochondria is only present at the highest CuHis dose. "N" represents the number of biological replicates. "n" represents the number of analyzed images. Adapted from Borchard et al., 2018 [201] with permission.

Consequently, the proportion of stage III and stage IV mitochondria was significantly increased at the higher copper-histidine dose but was unchanged in the presence of 2.5 µmol CuHis/1x10^6 cells. In contrast to these findings in copper-treated SH-SY5Y cells, mitochondria in U-87MG cells appeared largely unaffected in the presence of 2.5 µmol CuHis/1x10^6 cells as no significant changes in the prevalence of stage I to IV mitochondria was detectable. The higher CuHis dose resulted in a non-significant decrease of stage I and II mitochondria. Accordingly, the proportion of stage III and IV

increased slightly. In summary, mitochondria of copper-treated SH-SY5Y displayed massive structural alterations. In contrast, mitochondria from U-87MG were not affected by the applied copper challenges.

Table 6. Changes in mitochondrial structure in the presence of CuHis [µmol/1 x 10^6 cells] (taken from Borchard et al., 2018 [201] with permission).

	SH-SY5Y			U-87MG		
	Ctrl	*2.5*	*6.7*	*Ctrl*	*2.5*	*6.7*
Stage I [%]	5.5 ± 2.0	2.5 ± 1.2	1.3 ± 0.9	9.7 ± 5.8	6.4 ± 4.3	3.7 ± 3.1
Stage II [%]	27.5 ± 6.4	29.9 ± 1.3	10.2 ± 4.5 ***	36.9 ± 9.6	41.1 ± 8.5	30.8 ± 16.2
Stage III [%]	60.8 ± 5.7	59.0 ± 3.3	71.7 ± 11.0 *	38.8 ± 15.2	37.4 ± 8.3	44.3 ± 12.1
Stage IV [%]	6.3 ± 4.3	8.6 ± 1.7	17.4 ± 6.4 *	14.7 ± 3.1	15.1 ± 4.5	21.3 ± 7.2

3.1.6 Differentiation status of U-87MG and SH-SY5Y has no impact on the mitochondrial response to copper

To determine the consequences of the copper-induced structural alterations, the mitochondrial membrane potential as well as the production of reactive oxygen species (ROS) served as markers for mitochondrial functionality (**Figure 19**). Here, SH-SY5Y cells displayed a significantly lower $DiOC_6$ staining being related to a lower mitochondrial membrane potential in the presence of CuHis compared to control conditions (**Figure 19**A). This effect was significant at the highest dose of copper-histidine. In contrast, $DiOC_6$ staining of U-87MG cells revealed no differences between CuHis-treated and untreated cells. Additionally, MitoSOX staining as a measure of mitochondrially produced ROS showed no significant differences in both untreated or treated U-87MG or SH-SY5Y cells, respectively (**Figure 19**B).

The relevance of these findings was further validated by differentiating SH-SY5Y and U87MG cells (**Figure 19**). SH-SY5Y and U-87MG cells are neuroblastoma and glioblastoma cells. Thus, they are surrogates for adult neurons and glia cells, however differ, *e.g.*, in their proliferation behavior, protein expression pattern and morphology from primary neurons and glia [164, 208]. Upon differentiation with retinoic acid, however, these cells resemble adult neurons and glial cells with respect to morphological features (*e.g.*, extended long, branched processes) and the upregulation of proteins characteristic for adult neurons (e.g., MAP2, GAP-43, NeuN) [165, 208] or astrocytes (e.g., GFAP, S100B) [164, 209], respectively.

In full agreement with the observations in undifferentiated cells, a dose-dependent decrease of the mitochondrial membrane potential upon copper challenge in differentiated SH-SY5Y cells was observed (**Figure 19**A). In contrast, a slight increase of the MMP was detected in differentiated U-87MG cells, indicative of mitochondrial hyperpolarization. Moreover, the level of mitochondria-originating ROS was unaltered in differentiated SH-SY5Y, and slightly increased in differentiated U-87MG cells upon copper challenge (**Figure 19**B). Thus, SH-SY5Y cells, whether differentiated or undifferentiated, are affected by increasing copper amounts at the mitochondrial level.

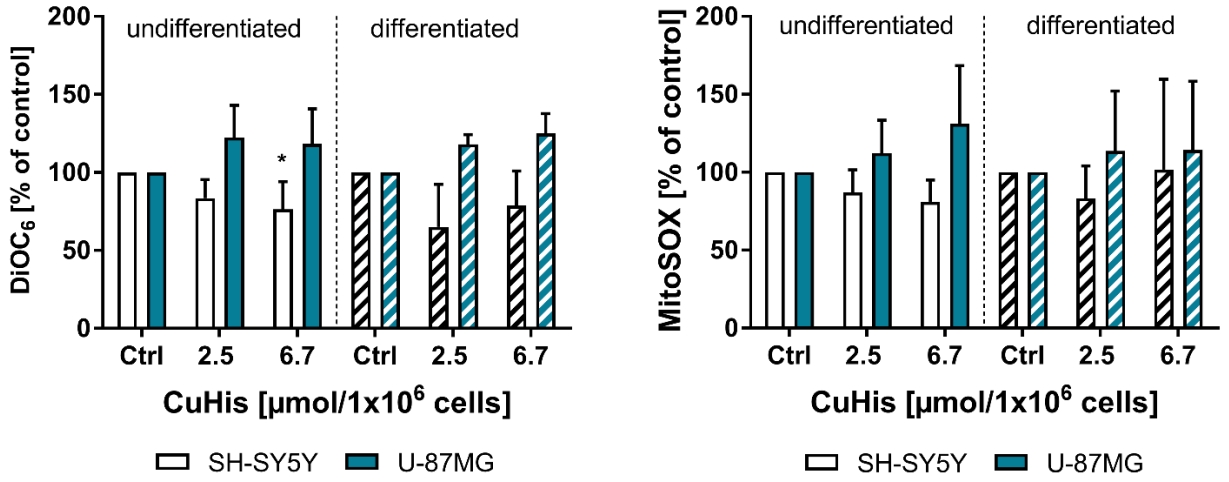

Figure 19. Undifferentiated and differentiated SH-SY5Y and U-87MG cells respond equally to copper challenges with respect to the mitochondrial membrane potential and ROS production.

(A) The mitochondrial membrane potential, assessed by DiOC6 staining, is reduced under copper treatment for 48 h in undifferentiated (N = 5, n = 15) as well as differentiated (N = 2, n = 6) SH-SY5Y cells. In contrast, undifferentiated (N = 5, n = 15) and differentiated (N = 2, n = 8) U-87MG cells displayed a slightly increased $DiOC_6$ signal, and possibly increased mitochondrial membrane potential. (B) Mitochondrial ROS production, assessed by MitoSOX staining, tends to be reduced in copper-treated, undifferentiated SH-SY5Y (N = 5, n = 15) cells and is unaltered in differentiated (N = 2, n = 6) SH-SY5Y cells. In contrast, U-87MG cells display a higher ROS production in the presence of copper independent of their differentiation status (undifferentiated: N = 5, n = 15; differentiated: N = 2, n = 8). Taken from Borchard et al., 2018 [201] with permission.

3.1.7 SH-SY5Y cells are highly susceptible to copper due to limited defense mechanisms

The higher copper susceptibility of SH-SY5Y mitochondria compared to U-87MG could be the result of two, not mutually exclusive, mechanisms. On the one hand, an increased copper uptake into SH-SY5Y cells may lead to an increased copper burden and thereby, dramatic structural and functional alterations of SH-SY5Y mitochondria. On the other hand, limited antioxidative defense mechanisms against copper-induced protein thiol oxidation, *e.g.*, glutathione or copper-binding metallothioneins, may lead to more severe impairments of mitochondrial functionality compared to U-87MG cells. Therefore, cellular

glutathione and metallothionein levels as well as the cellular copper content of both cell lines were investigated (**Figure 20**). Here, cellular total GSH levels of untreated SH-SY5Y were significantly lower compared to untreated U-87MG cells. Furthermore, metallothionein 1 and 2 (MT 1/2) levels were determined as these metallothionein isoforms are mainly responsible for the binding of metals, especially copper, for detoxification [210]. In SH-SY5Y, MT 1/2 were absent, even after a copper challenge of 48 h. In contrast, metallothionein 1 and 2 were abundantly present in U-87MG cells.

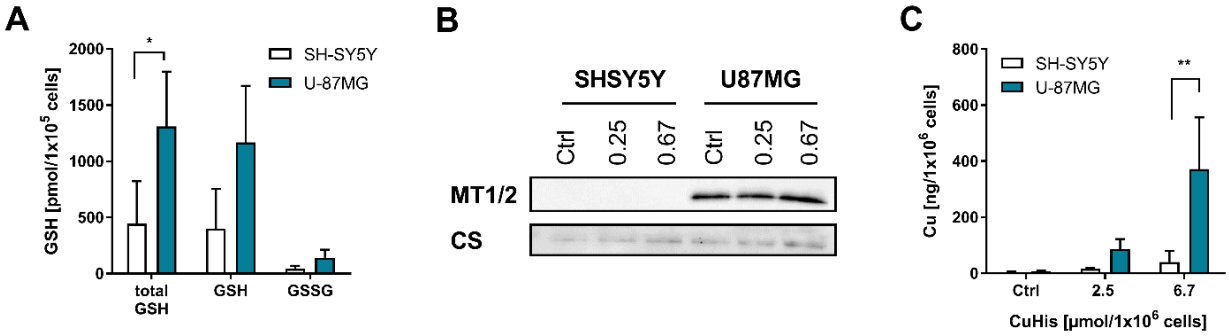

Figure 20. The high susceptibility of SH-SY5Y mitochondrial to copper is attributable to limited anti-oxidative defense mechanisms.

(A) The total GSH content of untreated SH-SY5Y cells is significantly lower compared to U-87MG cells (N = 3, n = 3). (B) Immunoblotting of metallothionein 1/2 (MT 1/2) shows absence of the copper-binding protein in SH-SY5Y cells. In contrast, MT1/2 is present in U-87MG cells. Citrate synthase served as loading control. For both cell lines, 1 x 10^5 cells per lane were applied to an SDS-PAGE (N = 3). (C) U-87MG cells accumulate significantly more copper in 48 h compared to SH-SY5Y cells (N = 3, n = 3). Adapted from Borchard et al., 2018 [201] with permission.

Additionally, the cellular copper content of SH-SY5Y and U-87MG after 48 h in the presence of 2.5 or 6.7 µmol CuHis/1x10^6 cells was measured. Here, SH-SY5Y cells accumulated significantly less copper compared to U-87MG cells at the highest applied copper dose. Thus, although U-87MG cells accumulate significantly more copper, these cells are relatively protected due to high MT1/2 and GSH levels. In contrast, SH-SY5Y cells lack such antioxidative protection plausibly explaining their high vulnerability to copper.

3.2 The high-affinity chelator WTX101 prevents copper-induced cell toxicity

3.2.1 Copper chelators increase serum copper levels

Current treatments in Wilson disease (WD) are mainly based on two concepts: a reduced intestinal copper uptake by zinc and/or the application of copper chelators like D-penicillamine (DPA) to reduce the hepatic copper burden. However, DPA was found to be a low affinity copper chelator [211, 212],

that is suitable for most patients suffering from hepatic WD but leads to massive side effects in WD patients suffering from neurological symptoms. This worsening of neurological symptoms is most probably due to the mobilization of copper from the liver and transport via the blood to peripheral organs, especially the brain, followed by the excretion of excess copper via the urine. In contrast to these current therapy options, the high affinity chelator bis-choline tetrathiomolybdate (WTX101) shows no neurological worsening in a phase 2 clinical trial [146].

The distribution of copper in untreated *Atp7b*$^{+/-}$ and *Atp7b*$^{-/-}$ rats in comparison to *Atp7b*$^{-/-}$ rats treated with WTX101 or DPA was investigated. Here, untreated *Atp7b*$^{-/-}$ animals revealed a significantly lower serum copper level than untreated *Atp7b*$^{+/-}$ control animals (**Figure 21**A). This can be mainly attributed to the lack of copper incorporation into ceruloplasmin in rats lacking functional ATP7B [213].

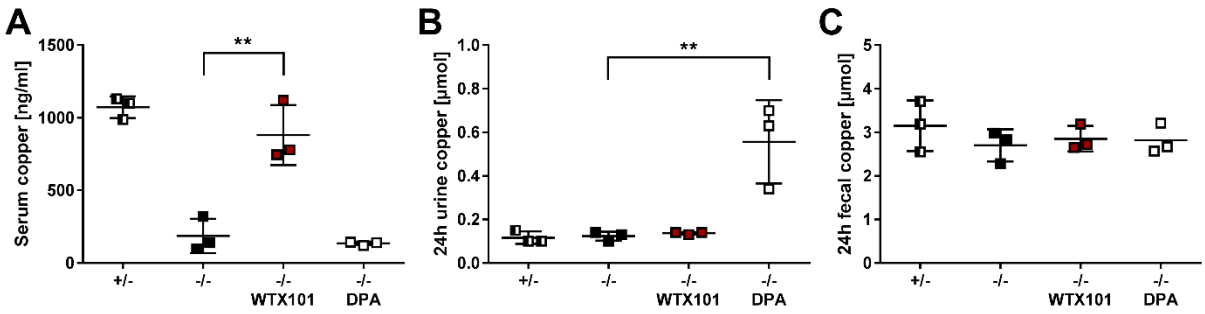

Figure 21. WTX101 and DPA cause differential distribution of copper in *Atp7b*$^{-/-}$ rats.

(A) Treatment of *Atp7b*$^{-/-}$ rats with WTX101 for four consecutive days results in increased serum copper levels, whereas serum copper levels were unchanged after treatment with DPA (N = 3). (B) Treatment of *Atp7b*$^{-/-}$ animals with DPA leads to a significant increase in urinary copper excretion (N = 3). (C) Fecal copper excretion is unchanged in WTX101- and DPA-treated *Atp7b*$^{-/-}$ rats compared to untreated animals (N = 3).

After treatment with WTX101, serum copper levels were significantly increased compared to untreated WD rats. In contrast, treatment with DPA revealed a low serum copper level, highly comparable to the untreated *Atp7b*$^{-/-}$ rats. To further elucidate the distribution of copper under the different treatments, the excretion of copper via urine (**Figure 21**B) and feces (**Figure 21**C) was investigated in these animals. Here, untreated *Atp7b*$^{+/-}$ and *Atp7b*$^{-/-}$ rats exhibited comparable levels of copper in urine and feces collected over 24 h. After treatment of WD rats with WTX101, excretion of copper in urine and feces was unchanged compared to untreated WD rats (**Figure 21**A). In contrast, DPA treatment led to significantly increased copper excretion via the urine whereas no increased copper level was detectable neither in blood nor feces. Thus, WTX101 and DPA increase the serum copper level and thereby may potentially cause neurological worsening due to the subsequent uptake of such mobilized copper into the brain.

3.2.2 WTX101 forms a stable complex with albumin and copper

To further investigate the different distribution of serum copper after chelator treatment of *Atp7b*$^{-/-}$ rats, the complexes formed by copper and the chelators DPA and WTX101 in the presence of bovine serum albumin were investigated by size-exclusion chromatography (**Figure 22**), as albumin is known to bind copper in the serum with high affinity [214].

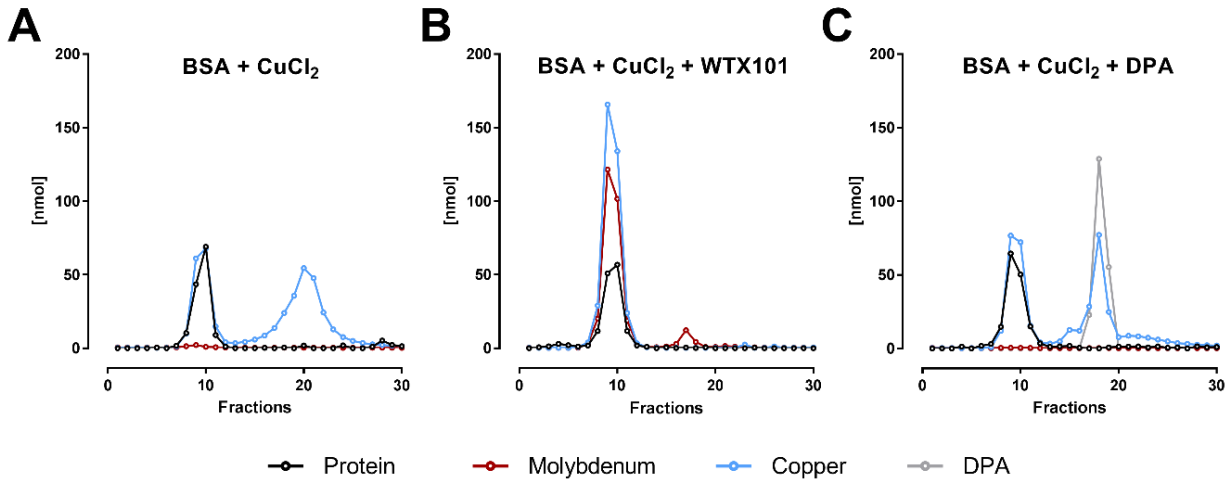

Figure 22. WTX101 associates with BSA and copper.

Size-exclusion chromatography of 250 µM BSA and 750 µM of copper shows the formation of a BSA-copper complex as well as a second copper peak representing unbound copper. In the presence of WTX101, BSA, molybdenum and copper are present in one peak, thereby suggesting the formation of a BSA-copper-WTX101 complex. In the presence of DPA, the distribution of copper is unchanged (N = 2).

Albumin, as the most abundant serum protein (35 – 50 g/l; 500 – 750 µM), is per se able to bind up to five copper ions at pH 7.4 [215]. The first copper ion is bound to the N-terminus with very high affinity ($K_d = 6.7 \times 10^{-17}$ M [214]), the second one is bound to a multi-metal binding site (MBS) with medium affinity ($K_d = 1.91 \times 10^{-7}$ M [215]) and the other three copper ions are bound to currently uncharacterized low affinity binding sites ($K_d = 6.25 \times 10^{-6}$ M [215]). Hence, the binding of 750 µM copper to 250 µM bovine serum albumin (BSA) was analyzed by size-exclusion chromatography. Here, one proportion of copper was found to be associated with albumin (**Figure 22**), whereas the other was present as unbound metal. In the presence of 750 µM WTX101, copper and the main proportion of the chelator, as represented by measuring molybdenum content of the fractions, eluted together with BSA (fractions 8-11). However, a small proportion of WTX101 eluted later representing unbound WTX101 (fractions 15-18). In the presence of DPA, the fraction of copper bound to albumin was unchanged. However, the fractions 17 to 19 represented copper bound to DPA, but no mobilization of copper from BSA was observed.

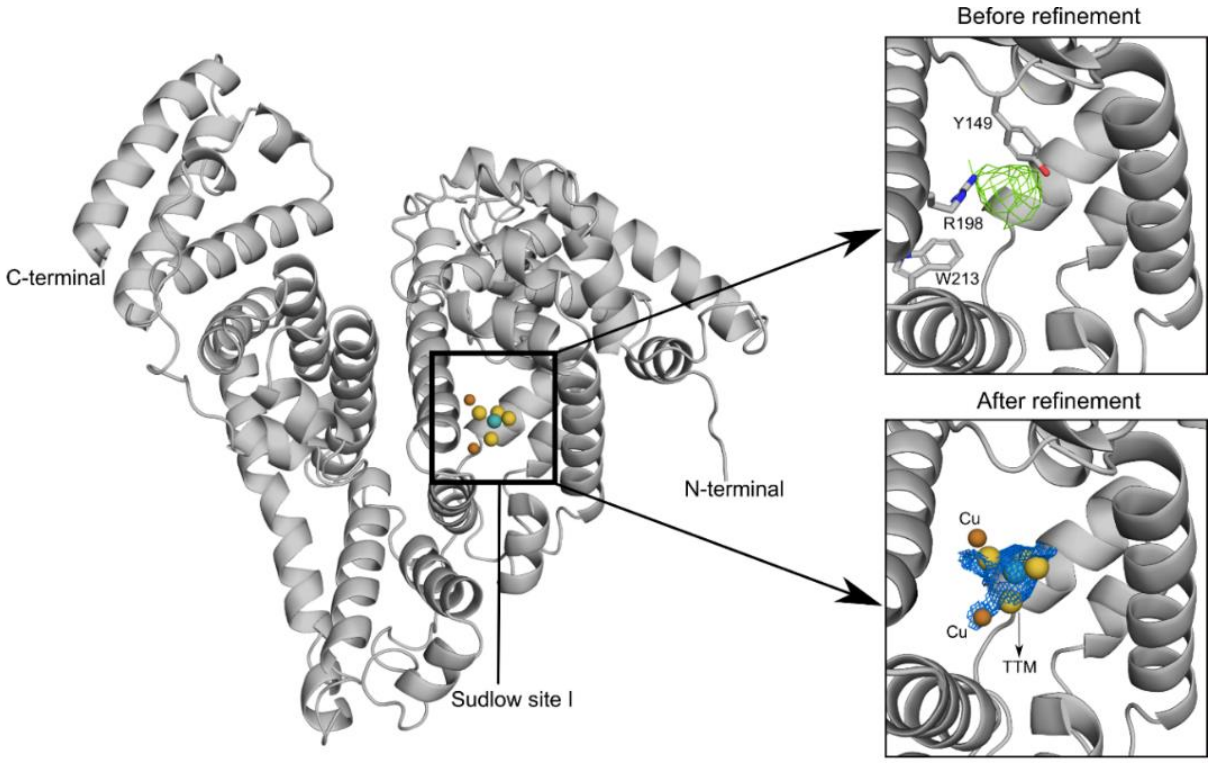

Figure 23. X-ray crystallographic analysis of the tripartite complex consisting of albumin, WTX101 and copper.

Analysis of the contents of the Sudlow site I (SsI) in the structure of BSA. The left panel presents overall structure of BSA with indicated Sudlow site I. The upper right panel presents a close-up of SsI with calculated difference map ($F_{obs} – F_{calc}$, colored green) before refinement. The difference map indicates the presence of additional molecules in this region. The lower right panel presents the same site of SsI after refinement. WTX101 and copper atoms are covered by calculated $2F_{obs}$ - F_{calc} map (colored blue) indicating presence of these molecules inside SsI.

To further characterize the tripartite complex formed by WTX101 and copper in the presence of albumin, X-ray crystallography was performed (**Figure 23**). Despite low resolution, X-ray crystallography of the *in vitro* generated complex revealed copper and WTX101 in the Sudlow Site 1 of BSA and the presence of two copper ions and one WTX101 molecule per albumin. Additionally, electron paramagnetic resonance (EPR) studies were performed to assess the oxidation status of the two copper ions in the tripartite complex (**Figure 24**). A complex consisting of BSA and copper revealed the typical Cu(II) signal. In the presence of WTX101, the signal intensity of the EPR-active cupric copper diminished by around 50 %, suggesting the reduction of one copper ion to Cu(I) and the second copper ion being still in the cupric form (Cu^{2+}). In the presence of the strong reduction agent sodium dithionite, the Cu(II) signal was completely depleted for both complexes, BSA and copper as well as in the presence of WTX101, due to the complete reduction of Cu(II) to EPR-silent Cu(I). Additionally, WTX101 and albumin alone did not show any EPR signal. In conclusion, EPR measurements revealed the reduction of one copper ion to cuprous copper, whereas the second metal ion is still bound as cupric copper.

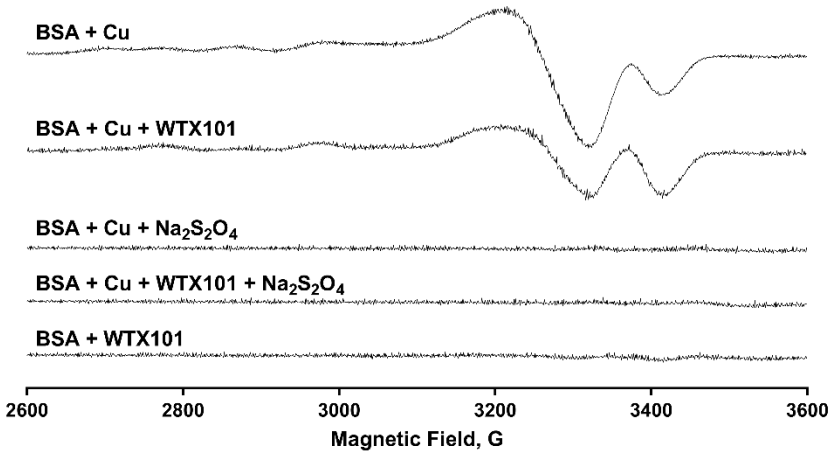

Figure 24. Electron paramagnetic resonance spectra of albumin-copper complexes in the absence or presence of WTX101. Electron paramagnetic resonance measurements reveal partial reduction of copper in the tripartite complex consisting of albumin, copper and WTX101. However, complete reduction of copper is only achieved by excess sodium dithionite ($Na_2S_2O_4$).

3.2.3 Copper-induced cell toxicity can be prevented by WTX101

To determine the pathophysiological consequences of the differential copper binding of the chelators WTX101 and DPA, four different cell lines namely HepG2 (human hepatocellular carcinoma) as model for the liver as well as EA.hy926 (human endothelium), U-87MG (human astrocytoma) and SH-SY5Y (human neuroblastoma) modelling the brain were investigated regarding cellular copper toxicity. The stated cell lines were treated with different ratios of BSA to copper to mimic an increasing amount of "loosely bound" or "free" copper in the blood. Here, a 1:1 ratio of BSA (250 µM) and copper (250 µM) results in a tight binding of copper mainly to the N-terminal binding site of albumin, thereby being unavailable for copper uptake via the copper transporter 1 (CTR1) and exhibiting no cell toxicity. Equally, a BSA to copper ratio of 1:2 (250 µM/500 µM) leads to a binding of the metal to the high-affinity N-terminal binding site as well as to the MBS with medium affinity resulting in the absence of cell toxic "loosely bound" copper. However, increasing BSA to copper ratios (from 1:3 to 1:10, 250 µM/750 µM to 250 µM/2.5 mM) result in increasing concentrations of cell toxic, free copper ions.

As shown in **Figure 25**, no signs of cellular toxicity were observed at ratios of BSA to copper of 1:1 and 1:2 after 24 h in all investigated cell lines measured by CellTiterGlo® assay and confirmed by Neutral red assay (**Figure S1**). However, all cell lines displayed a dose-dependent cell toxicity with increasing concentrations of "loosely bound" copper (ratios from 1:3 to 1:10). Here, HepG2 and EA.hy926 cells appeared to be most sensitive to copper-induced cell death compared to U-87MG and SH-SY5Y cells. In the presence of 750 µM WTX101, HepG2 and EA.hy926 cells presented with a significantly increased cell viability compared to the respective BSA to copper ratio (1:3 and 1:4). In contrast, the presence of

750 µM DPA was only beneficial in the presence of an albumin to copper ratio of 1:4 for HepG2 cells, but not beneficial at all for EA.hy926 cells.

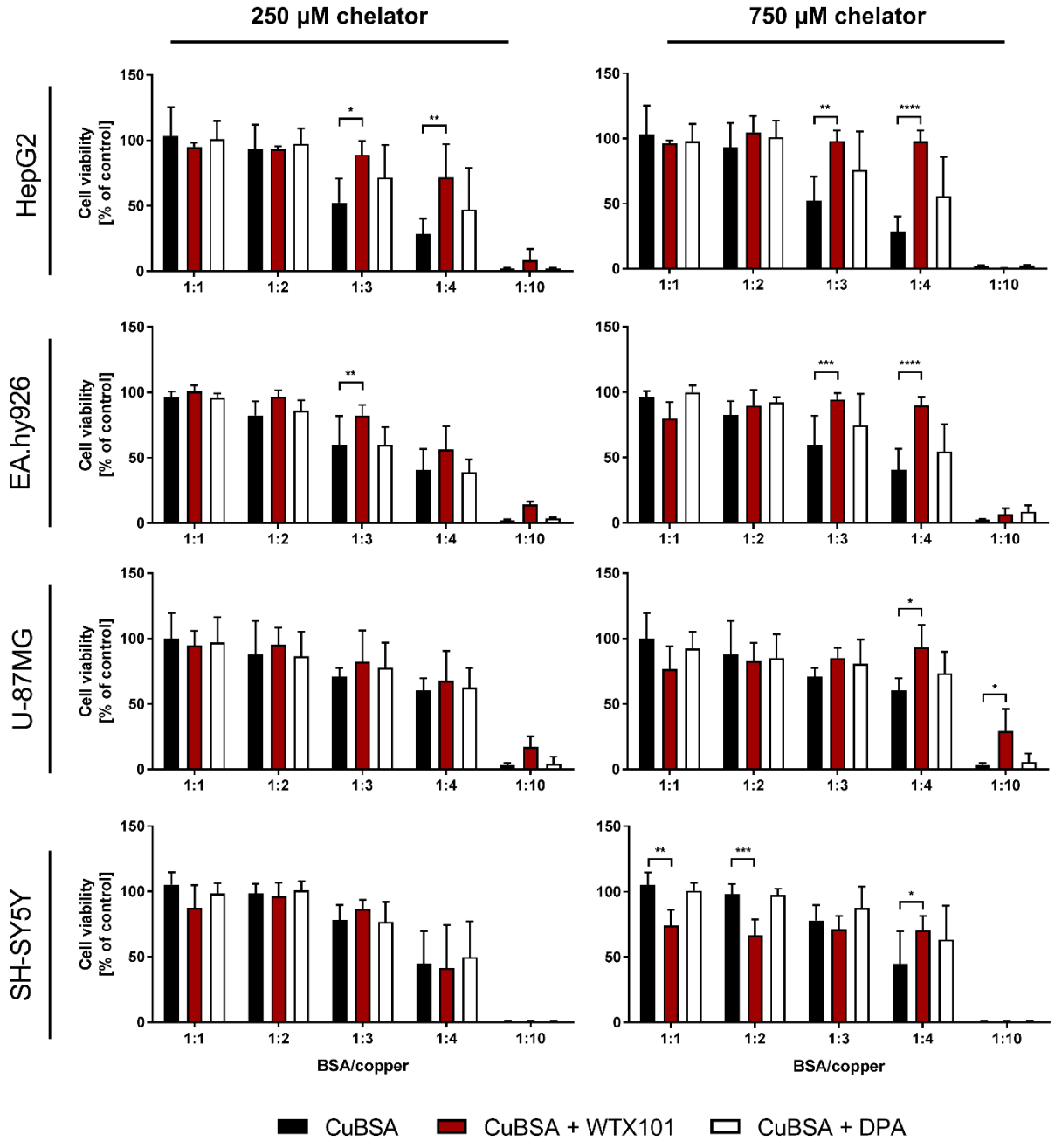

Figure 25. WTX101 protects EA.hy926 and U-87MG cells from copper toxicity (CellTiterGlo® assay).

All investigated cell lines show a dose-dependent decrease in cell viability under 24 h treatment with 250 µM BSA and increasing amounts of copper ranging from 250 to 2500 µM. In the presence of 750 µM DPA, this cytotoxic effect is not significantly diminished compared to BSA and copper alone. In contrast, the presence of 750 µM WTX101 protects mainly HepG2, EA.hy926 and U-87MG cells from cell death (N = 3 – 5, n = 6 - 10).

The toxic effect of increasing BSA/copper ratios was less pronounced in U-87MG astrocytoma cells compared to HepG2 and EA.hy926 cells. Nevertheless, the presence of 750 µM WTX101 significantly increased the cell viability in the presence of 250 µM BSA and 750 µM copper (ratio of 1:3), whereas a low dose of the chelator was not able to increase the cell viability significantly. In contrast, the presence of DPA did not influence the cell viability at any given albumin to copper ratio.

Considering the neuroblastoma cell line SH-SY5Y, a definite reduction in cell viability in the presence of albumin and copper was only detectable at a ratio of 1:4 and 1:10. In the presence of WTX101 at low BSA to copper ratios (1:1 and 1:2), cell viability of SH-SY5Y cells was significantly decreased. Most probably, the observed cell toxicity is caused by free WTX101 as detected by the above-mentioned size-exclusion chromatography (**Figure 22**). Upon excess of this chelator, a reduced cell viability per se can be observed (**Figure S2**) by de-coppering of vital enzymes that depend on adequate copper supply, here demonstrated by the activity of complex IV of the mitochondrial respiratory chain (**Figure S3**). Here, SH-SY5Y cells seem to be highly sensitive to changes in the cellular copper level as the effect of excess WTX101 is not detectable for HepG2, EA.hy926 and U-87MG cells. However, with increasing levels of unbound copper, the cell toxic effect of the metal predominates the chelator-dependent toxicity. At a BSA to copper ratio of 1:4, a highly significant reduction of cell viability ($p < 0.0001$) in the absence of chelators was observed for both cell lines. In the presence of 750 µM WTX101, the cell viability was significantly increased, but this effect was absent in the presence of 750 µM DPA. Thus, WTX101 can avoid copper-induced cell death in the investigated cell lines, whereas DPA cannot.

3.2.4 WTX101 reduces cellular copper content in EA.hy926 and U-87MG cells

The ability of the chelator WTX101 to rescue copper-induced cell toxicity in the investigated cell lines may be attributed to two possible, not mutually exclusive, mechanisms. First, complexation of copper by WTX101 could lead to a lower accessibility of the metal by CTR1. Thereby, the copper uptake is reduced resulting in reduced cell toxicity. Second, assuming an unchanged copper uptake, the high affinity of this copper chelator could lead to the formation of an inert complex that prevents the interaction of the metal with cellular targets, *e.g.*, mitochondrial protein thiols [84, 201].

Therefore, cellular copper levels in HepG2, EA.hy926, U-87MG and SH-SY5Y cells treated with an albumin to copper ratio of 1:3 in the absence or presence of 750 µM WTX101 or DPA were analyzed (**Figure 26**). Copper levels of all cell lines cultured for 24 h in normal DMEM (2 % FCS) served as controls.

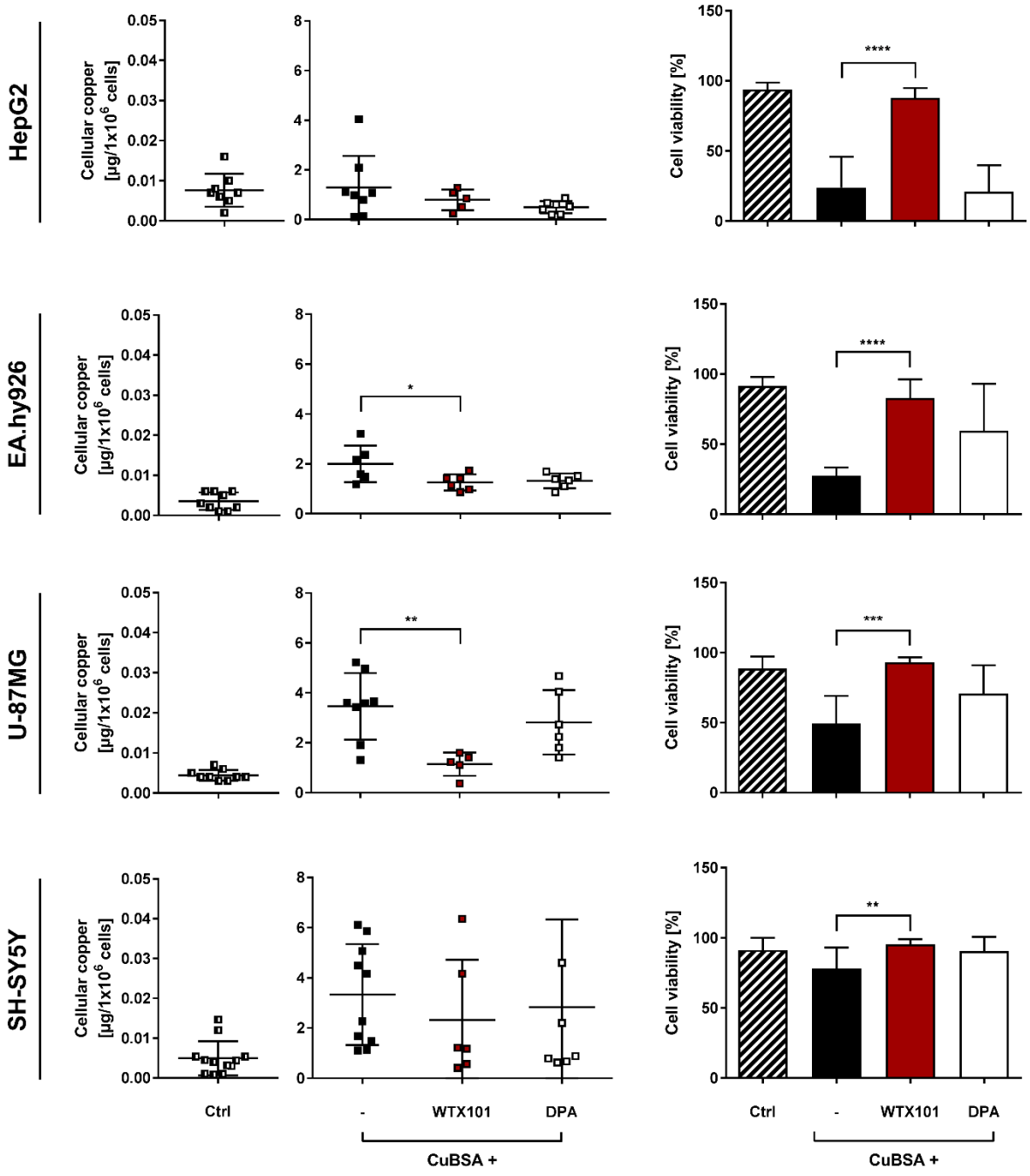

Figure 26. WTX101 leads to a decreased copper content in EA.hy926 and U-87MG cells.

Left panel: Under normal culture conditions, the copper levels of HepG2, EA.hy926, U-87MG and SH-SY5Y cells are low. The incubation of these cells with 250 µM BSA and 750 µM copper chloride leads to a massive accumulation of the metal in all investigated cell lines. In the presence of WTX101, U-87MG and EA.hy926 cells accumulate (significantly) less copper compared to albumin and copper alone. However, this effect is not present for HepG2 and SH-SY5Y cells. In contrast, the presence of DPA does not change the amount of copper in all cell lines. Right panel: The cell viability of HepG2, EA.hy926, U-87MG and SH-SY5Y significantly decreases in the presence of 250 µM BSA and 750 µM copper. 750 µM WTX101, but not DPA, protects all cell lines from copper-related cell toxicity (N = 3 - 13).

Here, all cell lines displayed a very comparable level of copper ranging from 3.5 to 8 ng copper per one million cells and strongly accumulated copper in the presence of BSA and copper alone (220 - 780 times more compared to basal levels). HepG2 and SH-SY5Y cells displayed unchanged copper levels independent of the absence or presence of chelators. However, cell viability determination by Trypan blue exclusion test revealed again a strong rescue effect of WTX101 in HepG2 cells in the presence of 250 µM BSA and 750 µM copper, whereas WTX101 and DPA were able to increase cell viability in SH-SY5Y cells. Concerning EA.hy926 and U-87MG cells, a tendency towards a lower cellular copper content in the presence of WTX101 compared to treatment with CuBSA only was observed. This effect was not present when DPA was used as a chelator. This decrease in cellular copper content correlated with the cell viability measured from the same cell sample. Control cells treated with medium only showed high cellular viability in both, EA.hy926 and U-87MG cells. In the presence of BSA and copper, the cellular copper of U-87MG and EA.hy926 cells increased profoundly leading to a strong decrease in cellular viability. In the presence of WTX101, the lower copper level in both cell lines was accompanied by a cell viability comparable to the untreated control. However, the presence of DPA was not changing the cellular copper content nor the viability of U-87MG and EA.hy926 cells

3.2.5 WTX101 prevents copper-induced mitochondrial damage

Early mitochondrial dysfunction plays a central role in Wilson disease patients as well as WD animal models and cell culture systems (for review see [87]) especially in terms of the liver pathology of the disease. In contrast, only a few publications hypothesize the involvement of mitochondria in the neurological presentation of WD. Here, brain mitochondria were found to be highly susceptible to copper overload regarding structural and functional alterations [112, 201]. Additionally, Stuerenburg [110] described an increased ratio of albumin in the cerebrospinal fluid to albumin in serum, a marker for disturbances of blood-brain barrier (BBB) function. Consequently, the following mitochondria-related experiments were performed in the endothelial cell line EA.hy926 and the astrocytoma cell line U-87MG, as endothelial cells and astrocytes are the major BBB components. Besides basic cellular parameters like cell viability, cellular protein content, cell size and cellular copper content (**Figure 27**), mitochondrial structure and respiration in intact EA.hy926 and U-87MG cells were analyzed (**Figure 28**). EA.hy926 and U-87MG cells were incubated for 24 h with an albumin to copper ratio of 1:3 (250 µM to 750 µM) in the absence or presence of 750 µM of the respective chelator. Here, the treatment conditions were modified to investigate mitochondrial dysfunction in the absence of cellular toxicity.

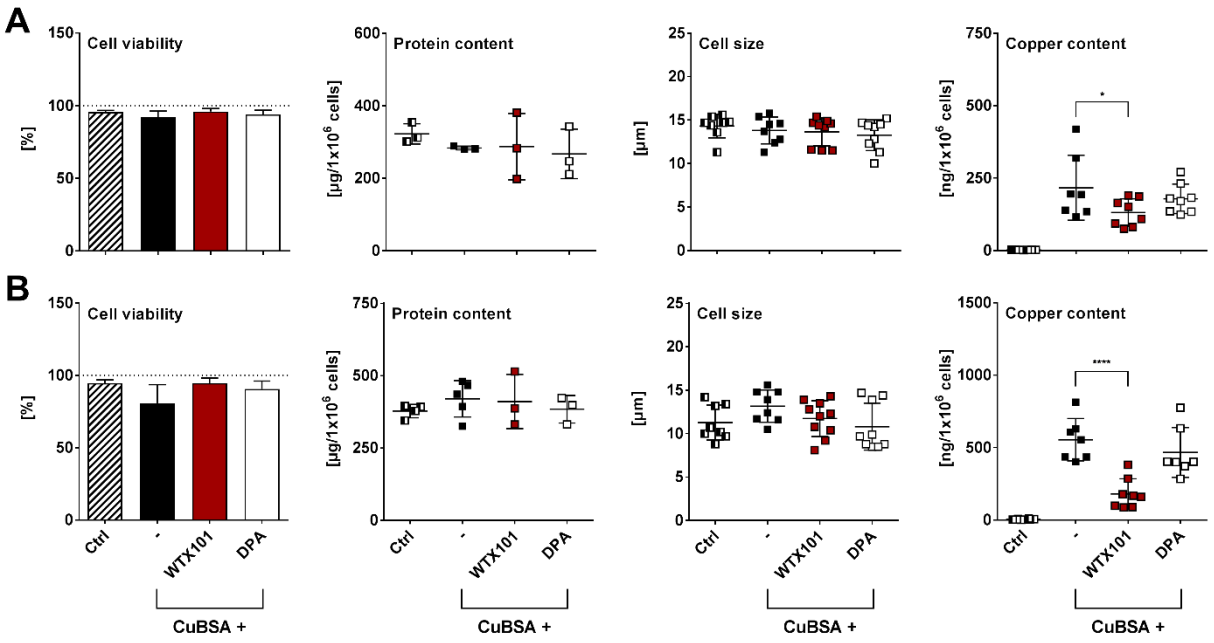

Figure 27. Cellular parameters of EA.hy926 and U-87MG cells subjected to high-resolution respirometry measurements.
Cell viability (N = 7 - 10), cellular protein content (N = 3 - 5) and cell size (N = 7 - 10) of EA.hy926 (A) and U-87MG (B) cells are comparable between untreated and CuBSA-treated cells in the absence or presence of WTX101 or DPA. In contrast, cellular copper content is significantly lower in CuBSA-treated EA.hy926 and U-87MG cells in the presence of WTX101 compared to cells treated with copper and BSA alone (N = 6 - 9).

The evaluation of basic cellular parameters revealed a comparable cell viability for all tested conditions in both, U-87MG and EA.hy926 cells (**Figure 27**). Additionally, cellular protein content and cell size were unaltered, when EA.hy926 or U-87MG cells were treated with CuBSA in the absence or presence of the the chelators WTX101 or DPA, compared to control conditions. However, cellular copper content was significantly increased in CuBSA-treated EA.hy926 ($p < 0.001$) and U-87MG ($p < 0.001$) cells in relation to untreated controls. Furthermore, the presence of WTX101 resulted in a significantly reduced cellular copper level compared to CuBSA treatment alone in both cell lines. On the contrary, EA.hy926 and U-87MG cells treated with CuBSA in the presence of DPA showed an unaltered cellular copper content compared to cells treated with CuBSA alone.

Subsequently, intact untreated and treated EA.hy926 and U-87MG were subjected to mitochondrial analysis by electron microscopy (**Figure 28**A) and high-resolution respirometry (**Figure 28**B - E) to determine potential detrimental effects of the high copper load on mitochondrial functionality in these cell lines. Electron micrographs of EA.hy926 cells treated with albumin and copper showed a loss of cristae structure and the presence of membranous inclusions compared to control cells (**Figure 28**A, upper panel).

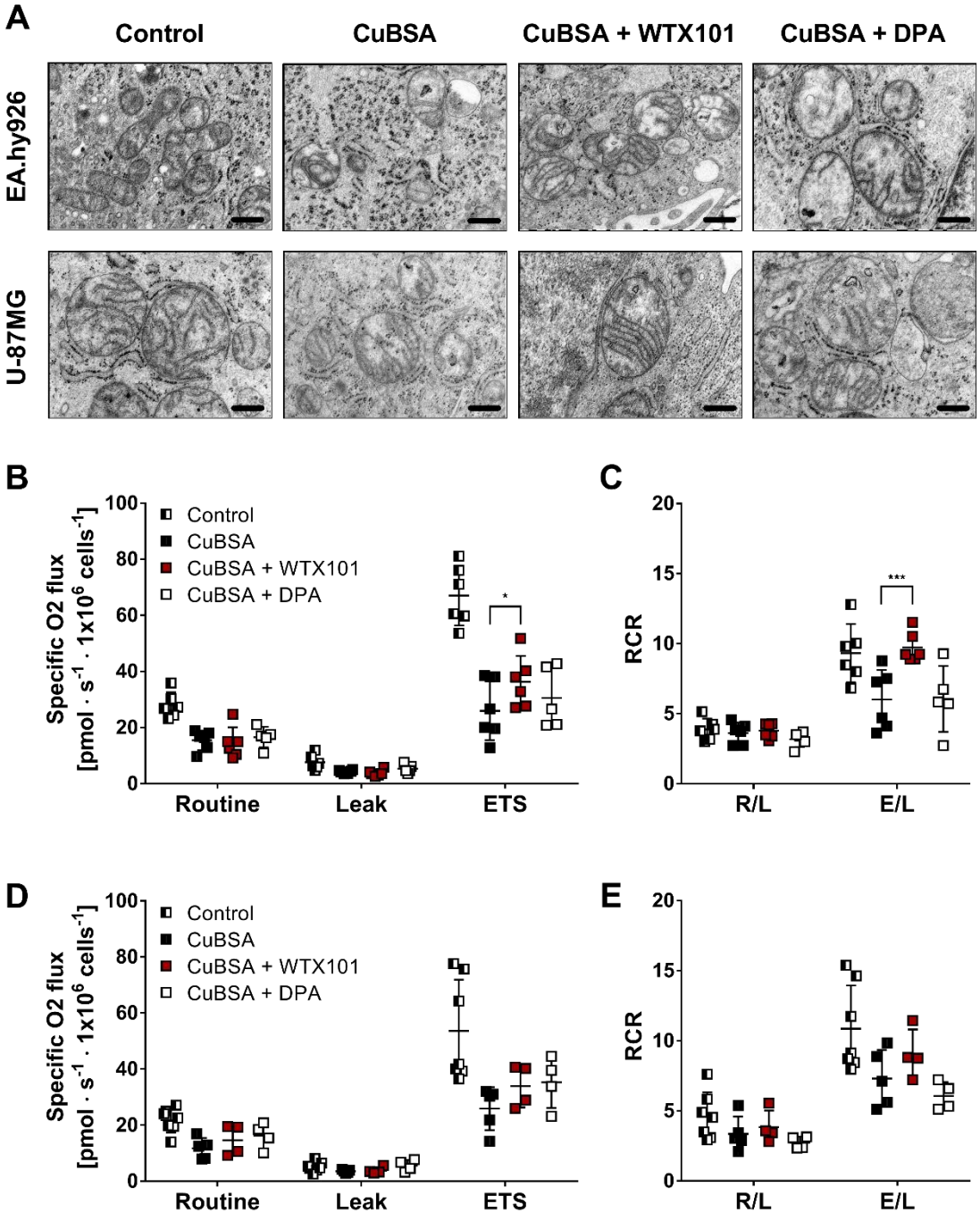

Figure 28. Copper-induced mitochondrial alterations can be avoided by WTX101, but not DPA.

(A) Mitochondrial structure of EA.hy926 and U-87MG cells is altered in the presence of copper and BSA. Here, membranous inclusions and unorganized cristae are present. In the presence of WTX101, these alterations are partially reversed, whereas DPA has no positive effect on mitochondrial structure in both cell lines. Scale bars equal 500 nm. Additionally, mitochondrial respiration is decreased in EA.hy926 (B) and U-87MG (D) cells in the presence of CuBSA and is increased in the presence of WTX101 in EA.hy926 cells (N = 4 - 7; ETS, capacity of the electron transport system). Accordingly, respiratory control ratios (RCRs) are significantly higher in WTX101-treated EA.hy926 (C) cells and slightly increased in U-87MG (E) cells (N = 4 - 7; R/L, routine to leak respiration; E/L, ETS to leak respiration).

The presence of WTX101 resulted in mitochondria with an electron-dense matrix and structured cristae as seen under control conditions, whereas the presence of DPA caused shortened and unstructured cristae. In accordance, EA.hy926 cells treated with albumin and copper displayed a strongly decreased routine respiration ($p < 0.01$) and a significantly reduced capacity of the electron transport system (ETS) ($p < 0.0001$) in comparison to untreated control cells (**Figure 28**B). In the presence of WTX101, routine and leak respiration were unchanged compared to albumin and copper treated cells, whereas respiration in the ETS state was significantly increased. Thereby, the respiratory control ratio routine to leak respiration (R/L) was unchanged, whereas the ratio of ETS to leak respiration (E/L) increased significantly compared to albumin and copper treated cells and reached the level of the untreated control cells (**Figure 28**C). In contrast, the presence of DPA showed no effects on mitochondrial respiration in all examined states compared to copper and albumin treated cells. Additionally, the described mitochondrial (dys)function of treated EA.hy926 cells was correlated with the cellular copper level (**Figure 28**A, upper panel) as well as the mitochondrial structure alterations (**Figure 27**A). Thus, copper levels were significantly lower in WTX101-treated EA.hy926 cells paralleled by an increased respiratory control ratio (E/L). In contrast, high copper levels in CuBSA-treated cells in the absence or presence of DPA coincided with a reduced maximal capacity of the electron transport system.

In U-87MG cells, CuBSA treatment resulted in slight alterations in cristae structure and membranous inclusions (**Figure 28**A, lower panel). Cristae organization was increased in the presence of WTX101, but unchanged in the presence of DPA. Additionally, inclusions were still present in WTX101 and DPA treated cells. Furthermore, CuBSA treatment of U-87MG cells led to a significantly reduced oxygen flux in the routine as well as ETS state in comparison to untreated control cells ($p < 0.0001$) (**Figure 28**D). The presence of all three investigated chelators did not change cellular respiration significantly. However, the calculated respiratory control ratios (**Figure 28**E) displayed a tendency to an increased E/L ratio in the presence of WTX101 that is not observable in the presence of DPA. However, the described tendency to an increased mitochondrial functionality in the presence of WTX101 correlated with a significantly reduced accumulation of copper under these conditions compared to CuBSA-treated cells in the absence or presence of DPA (**Figure 27**B).

3.2.6 Blood-brain barrier damage by albumin-bound copper is prevented by WTX101, but not DPA

In 2000, Stuerenburg [110] described disturbances of the blood-brain barrier (BBB) in neurologic Wilson disease patients. However, no further studies investigating the impact of BBB damage in Wilson disease are available. Consequently, the effects of copper challenges in the absence or presence of the chelators WTX101 or DPA on the BBB were analyzed using an *in vitro* BBB model. The BBB model involves primary

porcine brain capillary endothelial cells (PBCECs) seeded on Transwell® inserts and the continuous measurement of their transepithelial electrical resistance (TEER) and monolayer capacitance as a measure of the barrier integrity.

First, the impact of increasing concentrations of BSA-bound copper on the PBCEC monolayer integrity (**Figure S4**A) paralleled by the determination of cell toxicity by Neutral red assay (**Figure S4**B) were tested. Here, a decrease in TEER values was observed already at non-toxic copper concentrations (up to 250 µM copper/83.3 µM BSA), whereas a toxic concentration of 300 µM copper (and 100 µM BSA) resulted in an early disruption of the PBCEC monolayer as the TEER decreased and the capacitance increased strongly within the 50 h of observation. Hence, the capability of the copper chelators WTX101 and DPA to prevent CuBSA-induced (250 µM copper and 83.3 µM BSA) blood-brain barrier damage was determined (**Figure 29**).

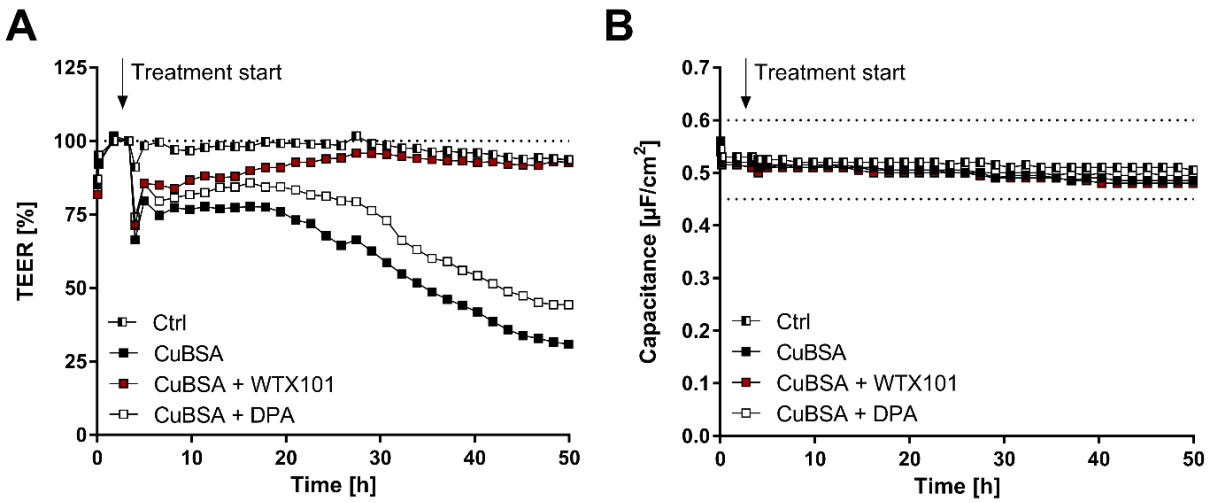

Figure 29. WTX101 prevents the copper-induced TEER loss of the PBCEC monolayer.

(A) Exemplary curves of transepithelial electrical resistance (TEER) values of PBCEC monolayers. The TEER of an untreated PBCEC monolayer is stable for 50 h. Treatment with CuBSA (250 µM copper and 83.3 µM BSA) results in a dramatic reduction of the TEER value. The presence of DPA delays the effect of CuBSA on the TEER, whereas WTX101 completely blocks the copper-induced TEER reduction (N = 2, n = 4). (B) Capacitance values of all tested conditions are stable over 50 h (N = 2, n = 4).

The presence of DPA resulted in a slightly delayed decrease of the TEER compared to monolayers treated with CuBSA alone, but DPA was not able to prevent the copper-induced TEER loss (**Figure 29**A). In contrast, PBCEC monolayers treated with BSA-bound copper in the presence of WTX101 demonstrated stable TEER values for 50 h comparable to untreated monolayers. Capacitance values were stable for all investigated conditions (**Figure 29**B) indicating the absence of cellular toxicity.

Additionally, the distribution of copper upon incubation of PBCECs in the Transwell® system was analyzed (**Figure 30**). Therefore, samples were taken from the apical and basolateral compartment right after treatment initiation and after approximately 24 and 48 h. Here, untreated control PBCEC monolayers displayed unchanged low copper levels in the apical and basolateral compartment. As CuBSA was added to the apical compartment for all other conditions, the start value at treatment initiation was 125 nmol Cu (**Figure 30**, upper panel). In the apical compartment, the concentration of copper decreased significantly ($p < 0.01$) after 24 h independent from the absence or presence of the chelators and remained stable until the end of the experiment. A time-dependent increase in copper was detectable in the basolateral compartment when PBCEC monolayers were treated with CuBSA alone (**Figure 30**, lower panel).

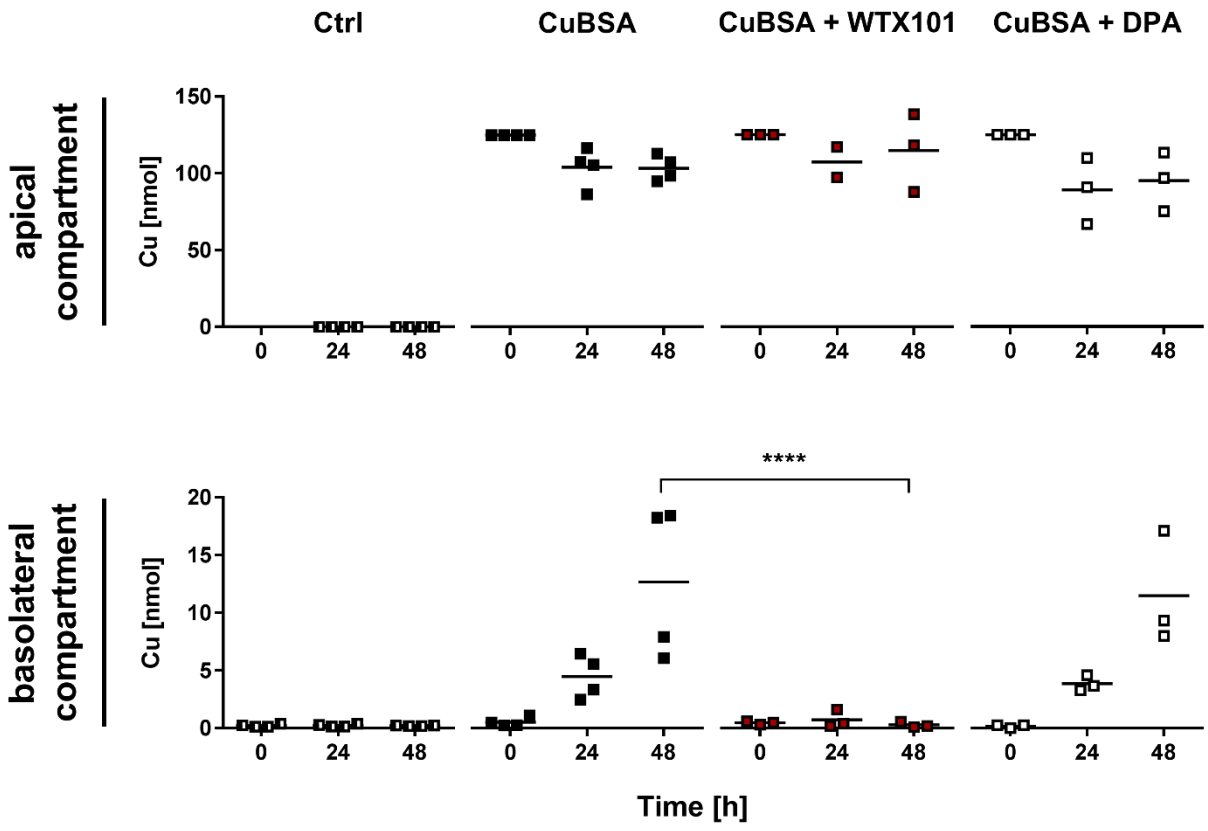

Figure 30. The basolateral copper concentration is significantly diminished in the presence of WTX101.

BSA-bound copper (BSA) decreases in the apical compartment and increases in the basolateral compartment of the Transwell® system in a time-dependent manner. In the presence of the chelators WTX101 or DPA, the apical copper concentration decreases similarly. However, only WTX101 prevents copper transport into the basolateral compartment whereas DPA is not able to interfere with it.

In the presence of WTX101, no increase of copper concentration in the basolateral compartment was detectable after 24 and 48 h of incubation resulting in a significantly lower copper concentration at

treatment termination compared to CuBSA treament. On the contrary, the presence of DPA resulted in a time-dependent increase of copper in this compartment comparable to CuBSA treatment alone.

Furthermore, immunostaining against Claudin-5 and Zonula occludens-1 (ZO-1) was performed on PBCECs grown on Transwell® inserts for TEER measurements (**Figure 31**). Claudin-5, as part of the claudin protein family, is an integral component of the tight junction protein complexes that eliminate the paracellular space between endothelial cells. Thereby, it promotes a tight BBB with limited molecular exchange between the blood and the central nervous system [216]. Staining of claudin-5 in control cells revealed a continuous distribution of the tight junction protein at the cell margins (**Figure 31**, upper panel).

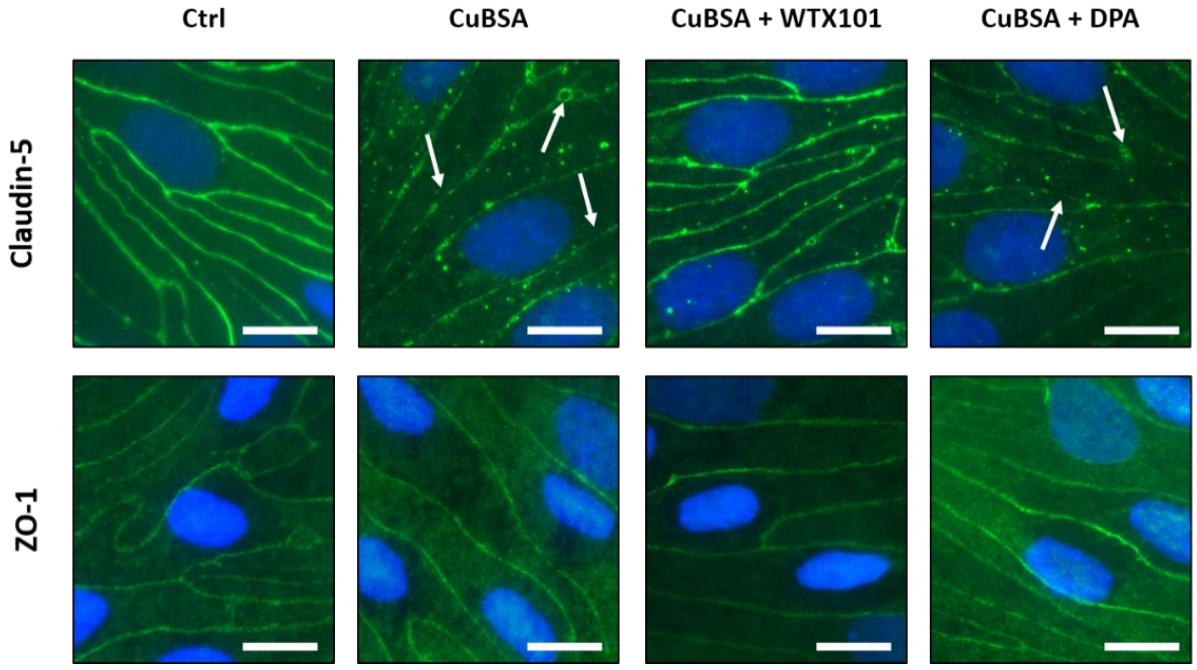

Figure 31. Immunocytochemistry analysis of PBCECs grown on Transwell® inserts against Claudin-5 or Zonula occludens-1. PBCECs were treated for 48 h with BSA-bound copper (250 µM copper and 83.3 µM BSA) in the absence or presence of 250 µM WTX101 or DPA. Directly after TEER measurements, cells were stained with a Claudin-5 (upper panel) or ZO-1 (lower panel) antibody (green) and cell nuclei were stained with Hoechst 33258 (blue). CuBSA-treated PBCECs display morphological alterations that were prevented by the presence of WTX101, but not DPA. Scale bars equal 10 µm.

PBCECs appeared spindle-like with prominent cell nuclei as shown by counterstaining with Hoechst 33258. In contrast, copper-treated PBCECs displayed gap formations between cells as well as serrated and diffuse claudin-5 expression. However, no loss of nuclei structure was observable emphasizing the absence of cell toxicity. In the presence of WTX101, these morphology alterations were much less

pronounced. Here, claudin-5 expression was continuous and uninterrupted, whereas the presence of DPA could not prevent copper-induced gap formation.

Additionally, PBCECs were stained for Zonula occludens-1, a protein located on the cytoplasmic membrane surfaces of intercellular tight junctions that cross-links and anchors these proteins to the cytoskeleton [217]. Allover, the effects of copper on ZO-1 staining and localization were less pronounced (**Figure 31**, lower panel) compared to immunocytochemistry staining against claudin-5. In untreated PBCECs, ZO-1 staining appeared continuous and uninterrupted at the cell borders. Additionally, ZO-1 staining was evenly distributed throughout the cytosol of control PBCECs. However, CuBSA-treated PBCECs displayed with a continuous ZO-1 staining along the cell margins but unregular invaginations and partly uneven intracellular distribution of ZO-1. In the presence of WTX101, these morphological differences were absent and PBCECs cells were not distinguishable from control cells. In the presence of DPA, the distribution of ZO-1 at the cell margins was continuous, but the intracellular distribution of the tight-junction-associated protein was uneven as seen in CuBSA-treated cells.

Finally, the ultrastructure of copper-treated PBCEC monolayers was analyzed by electron microscopy (**Figure 32**). Here, the paracellular connections that enable a tight barrier, the tight junctions, are visible as electron-dense, close contacts between neighboring plasma membranes of PBCECs (**Figure 32**, upper panel). In control PBCEC monolayers, the tight junctions were strongly expressed, whereas treatment with CuBSA resulted in a reduced electron density at the cell margins. In the presence of WTX101, PBCEC tight junctions appeared more prominent and comparable to the control cells, whereas DPA co-treatment resulted in reduced tight junction presence. Additionally, the mitochondrial ultrastructure was analyzed (**Figure 32**, lower panel). Here, only slight changes in mitochondrial structure were observable due to sample quality. However, mitochondria in CuBSA-treated PBCECs appeared with less organized cristae and partial electron-transmissive matrices. These structural alterations were not avoided in the presence of DPA. Indeed, DPA co-treatment seemed to even worsen mitochondrial structure as indicated by irregular and shortened cristae and electron-transmissive matrices. In contrast, co-incubation with WTX101 resulted in mitochondria with organized cristae and electron-dense matrices comparable to untreated PBCECs.

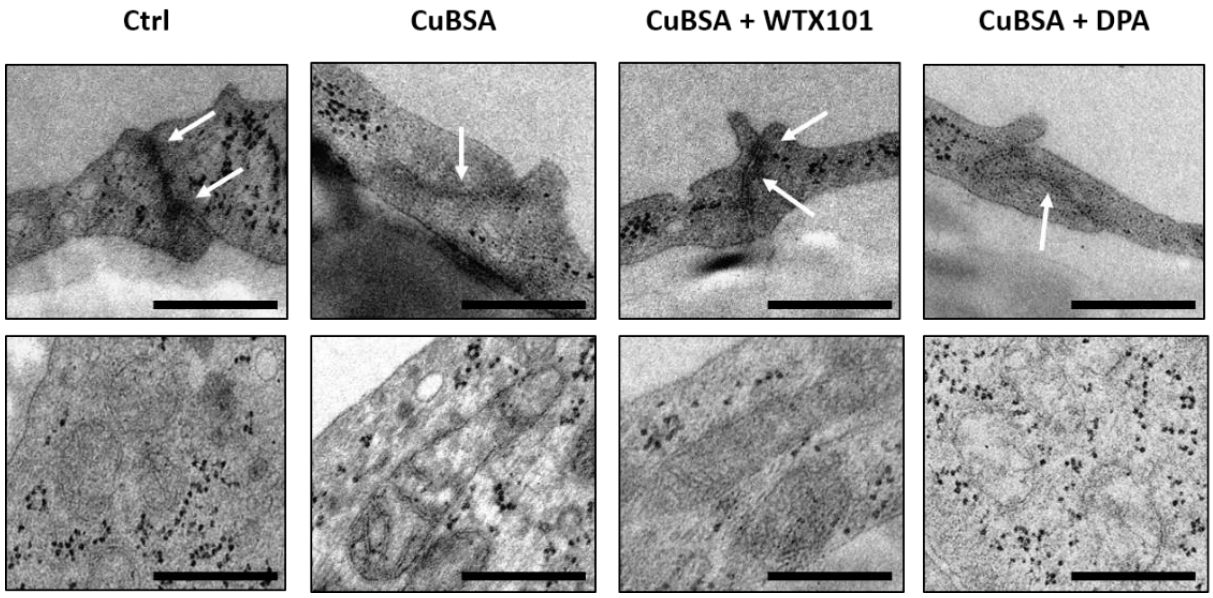

Figure 32. Electron micrographs of the tight junctions between PBCECs upon CuBSA treatment in the absence or presence of WTX101 or DPA.

Upper panel: Tight junctions (TJ) appear as electron dense spots on the cell margins of adjacent PBCECs. CuBSA treatment results in lower expression of TJ proteins, that can be prevented by the presence of WTX101, but not DPA. Scale bars equal 500 nm. Lower panel: Mitochondrial alterations upon CuBSA treatment are absent when PBCECs are co-incubated with WTX101, but not DPA. Scale bars equal 500 nm.

3.3 Mitochondrial thiol modification leads to deficits in NADH-linked respiration

Mitochondria are central organelles in the pathophysiology of Wilson disease. Here dramatic copper accumulation causes massive structural and functional alterations leading to cell death. In accordance, reduced activity of the mitochondrial respiratory complexes I - IV was described previously in WD animal models [88, 218] and patients [95]. All complexes of the electron transport system of mitochondria contain various numbers of thiol groups, ranging from 14 – 16 in complex IV [219] to 130 in complex I [220]. As described in 3.1.4, these thiol residues can be modified by copper, thereby making ETS complexes potential targets of copper-induced thiol oxidation.

Therefore, mitochondrial membrane potential (**Figure 33**, upper panel) and respiration (**Figure 33**, lower panel) of isolated U-87MG mitochondria were analyzed in the presence of two substrate combinations, either promoting complex I - related (pyruvate/malate) or complex II - linked (succinate/rotenone) respiration. To restrict the observed effects to the modification of thiol residues, mitochondria were

treated with N-ethylmaleimide, a compound that irreversibly interacts with thiol residues [221], instead of copper.

The mitochondrial membrane potential was unaffected by NEM treatment independent from the used substrate combination. In contrast, NEM treatment resulted in significantly reduced mitochondrial respiration in the OXPHOS state. Additionally, the capacity of the electron transport system (ETS) was significantly lower in NEM-treated U-87MG mitochondria compared to the untreated control in the presence of pyruvate and malate.

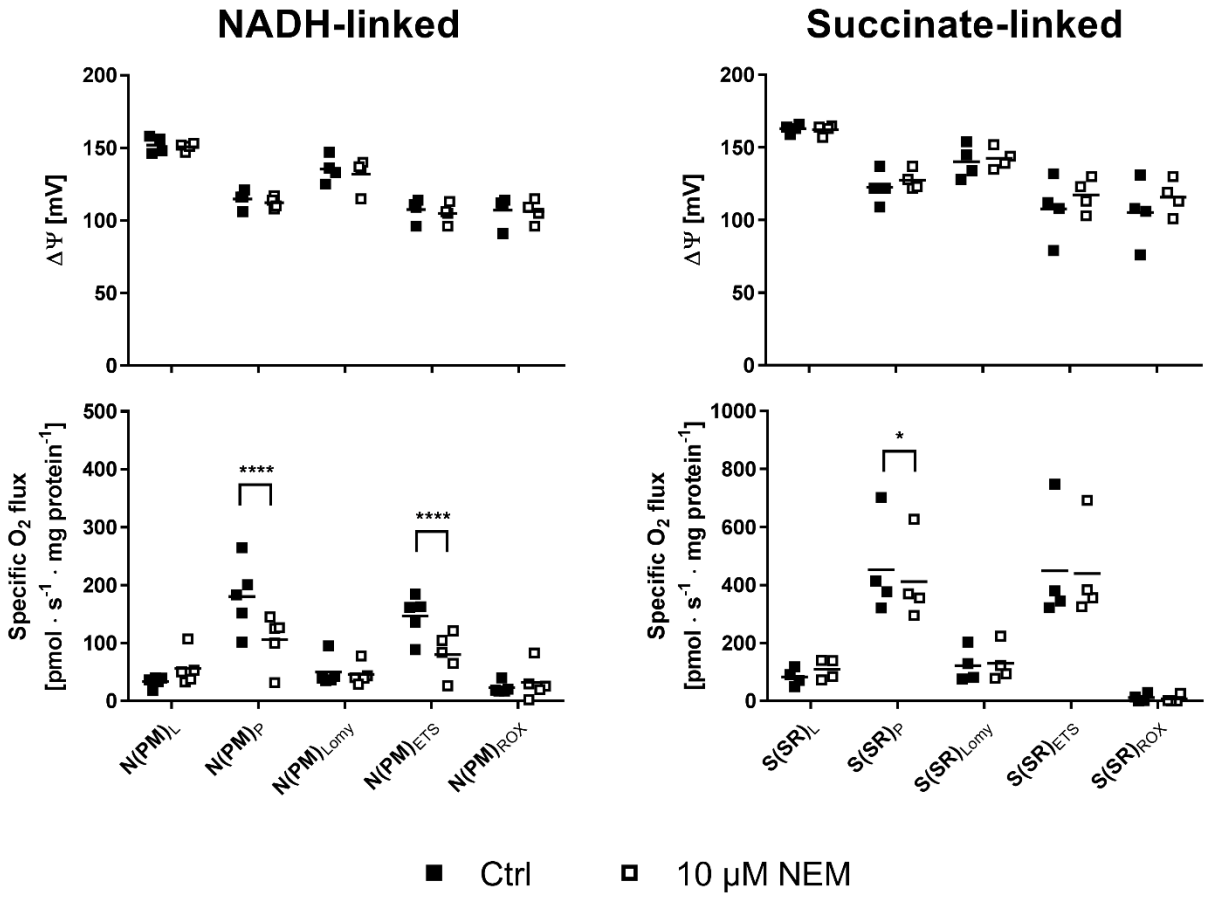

Figure 33. NADH-linked vs. succinate-linked respiration of isolated U-87MG mitochondria in the absence or presence of NEM under tissue hyperoxic conditions (180 µM O_2).

The mitochondrial membrane potential (ΔΨ, upper panels) is unaffected by N-ethylmaleimide (NEM) in the presence of pyruvate/malate (NADH-linked) or succinate/rotenone (succinate-linked) as substrates. However, NADH-linked respiration in the OXPHOS ($N(PM)_P$) and ETS state ($N(PM)_{ETS}$) is reduced in the presence of NEM. Succinate-linked respiration is affected only in the OXPHOS state ($S(SR)_P$) (N = 4 - 5).

The finding of the OXPHOS capacity being higher than the capacity of the ETS is most probably due to an experimental artefact, *e.g.*, due to over titration of the uncoupler and thereby, inhibition of the

electron transport system. In contrast, succinate-linked respiration was less affected by NEM treatment. Here, the oxygen flux in the ETS state was unaffected, whereas respiration in the OXPHOS state was slightly but significantly reduced. In summary, the modification of mitochondrial thiols by NEM affected complex I-linked respiration stronger than complex II-linked respiration in isolated U-87MG mitochondria.

A unique feature of complex I is its ability to shift between the active and the de-active form [222, 223]. During this A/D transition, cysteine 39 of the mitochondrially-encoded ND3 subunit gets exposed. Hence, the D-form is more susceptible to reversible or irreversible modification that results in the arrest of the enzyme in the de-active state and consequently, the inhibition of the enzyme [224].

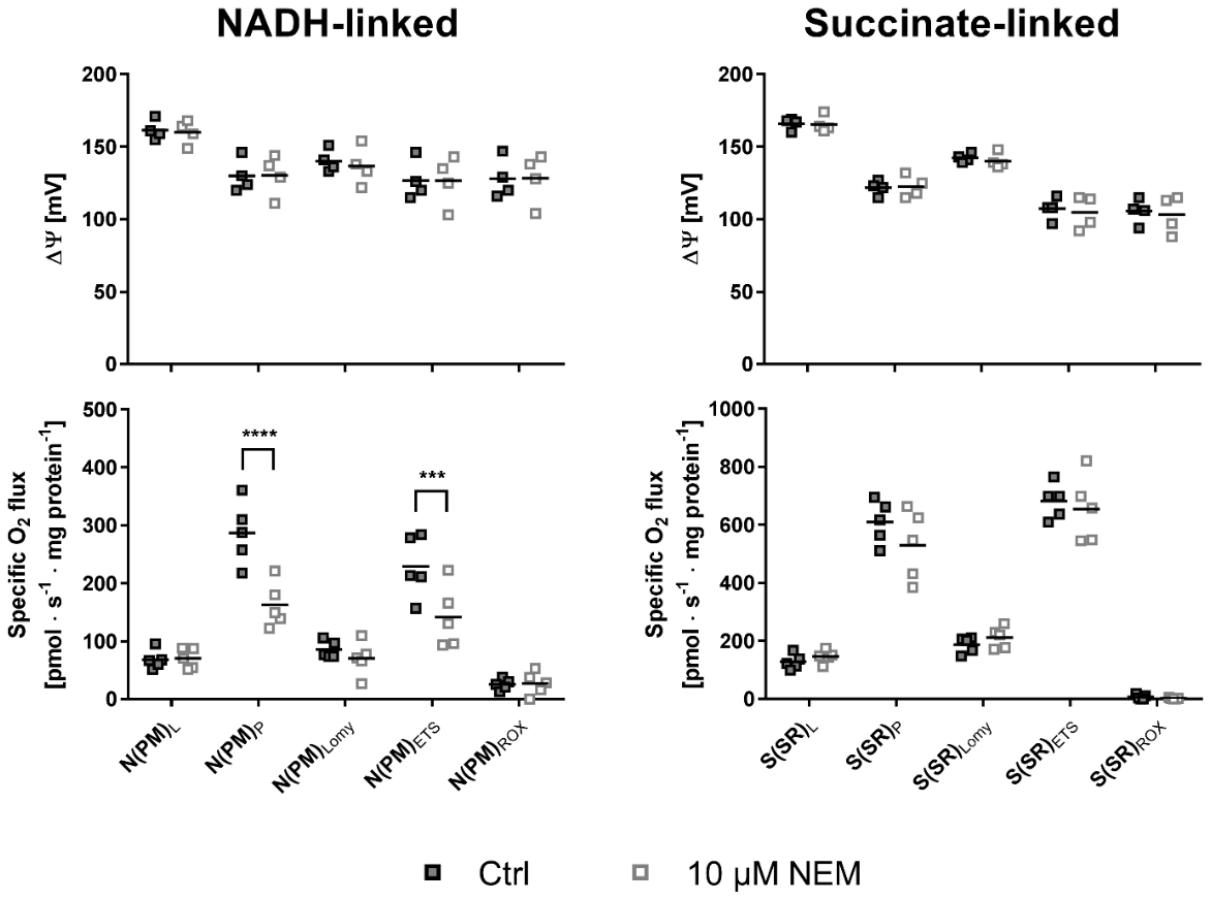

Figure 34. NADH-linked vs. succinate-linked respiration of isolated U-87MG mitochondria in the absence or presence of NEM under tissue normoxic conditions (30 µM O_2).

The mitochondrial membrane potential (ΔΨ, upper panels) is unaffected by N-ethylmaleimide (NEM) in the presence of either pyruvate/malate (NADH-linked) or succinate/rotenone (succinate-linked) as substrates. However, NADH-linked respiration in the OXPHOS ($N(PM)_P$) and ETS state ($N(PM)_{ETS}$) is reduced in the presence of NEM. Succinate-linked respiration is not affected by NEM (N = 5).

Such deactivation occurs in the absence of substrates or oxygen. Therefore, isolated U-87MG mitochondria were exposed to lower oxygen levels (30 µM O_2 instead of 180 µM O_2) prior to NEM treatment and determination of the mitochondrial membrane potential (**Figure 34**, upper panel) and respiration (**Figure 34**, lower panel) to increase the amount of complex I in the de-active form. Here, the mitochondrial membrane potential was unaffected by NEM treatment as already shown under tissue hyperoxic conditions (180 µM O_2, **Figure 33**). However, mitochondrial oxygen consumption was strongly reduced in the presence of NEM and the complex I-linked substrates pyruvate/malate in the OXPHOS and ETS state. Additionally, this reduction was even more pronounced compared to the effect observed under tissue hyperoxic conditions. In contrast, succinate-linked respiration was unaffected by NEM treatment.

For translation of these findings into the context of copper overload, U-87MG were either treated with medium alone or in the presence of BSA-bound copper for 24 h and subsequently subjected to HRR (**Figure 35**), as mitochondrial thiol modification had no effect on the mitochondrial membrane potential.

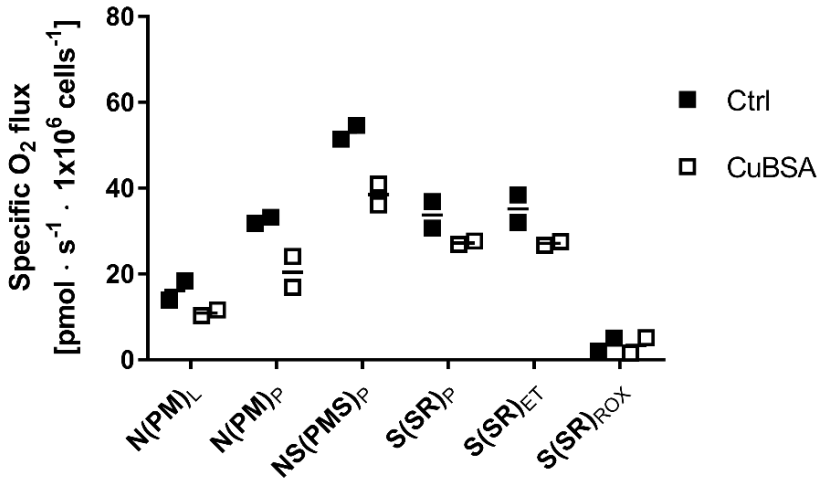

Figure 35. Oxygen consumption rates of permeabilized U-87MG cells either untreated or CuBSA-treated for 24 h.
U-87MG cells were either treated with medium only or in the presence of CuBSA (ratio of 1:3) for 24 h. Cells were permeabilized with digitonin and subjected to HRR. CuBSA-treated cells exhibit lower respiration rates in the presence of NADH-linked substrates compared to respiration in the presence of succinate (N = 2).

Here, CuBSA-treated permeabilized U-87MG cells exhibited lower oxygen consumption rates in the OXPHOS state under NADH-linked respiration compared to control cells (N(PM)$_P$). Furthermore, addition of succinate resulted in an increased respiration for both, untreated and treated U-87MG cells. However, CuBSA-treated cells respired less than control cells. Addition of the complex I inhibitor rotenone led to the determination of the succinate-linked oxygen flux in the OXPHOS state (S(SR)$_P$).

Here, no difference between CuBSA-treated and control cells was detectable anymore. This holds also true for the succinate-linked respiration in the ETS state after addition of the uncoupling agent CCCP ($S(SR)_{ET}$). Thus, copper-induced mitochondrial dysfunction in U-87MG is characterized by a predominant reduction of NADH-linked respiration, whereas Succinate-linked respiration is less affected, revealing a direct impact of copper on complex I.

4 DISCUSSION

4.1 Brain mitochondria are sensitive targets of copper overload in the context of Wilson disease

4.1.1 Brain mitochondria are highly susceptible to copper

Wilson disease (WD) is characterized by a disrupted copper homeostasis resulting in massively increased copper levels, mainly in the liver and brain. Liver mitochondria were identified as first responders to excessive copper in hepatocytes of WD patients [85, 91, 225] and WD animal models [84, 85, 88]. In the latter, the capacity of liver mitochondria to produce ATP was strongly reduced. Furthermore, this functional deficit was paralleled by an increasing mitochondrial copper load and coincided with progressive disease states [85]. In line with these observations, a reduction of the mitochondrial copper burden by copper chelators avoided hepatocyte death whereas the cytosolic copper load was unchanged [84, 85]. Taken together, copper-induced mitochondrial dysfunction decisively contributes to hepatocyte death in WD.

In contrast to this well-established role of mitochondria in the hepatic phenotype of WD, the copper-related detrimental effects are much less understood for other organs affected in WD, *e.g.*, heart, kidney and brain. Here, the brain is of special interest as copper massively accumulates in the brain of WD patients [49, 70, 99, 100] and leads to various psychiatric and neurologic symptoms [107, 120]. Due to ethical aspects, studies in neurologic WD patients are largely missing. Furthermore, animal models only partially resemble the pathologic situation of this subset of WD patients [116-118]. However, early studies in cats demonstrated the neurotoxicity of copper [112]. Furthermore, neuronal copper intoxications were demonstrated to cause a massively increased oxygen consumption due to a strong uncoupling effect. The authors concluded that brain mitochondria are highly vulnerable to copper [114]. Unfortunately, further studies along this line are largely missing although the stated publications indicate a pivotal role of mitochondria in copper-induced neurotoxicity.

Therefore, the direct sensitivity of mitochondria from different tissues to copper was tested. To this end, rat liver, kidney, heart and brain mitochondria were subjected to equal copper challenges and structural and functional consequences were determined. Indeed, a tissue-specific mitochondrial copper sensitivity can be hypothesized as these organelles differ markedly in their molecular composition [28, 29], their structure (**Figure 9**A), and their sensitivities to applied challenges, as exemplified by calcium (**Figure 9**C). The latter observations agree with previous reports [226, 227], describing the swelling of a

subfraction of brain mitochondria only, whereas the same stimulus caused a pronounced swelling in liver and heart mitochondria. In the presence of cuprous copper (Cu^{1+}, Cu/GSH ratio of 2:10), brain mitochondria presented with an early mitochondrial membrane potential (MMP) loss compared to organelles from rat liver, kidney and heart (**Table 5**). This functional deficit was paralleled by profound structural changes already at low Cu^{1+} concentrations as determined by a change in optical density at 540 nm (**Figure 10**). Here, brain mitochondria displayed $OD_{540\,nm}$ changes already at a Cu/GSH ratio of 1:10, although an MMP loss was only present at a ratio of 2:10 and higher. Typically, changes in $OD_{540\,nm}$ are used to determine mitochondrial swelling upon a calcium challenge that induces the mitochondrial permeability transition (MPT) [228] and is paralleled by an MMP loss [179]. However, the optical density of a mitochondrial suspension is directly dependent on their light diffraction properties and thereby, displays a summation parameter [229]. Consequently, substantial structural alterations of mitochondria, different from the MPT, are detected as well. Indeed, electron microscopy analysis of the investigated rat mitochondrial populations upon copper challenges revealed distinct structural alterations in brain mitochondria already after 30 min of Cu^{1+} exposure (**Figure 11**). Here, brain mitochondria appeared uniformly greyish with strongly thinned cristae. Nevertheless, these cristae seemed to sustain an intact MMP. This could explain a change in optical density already at a Cu/GSH ratio of 1:10, but an MMP loss occurring at a ratio of 2:10 and strengthens the notion of an exceptional vulnerability of brain mitochondria to copper. In contrast to the highly sensitive brain mitochondria, organelles isolated from rat heart were much less sensitive to copper challenges as shown by less pronounced structural alterations (**Figure 11**) in parallel with dramatic $OD_{540\,nm}$ changes only at the highest Cu/GSH ratio (**Figure 10**). This finding agrees well with the only very rare occurring heart problems in WD patients [61, 64, 65] and strongly suggests that the tissue-specific mitochondrial vulnerabilities, at least partially, determine the observed copper-induced organ toxicities in Wilson disease.

4.1.2 The formation of reactive oxygen species is a late-stage event in copper toxicity

The redox activity of copper and thereby, its participation in Fenton chemistry-based reactions led many authors to the hypothesis that the formation of reactive reaction species may be a causative factor of mitochondrial dysfunction and hepatocyte death in hepatic WD patients [72-76]. However, this was challenged by findings in still healthy WD animals (LEC rats) that displayed no oxidative stress at an early disease stage, but profound ROS production only in the late stages of liver damage [78-80].

Therefore, hydrogen peroxide production was analyzed in rat liver, heart, kidney and brain mitochondria upon copper challenges and revealed prominent ROS production only at the highest Cu/GSH ratio (5:10) in all investigated mitochondrial populations. Hence, the observed mitochondrial structural and functional impairments (**Figure 10**, **Figure 11**) at low Cu/GSH ratios cannot be explained by a Fenton chemistry-based reaction of copper. To further strengthen these observations, rat liver and brain mitochondria were subjected to activity measurements of the redox-sensitive aconitase (**Figure 13**A) and to the determination of lipid peroxidation (**Figure 13**B). In agreement, profound mitochondrial oxidative damage occurred only at the highest Cu/GSH ratio and therefore, in the presence of Cu^{2+}. Although under physiological conditions, intracellular copper is present in its cuprous form (Cu^{1+}) and bound to copper chaperones [15, 24], excessive copper accumulation in WD could lead to the presence of unbound cuprous and/or cupric copper (Cu^{2+}). Cupric copper is known to cause rapid mitochondrial dysfunction already at low concentrations paralleled by a dramatic increase in ROS production [230]. Accordingly, rat liver and brain mitochondria exposed to Cu^{2+} (Cu/GSH ratio of 5:10) were readily destroyed as shown by electron microscopy (**Figure 13**C) and displayed a burst of mitochondria-derived ROS (**Figure 12**). Hence, liver and brain mitochondria produced significant ROS **after** their disintegration by excess copper. This dramatic mitochondrial destruction can be explained in several, not mutually exclusive, ways. On the one hand, copper could cause the disintegration of the highly organized electron transport system (ETS) [231] followed by an electron leakage and massive ROS production (mainly at complexes I and III [232]). This possible explanation is substantiated by reports describing copper-induced dysfunction of ETS complexes in parallel with oxidative damage [95, 230]. On the other hand, the presence of either cupric or loosely-bound cuprous copper may cause their participation in Fenton chemistry-based reactions and thereby, the production of highly detrimental hydroxyl radicals, that subsequently cause damage to proteins, lipids and DNA [25]. Nevertheless, a vicious cycle appears plausible under such excessive conditions causing an exploding emergence of ROS. In conclusion, these data demonstrate that Cu^{1+}-related mitochondrial damage, especially to brain mitochondria, is an early event as shown by MMP loss and structural alterations. In contrast, an increased mitochondrial ROS production appears to be a secondary consequence rather than the cause of organelle impairment.

4.1.3 Mitochondrial thiols are susceptible to copper

As massive ROS production can be excluded as primary cause of copper-induced damage in isolated mitochondria, an alternative hypothesis for copper toxicity could be its direct impact on proteins. Free protein thiols were found to be dose-dependently decreased upon Cu^{1+} challenges in both mitochondrial populations (**Figure 14**A, C). This finding agrees with previous reports that copper may specifically

attacks susceptible proteins at their thiol groups [82, 233] and is in line with the earlier identification of mitochondrial membrane proteins that were sensitive to copper-induced modifications of their cysteine residues [84]. This suggested mechanism of copper-mediated protein impairment resembles "classical" protein damage by direct attack of target amino acid residues (*e.g.*, cysteine and methionine) [234]. Additionally, conformational changes and/or protein activity losses may occur [14, 235], which are especially critical for proteins of the mitochondrial oxidative phosphorylation system. Hence, the question arises, why brain mitochondria are comparatively highly sensitive to copper-induced oxidation of thiol residues. A possible explanation could be their significantly lower level of mitochondrial glutathione compared to liver mitochondria (**Figure 14**B) as already described in the literature [236]. This is of main interest as glutathione is the major intracellular reductant, complexes copper in the cytosol and thereby, participates in the defense against oxidative protein damage [168, 169, 207]. However, the absolute levels of free thiols were comparable between rat liver (42.9 ± 7.0 nmol/mg mitochondrial protein, [237]) and brain (43.5 ± 21.2 nmol/mg mitochondrial protein) mitochondria suggesting the impairment of different cysteine residues by copper in brain mitochondria compared to liver mitochondria. Accordingly, fluorescent labeling of thiol residues in both mitochondrial populations revealed the oxidation of different proteins in brain compared to liver mitochondria (**Figure 14**C). However, these specific protein targets in brain mitochondria need to be characterized in the future studies. Finally, brain mitochondria displayed a significantly reduced ATP production capacity at a low Cu/GSH ratio (1:10), whereas liver mitochondria exhibited a stable ATP production in the presence of this copper challenge (**Figure 15**A). In conclusion, a limited defense against oxidative protein damage, *i.e.*, a lowered GSH content, could plausibly explain the high sensitivity of brain mitochondria to copper challenges.

The liver consists mainly of hepatocytes (approximately 80 % of liver mass [238]) that contain the vast majority of mitochondria. Thus, isolated liver mitochondria can be considered as hepatocytic mitochondria, whereas the brain consists of several different cell types, including neurons, astrocytes and endothelial cells. Therefore, the isolation of mitochondria from whole brain leads to a comparably inhomogeneous population of organelles with different origin. Hence, the neuroblastoma cell line SH-SY5Y and the astrocytoma cell line U-87MG were used to gain further insight into the specific copper sensitivity of different brain cell types. In agreement with earlier reports [239], isolated SH-SY5Y mitochondria were highly susceptible to copper in functional aspects (**Figure 15**B). In line with the findings on isolated brain mitochondria, a loss of free protein thiols was detectable in isolated SH-SY5Y mitochondria upon copper challenges (**Figure 15**C). In contrast, isolated U-87MG mitochondria were

unaffected by the applied copper challenges with regard to their ATP production capacity and displayed a reduction in free protein thiols only at the highest copper concentration (**Figure 15**B, C). Although isolated SH-SY5Y mitochondria were highly sensitive to copper, cell toxicity of histidine-bound copper was comparable in SH-SY5Y and U-87MG cells (**Figure 16**), whereas structural alterations were observable in SH-SY5Y cells in a dose-dependent manner, but not in U-87MG (**Figure 17**,**Figure 18**). Accordingly, structural alterations of SH-SY5Y mitochondria can be considered as an early feature of copper-induced toxicity prior to cell death. In line with the observations in rat brain mitochondria, excessive production of ROS was not observed under the applied copper challenges (**Figure 19**, right panel), further supporting the role of ROS as a consequence of massive mitochondrial damage, and not its cause. As shown for rat brain mitochondria compared to liver organelles, SH-SY5Y cells exhibited limited antioxidative defense mechanisms against copper overload indicated by significantly reduced GSH levels (**Figure 20**A) and the absence of metallothionein (**Figure 20**B). In line with this finding, previous studies similarly described the absence of metallothionein isotypes 1 and 2 (MT1/2) in neurons [240-242]. Indeed, these protein isotypes are mainly responsible for the safe storage of intracellular metals, *i.e.*, copper [241], thereby diminishing its redox activity within the cell. Hence, the absence of MT1/2 along with the comparatively low level of cellular GSH could explain the high susceptibility of SH-SY5Y mitochondria to copper. Interestingly, U-87MG cells accumulated significantly more copper compared to SH-SY5Y cells (**Figure 20**C), but only the latter presented with mitochondrial structural and functional deficits (**Figure 15**, **Figure 18**). From these data, it is tempting to speculate that astrocytes in WD patients' brains should be capable of buffering high amounts of copper quite longstanding, but overload of their storage capacity may lead to copper release that impairs neuronal function. This would provide a plausible explanation why neuronal symptoms are rather late occurring features in WD. However, this needs to be validated in the future.

4.2 The high-affinity chelator WTX101 prevents copper-induced mitochondrial damage and subsequent cell death

4.2.1 Copper chelators bear a potential risk for neurological worsening in WD

D-penicillamine (DPA), the copper chelator mainly used in the treatment of hepatic WD, may cause (partially irreversible) worsening of symptoms in up to 50 % of neurologic WD patients [68, 131, 135, 136, 243]. This dramatic side effect was attributed to the mobilization of copper from the liver into the systemic circulation, thereby leading to an increased copper accumulation in the brain [137].

Therefore, the distribution of copper was analyzed in the *Atp7b*$^{-/-}$ rat model upon treatment with DPA, but also with WTX101 (bis-choline tetrathiomolybdate, TTM), a clinical phase 3 drug for WD [103]. In accordance to the literature [134, 244], DPA led to an increased urinary metal excretion (**Figure 21**). However, no increase in blood copper was observable revealing a rapid clearance of the metal by the kidneys. This is in accordance with the literature describing a peak of blood DPA levels 1 to 3 h after oral administration in WD patients [245]. Hence, the intraperitoneal application of DPA in *Atp7b*$^{-/-}$ rats could result in an even earlier peak of blood DPA levels that is undetectable by blood sampling after several days after administration. Additionally, WTX101-treated animals revealed a significant increase in serum copper levels but no increase in urinary copper excretion suggesting the formation of a complex which cannot be eliminated via the kidneys. This phenomenon was already described for ammonium TTM and Ogra and co-workers suggested the formation of a tripartite complex consisting of TTM, albumin and copper [144]. Altogether, these findings demonstrate a potential risk of neurological deterioration for DPA and WTX101. However, in a phase 2 clinical study, no WTX101-treated patient suffered from neurological deterioration [145].

For further characterization of the chelator complexes formed in the blood, size-exclusion chromatography of premixed solutions of BSA, copper and DPA or WTX101, respectively, was performed (**Figure 22**). Here, the copper elution was unchanged in the presence of DPA compared to copper and BSA alone. This is in agreement with a previous report describing the inability of DPA to mobilize copper from BSA [246] and can be further ascribed to the binding affinities of DPA ($K_d = 2.4 \times 10^{-16}$ M [212]) and albumin (K_d (N-terminal) $= 6.7 \times 10^{-17}$ M [214]), to copper. Hence, only very high levels of DPA would be able to compete for the copper ion bound to the N-terminus of BSA. The concurrent elution of copper and DPA in a second peak suggests the formation of a low molecular copper-DPA complex as suggested previously [246]. In contrast, elution of WTX101 was paralleled by copper and BSA co-elution. This agrees well with the tripartite complex formation as described previously [144]. Therefore, this complex consisting of WTX101, copper and BSA was further characterized by X-ray crystallography. Here, two copper ions and one WTX101 molecule presented in the Sudlow Site 1 of BSA (**Figure 23**). Hence, the data suggest a tight incorporation of copper into albumin in the presence of WTX101 independent from the copper-binding sites of albumin on the N-terminus of the molecule as well as the multi-metal binding site. Consequently, tripartite complex formation could result in the unavailability of copper for uptake into the brain and thereby, a low risk of neurological worsening. Reconsidering the results from the size-exclusion chromatography (**Figure 22**), one further copper ion needs to be bound separately from the Sudlow Site 1 in the TPC. Most possibly, this copper ion is bound to the high-affinity site at the

N-terminus of albumin. However, due to the low resolution of the data and the conformational flexibility of the N-terminus the occupancy with copper is not determinable in this data set. Due to the strong reductive activity of tetrathiomolybdate [247], the oxidation state of the incorporated copper ions (**Figure 24**) was determined by paramagnetic electron resonance measurements. Here, one copper ion was found to be reduced to Cu(I), whereas the second copper ion remained in the cupric form.

4.2.2 Copper-induced cell death can be avoided by the high-affinity chelator WTX101

Taken the previous results and the available clinical data together, the chelator-related mobilization of copper into the serum seems not to be problematic *per se*. Whereas both DPA and WTX101 caused elevated serum copper levels in treated *Atp7b*$^{-/-}$ animals (**Figure 21**), neurological worsening is mainly observable in DPA-treated, but not WTX101-treated WD patients. Therefore, it can be hypothesized that the risk for neurologic deterioration depends also on further factors, *e.g.*, the copper affinity of the respective chelator. Here, tetrathiomolybdate reveals an extremely high affinity for copper (K_d (TTM) = 2.3 × 10^{-20} M [212],), whereas DPA is known to be a chelator with comparatively low copper affinity (K_d = 2.4 × 10^{-16} M [212]).

Unfortunately, *in vivo* studies using *Atp7b*$^{-/-}$ rats were not applicable as these animals do not display any obvious neurological symptoms (unpublished observations). This can be attributed to the disease progression in these animals characterized by a fulminant hepatitis at an age of 85 - 95 d and subsequent animal death [84, 85]. Thus, a progressive accumulation of copper in *Atp7b*$^{-/-}$ brains is rather unlikely. Therefore, the consequences of the differential copper binding by DPA and WTX101 were analyzed by determining the cellular toxicity of increasing copper to BSA ratios in the absence or presence of the stated chelators in HepG2, EA.hy926, U-87MG and SH-SY5Y cells (**Figure 25**, **Figure S2**). Here, the high-affinity chelator WTX101 exhibited protective effects on copper-induced cell toxicity in all investigated cell lines. These effects were paralleled by a decreased cellular copper content in WTX101-treated EA.hy926 and U-87MG cells (**Figure 26**). Here, the presence of WTX101 and thereby, the formation of the tripartite complex could lead to a decrease in CTR1-available copper by its tight incorporation into BSA and thereby, a decreased cellular copper content. In contrast, the cellular copper content of EA.hy926 and U-87MG cells was unchanged in the presence of DPA. This observation is in line with the literature describing equal copper levels in mouse hepatocytes treated with copper in the absence or presence of DPA [248]. However, the cellular copper content of HepG2 and SH-SY5Y was unaltered in the presence of the investigated chelators compared to CuBSA-treated cells. Nevertheless, cellular viability was significantly enhanced by WTX101, but not DPA in these cell lines (**Figure 25**). This

could be attributed to the tight incorporation of the metal into inert metal-chelator complexes within the cells that prevents copper-induced oxidative damage at comparable cellular copper levels. Taken together, the protective effects of the high-affinity chelator WTX101 concerning copper-induced cellular toxicity coincide with a statistically significant reduction in cellular copper levels in U-87MG and EA.hy926 cells.

4.2.3 The high-affinity chelator WTX101 prevents copper-induced blood brain barrier damage

Mitochondria are first responders of copper toxicity in hepatic WD patients and animal models [84-86, 89]. Additionally, studies in animal [112, 114] and *in vitro* models [201] indicate a critical role of mitochondria also in the neurologic phenotype of the disease. For the sake of conciseness, the subsequent analyses of mitochondrial function and structure upon copper challenge were restricted to EA.hy926 and U-87MG cells (**Figure 27**, **Figure 28**). Here, CuBSA-treated U-87MG and EA.hy926 cells displayed a decreased capacity of the electron transport system and mitochondrial structure alterations. Copper-induced mitochondrial dysfunction was prevented by WTX101, but not DPA. Additionally, mitochondrial alterations correlated with the cellular copper level, whereas no changes in basic cellular parameters like protein concentration and size were detectable (**Figure 27**). Taken together, mitochondrial dysfunction upon copper challenges appears as an early feature of copper toxicity in these cells before pronounced cell death is detectable.

Interestingly, these two cell types, endothelial (EA.hy926) and astrocytoma cells (U87MG), represent two major constituents of the blood-brain barrier. Previously, Stuerenburg suggested an involvement of the blood-brain barrier in four neurologic WD patients showing neurological deterioration under penicillamine treatment paralleled by an increased blood-brain barrier (BBB) leakiness [110]. Furthermore, Doll et al. described mitochondria as “key players in BBB permeability” [249]. Here, manipulation of mitochondrial respiration led to a rapid increase in BBB permeability and disruption of the tight junctions. Consequently, the impact of copper on BBB integrity in a Transwell® system using a CellZscope® device was investigated. However, EA.hy926 were not a suitable BBB model due to low transepithelial electrical resistance (TEER) values [250]. Hence, the effect of BSA-bound copper in the absence or presence of the chelators WTX101 and DPA was evaluated using primary porcine brain capillary endothelial cells (PBCECs) as an *in vitro* model of the blood-brain barrier. Here, PBCECs treated with a non-toxic BSA-bound copper concentration displayed decreasing TEER values over 48 h (**Figure *29***, **Figure S4**), which was avoided by WTX101, but not by DPA. Additionally, only the presence of the

high-affinity chelator WTX101 reduced the transport of copper through the PBCEC monolayer (**Figure 30**). This can be attributed to the detrimental impact of BSA-bound copper on the tight junction integrity, as shown by ICC against claudin-5 and ZO-1 (**Figure 31**) that can only be prevented by WTX101. Furthermore, electron micrographs (**Figure 32**, upper panel) of PBCECs grown on Transwell® inserts revealed a reduction of the tight junctions in copper-treated PBCECS in the absence or presence of DPA, whereas WTX101-treated PBCECs displayed with electron-dense tight junctions at the cell margins further strengthening an impact of copper on tight junction integrity as shown by immunocytochemistry. However, conclusions concerning the involvement of mitochondrial dysfunction in copper-treated PBCECs proved to be difficult (**Figure 32**, lower panel) due to the low number of organelles per cell (2 – 6 % of cytoplasm volume [251]). Only slight structural alterations were observable upon copper treatment. In the presence of WTX101, PBCEC mitochondria appeared with more structured cristae, whereas co-treatment with DPA resulted in disintegrated cristae. Thus, a clear connection between mitochondrial dysfunction and tight junction disruption in PBCECs upon copper challenge remains for future studies. Nevertheless, the gained data further strengthen the potential role of the blood-brain barrier in neurologic WD as described by Stuerenburg [110]. Furthermore, the ability of the high-affinity chelator WTX101 to prevent copper-induced BBB leakage could be one explanation for the absence of neurological worsening in WTX101-treated WD patients [145]. In contrast, the presence of DPA could not diminish the copper-related increase in PBCEC barrier permeability.

4.3 Complex I as a potential target of copper-induced mitochondrial thiol modification

Mitochondrial protein thiols were identified as critical targets in liver and brain mitochondria (see 3.1.4). Although both mitochondrial populations displayed the same level of free thiols per mg of mitochondrial protein, brain mitochondria were more sensitive to copper challenges with respect to functional and structural aspects (see 3.1.2). Furthermore, fluorescent labeling of protein thiols suggested the oxidation of different proteins in brain and liver mitochondria, respectively (see 3.1.4). Mitochondria are enriched in proteins with thiol residues that are critical for their redox homeostasis and thereby, their functionality, *e.g.*, oxidative phosphorylation and ROS production. Indeed, 19 of the 50 most reactive cysteine residues within cells are found in mitochondria [252]. Furthermore, most of these highly active cysteine residues are located within the reactive centers of mitochondrial metabolic enzymes [252], *e.g.*, aconitase [253] and acetyl-CoA acetyltransferases [254]. Additionally, all complexes of the oxidative phosphorylation system (complex I - V) were shown to be sensitive to redox

modification of thiol residues [255], but physiological functions and consequences are still a matter of research.

To demonstrate this thiol sensitivity, mitochondria isolated from U-87MG cells were treated with 10 µM NEM and their substrate-specific functionality was analyzed by high-resolution respirometry (HRR) under tissue hyperoxic (≈ 180 µM O_2) conditions (**Figure 33**). NEM treatment resulted in a significant reduction in NADH-linked respiration (36 % reduction in NEM-treated mitochondria), promoted by pyruvate and malate as substrates, whereas succinate-linked respiration, promoted by succinate and rotenone, was rather unchanged. This suggests a specific sensitivity of complex I or upstream protein relays that facilitate the entry of pyruvate and malate into the mitochondrial matrix and their processing until their entry into the ETS via the tricarboxylic acid cycle. Here, complex I itself seems to be of special interest due to its extremely high number of thiol groups (130 [220]) compared to complex II (41 thiol groups according to Uniprot database: P31040, P21912, Q99643, O14521). Furthermore, a unique feature of complex I is its ability to shift between an active (A) and de-active (D) form [222, 223]. This A/D transition involves a specific and conserved cysteine (cys39) in the ND3 subunit of complex I that is not accessible in the active state [224]. In the absence of substrates and/or oxygen, complex I converts into the de-active form [256]. Thereby, this single cysteine residue gets exposed and prone to inhibition by divalent cations (*i.e.*, Ca^{2+} [255]) or modification, *e.g.*, by ROS [257]. Consequently, the reactivation of complex I is prevented, and its catalytic activity is reduced.

Hence, isolated U-87MG mitochondria were exposed to lower oxygen levels (tissue normoxia, ≈ 30 µM O_2) prior to modification by NEM and subsequently analyzed concerning their NADH- vs. succinate-linked mitochondrial respiration under tissue hyperoxic conditions (**Figure 34**). Here, NADH-linked respiration in the OXPHOS and ETS state was significantly decreased in the presence of NEM (52 % reduction in NEM-treated mitochondria), whereas succinate-linked respiration was unaffected as seen under tissue hyperoxic conditions (**Figure 33**). Assuming a linear relationship between oxygen concentration and the proportion of complex I in the de-active state, exposing mitochondria to a lower oxygen concentration (≈ 30 µM O_2) should result in a partial shift of complex I from the active into the de-active state enabling the modification of the cysteine residue of the ND3 subunit. Accordingly, the extent of respiration reduction was more pronounced after NEM treatment under tissue normoxia (36 % reduction at 180 µM O_2 vs. 52 % reduction at 30 µM O_2). However, two limitations need to be considered. First, tissue normoxic conditions led to an increased NADH-linked respiration of untreated mitochondria after reoxygenation to tissue hyperoxic levels. Hence, considering the absolute respiration rates, no further reduction of NADH-linked respiration was observable after NEM treatment at tissue

normoxia. Second, the applied oxygen concentrations are still not reflecting the physiological situation. Here, mitochondria are usually exposed to low micromolar oxygen concentrations (≈ 1 µM O_2) [256]. Hence, a reduction from 180 µM to 30 µM oxygen is still not mirroring the physiological condition. To sum up, irreversible thiol modification leads to a decreased NADH-linked respiration, whereas succinate-linked respiration is not affected. However, further studies are needed to gain insight into the role of complex I in NEM-induced impairment of mitochondrial respiration.

Besides this *in vitro* NEM treatment of isolated mitochondria, U-87MG cells were incubated with copper for 24 h and HRR was applied to analyze copper-induced mitochondrial dysfunction (**Figure 35**). Here, preliminary results suggest a reduced oxygen consumption of copper-treated U-87MG cells in NADH-linked respiration in the OXPHOS state compared to untreated cells. Addition of succinate and rotenone, enabling the determination of succinate-linked respiration in the OXPHOS state, revealed only slight differences between copper- and untreated U-87MG cells. As shown for NEM treatment, copper also seems to specifically affect NADH-linked respiration. As cys39 of the ND3 subunit is facing the mitochondrial matrix [224, 258], one prerequisite of copper-induced modification of this thiol residue is the transport of copper into the mitochondrial matrix. Indeed, a low-molecular weight non-proteinaceous copper ligand was described to be present within the mitochondrial matrix [20, 259], but the identity of the ligand is still unclear. Furthermore, the hypothesized copper-induced modification of cys39 assumes that copper is present in an un- or loosely-bound and thereby, reactive form within the matrix. Hence, future studies are needed to clarify whether the stated hypothesis of complex I as a target of copper toxicity holds true and if the oxidation of cys39 contributes to the reduced NADH-linked respiration of copper-treated cells.

5 CONCLUSIONS

The present thesis demonstrates implications of the involvement of brain mitochondria in the pathogenesis of neurologic Wilson disease. In a comparative setting, isolated rat brain mitochondria presented with the highest sensitivity to copper challenges regarding their structure and function compared to organelles isolated from rat liver, kidney and heart. Here, a direct copper-dependent oxidation of mitochondrial free protein thiols was proposed as the major mechanism of mitochondrial copper toxicity in agreement with earlier reports [14, 84]. In contrast to previous hypotheses, an increased production of reactive oxygen species was only a late-stage event, occurring in severely damaged mitochondria. Furthermore, SH-SY5Y mitochondria were identified to be highly susceptible to copper. This was linked to a decreased antioxidative defense system of SH-SY5Y cells. Taken together, brain mitochondria, and even more neuronal mitochondria, seem to be key players in neurologic Wilson disease that present with structural and functional alterations prior to massive ROS production and cell death. Furthermore, their efficient de-coppering might be a promising treatment approach as already demonstrated for the hepatic phenotype of the disease.

The blood-brain barrier was identified as a pivotal target of copper overload. Here, a copper-induced increased permeability of the endothelial cell layer enabled the passage of copper into the basolateral compartment, mimicking the brain parenchyma. This finding implies that blood-brain damage can occur in Wilson disease patients with high levels of non-ceruloplasmin bound copper. The following unrestricted transport of blood components into the parenchyma could lead to the unhindered exposition of neurons to potential toxic agents present in the blood, *e.g.*, loosely-bound copper, but also the entrance of otherwise excluded immune cells and cytokines. However, further studies in neurologic WD patients, as already done in small scale by Stuerenburg [110], are necessary to validate the herein proposed role of the blood-brain barrier in neurologic WD. Importantly, the high-affinity chelator WTX101 prevented the increase in endothelial cell layer permeability by copper, whereas the low-affinity chelator DPA failed to achieve this protective effect.

Finally, first indications for the specific oxidation of protein thiol residues of the mitochondrial complex I by copper were described. This could be of major interest as a decreased activity of complex I was observed in WD animal models [95, 230], but the mechanism is still unclear. Furthermore, as the amount of complex I in its de-active form is higher in the brain compared to the liver [257], the copper-induced modification of cys39 might be organ-specific and limited to the neurological phenotype of Wilson disease.

6 REFERENCES

1. Vander Wende, C. and W.W. Wainio, *The state of the copper in cytochrome c oxidase.* J Biol Chem, 1960. **235**: p. PC11-2.
2. McCord, J.M. and I. Fridovich, *Superoxide dismutase. An enzymic function for erythrocuprein (hemocuprein).* J Biol Chem, 1969. **244**(22): p. 6049-55.
3. Friedman, S. and S. Kaufman, *3,4-dihydroxyphenylethylamine beta-hydroxylase. Physical properties, copper content, and role of copper in the catalytic acttivity.* J Biol Chem, 1965. **240**(12): p. 4763-73.
4. Johnson, P.E., D.B. Milne, and G.I. Lykken, *Effects of age and sex on copper absorption, biological half-life, and status in humans.* Am J Clin Nutr, 1992. **56**(5): p. 917-25.
5. King, J.C., W.L. Raynolds, and S. Margen, *Absorption of stable isotopes of iron, copper, and zinc during oral contraceptives use.* Am J Clin Nutr, 1978. **31**(7): p. 1198-203.
6. Pena, M.M., J. Lee, and D.J. Thiele, *A delicate balance: homeostatic control of copper uptake and distribution.* J Nutr, 1999. **129**(7): p. 1251-60.
7. Gubler, C.J., et al., *Studies on copper metabolism. IX. The transportation of copper in blood.* J Clin Invest, 1953. **32**(5): p. 405-14.
8. Neumann, P.Z. and A. Sass-Kortsak, *The state of copper in human serum: evidence for an amino acid-bound fraction.* J Clin Invest, 1967. **46**(4): p. 646-58.
9. Nose, Y., E.M. Rees, and D.J. Thiele, *Structure of the Ctr1 copper trans'PORE'ter reveals novel architecture.* Trends Biochem Sci, 2006. **31**(11): p. 604-7.
10. Hassett, R. and D.J. Kosman, *Evidence for Cu(II) reduction as a component of copper uptake by Saccharomyces cerevisiae.* J Biol Chem, 1995. **270**(1): p. 128-34.
11. Ohgami, R.S., et al., *The Steap proteins are metalloreductases.* Blood, 2006. **108**(4): p. 1388-94.
12. Wu, F., et al., *Wilson's disease: a comprehensive review of the molecular mechanisms.* Int J Mol Sci, 2015. **16**(3): p. 6419-31.
13. Palida, F.A., et al., *Cytosolic copper-binding proteins in rat and mouse hepatocytes incubated continuously with Cu(II).* Biochem J, 1990. **268**(2): p. 359-66.
14. Saporito-Magrina, C.M., et al., *Copper-induced cell death and the protective role of glutathione: the implication of impaired protein folding rather than oxidative stress.* Metallomics, 2018. **10**(12): p. 1743-1754.
15. Banci, L., et al., *Affinity gradients drive copper to cellular destinations.* Nature, 2010. **465**(7298): p. 645-8.
16. Roelofsen, H., et al., *Copper-induced apical trafficking of ATP7B in polarized hepatoma cells provides a mechanism for biliary copper excretion.* Gastroenterology, 2000. **119**(3): p. 782-93.
17. Lorinczi, E., et al., *Delivery of the Cu-transporting ATPase ATP7B to the plasma membrane in Xenopus oocytes.* Biochim Biophys Acta, 2008. **1778**(4): p. 896-906.
18. Polishchuk, E.V., et al., *Wilson disease protein ATP7B utilizes lysosomal exocytosis to maintain copper homeostasis.* Dev Cell, 2014. **29**(6): p. 686-700.
19. Culotta, V.C., et al., *The copper chaperone for superoxide dismutase.* J Biol Chem, 1997. **272**(38): p. 23469-72.
20. Cobine, P.A., et al., *Yeast contain a non-proteinaceous pool of copper in the mitochondrial matrix.* J Biol Chem, 2004. **279**(14): p. 14447-55.
21. Horn, D. and A. Barrientos, *Mitochondrial copper metabolism and delivery to cytochrome c oxidase.* IUBMB Life, 2008. **60**(7): p. 421-9.
22. Giorgi, C., et al., *Mitochondria and Reactive Oxygen Species in Aging and Age-Related Diseases.* Int Rev Cell Mol Biol, 2018. **340**: p. 209-344.

23. Rae, T.D., et al., *Undetectable intracellular free copper: the requirement of a copper chaperone for superoxide dismutase.* Science, 1999. **284**(5415): p. 805-8.
24. Kim, B.E., T. Nevitt, and D.J. Thiele, *Mechanisms for copper acquisition, distribution and regulation.* Nat Chem Biol, 2008. **4**(3): p. 176-85.
25. Leonard, S.S., G.K. Harris, and X. Shi, *Metal-induced oxidative stress and signal transduction.* Free Radic Biol Med, 2004. **37**(12): p. 1921-42.
26. Altmann, R., *Die Elementarorganismen und ihre Beziehungen zu den Zellen*. 1890: Veit.
27. Palade, G.E., *The fine structure of mitochondria.* Anat Rec, 1952. **114**(3): p. 427-51.
28. Mootha, V.K., et al., *Integrated analysis of protein composition, tissue diversity, and gene regulation in mouse mitochondria.* Cell, 2003. **115**(5): p. 629-40.
29. Fernandez-Vizarra, E., et al., *Tissue-specific differences in mitochondrial activity and biogenesis.* Mitochondrion, 2011. **11**(1): p. 207-13.
30. Alberts, B., *Molecular biology of the cell*. 4th ed. 2002, New York: Garland Science. xxxiv, 1548 p.
31. Dempsey, E.W., *Variations in the structure of mitochondria.* J Biophys Biochem Cytol, 1956. **2**(4 Suppl): p. 305-12.
32. Freeman, J.A., *The ultrastructure of the double membrane systems of micochondria.* J Biophys Biochem Cytol, 1956. **2**(4 Suppl): p. 353-4.
33. Correa, T.D., et al., *Time course of blood lactate levels, inflammation, and mitochondrial function in experimental sepsis.* Crit Care, 2017. **21**(1): p. 105.
34. Fearnley, I.M. and J.E. Walker, *Conservation of sequences of subunits of mitochondrial complex I and their relationships with other proteins.* Biochim Biophys Acta, 1992. **1140**(2): p. 105-34.
35. Walker, J.E., *The NADH:ubiquinone oxidoreductase (complex I) of respiratory chains.* Q Rev Biophys, 1992. **25**(3): p. 253-324.
36. Walker, J.E., J.M. Skehel, and S.K. Buchanan, *Structural analysis of NADH: ubiquinone oxidoreductase from bovine heart mitochondria.* Methods Enzymol, 1995. **260**: p. 14-34.
37. Malatesta, F., et al., *Structure and function of a molecular machine: cytochrome c oxidase.* Biophys Chem, 1995. **54**(1): p. 1-33.
38. Musser, S.M., M.H. Stowell, and S.I. Chan, *Cytochrome c oxidase: chemistry of a molecular machine.* Adv Enzymol Relat Areas Mol Biol, 1995. **71**: p. 79-208.
39. Schultz, B.E. and S.I. Chan, *Structures and proton-pumping strategies of mitochondrial respiratory enzymes.* Annu Rev Biophys Biomol Struct, 2001. **30**: p. 23-65.
40. Xu, T., V. Pagadala, and D.M. Mueller, *Understanding structure, function, and mutations in the mitochondrial ATP synthase.* Microb Cell, 2015. **2**(4): p. 105-125.
41. Mitchell, P., *Coupling of phosphorylation to electron and hydrogen transfer by a chemi-osmotic type of mechanism.* Nature, 1961. **191**: p. 144-8.
42. Chance, B. and G.R. Williams, *Respiratory enzymes in oxidative phosphorylation. I. Kinetics of oxygen utilization.* J Biol Chem, 1955. **217**(1): p. 383-93.
43. Steffens, G.C., R. Biewald, and G. Buse, *Cytochrome c oxidase is a three-copper, two-heme-A protein.* Eur J Biochem, 1987. **164**(2): p. 295-300.
44. Zhen, Y., et al., *Definition of the interaction domain for cytochrome c on cytochrome c oxidase. I. Biochemical, spectral, and kinetic characterization of surface mutants in subunit ii of Rhodobacter sphaeroides cytochrome aa(3).* J Biol Chem, 1999. **274**(53): p. 38032-41.
45. Kaila, V.R., et al., *The chemistry of the CuB site in cytochrome c oxidase and the importance of its unique His-Tyr bond.* Biochim Biophys Acta, 2009. **1787**(4): p. 221-33.
46. Bereiter-Hahn, J. and M. Voth, *Dynamics of mitochondria in living cells: shape changes, dislocations, fusion, and fission of mitochondria.* Microsc Res Tech, 1994. **27**(3): p. 198-219.
47. Wilson, S.A.K., *Progressive Lenticular Degeneration: A Familial Nervous Disease Associated with Cirrhosis of the Liver.* Brain, 1912. **34**(4): p. 295-507.

48. Bearn, A.G., *Genetic and biochemical aspects of Wilson's disease.* Am J Med, 1953. **15**(4): p. 442-9.
49. Cumings, J.N., *The copper and iron content of brain and liver in the normal and in hepato-lenticular degeneration.* Brain, 1948. **71**(Pt. 4): p. 410-5.
50. Haurowitz, F., *Über eine Anomalie des Kupferstoffwechsels*, in *Hoppe-Seyler´s Zeitschrift für physiologische Chemie*. 1930. p. 72.
51. Glazebrook, A.J., *Wilson's Disease.* Edinburgh Medical Journal, 1945. **52**(2): p. 83-87.
52. Frydman, M., et al., *Assignment of the gene for Wilson disease to chromosome 13: linkage to the esterase D locus.* Proc Natl Acad Sci U S A, 1985. **82**(6): p. 1819-21.
53. Bull, P.C., et al., *The Wilson disease gene is a putative copper transporting P-type ATPase similar to the Menkes gene.* Nat Genet, 1993. **5**(4): p. 327-37.
54. Petrukhin, K., et al., *Mapping, cloning and genetic characterization of the region containing the Wilson disease gene.* Nat Genet, 1993. **5**(4): p. 338-43.
55. Tanzi, R.E., et al., *The Wilson disease gene is a copper transporting ATPase with homology to the Menkes disease gene.* Nat Genet, 1993. **5**(4): p. 344-50.
56. Scheinberg, I.H. and D. Gitlin, *Deficiency of ceruloplasmin in patients with hepatolenticular degeneration (Wilson's disease).* Science, 1952. **116**(3018): p. 484-5.
57. Bearn, A.G. and H.G. Kunkel, *Abnormalities of copper metabolism in Wilson's disease and their relationship to the aminoaciduria.* J Clin Invest, 1954. **33**(3): p. 400-9.
58. Ferenci, P., et al., *Diagnostic value of quantitative hepatic copper determination in patients with Wilson's Disease.* Clin Gastroenterol Hepatol, 2005. **3**(8): p. 811-8.
59. Roche-Sicot, J. and J.P. Benhamou, *Acute intravascular hemolysis and acute liver failure associated as a first manifestation of Wilson's disease.* Ann Intern Med, 1977. **86**(3): p. 301-3.
60. Schilsky, M.L., I.H. Scheinberg, and I. Sternlieb, *Prognosis of Wilsonian chronic active hepatitis.* Gastroenterology, 1991. **100**(3): p. 762-7.
61. Ala, A., et al., *Wilson's disease.* Lancet, 2007. **369**(9559): p. 397-408.
62. Bearn, A.G., T.F. Yu, and A.B. Gutman, *Renal function in Wilson's disease.* J Clin Invest, 1957. **36**(7): p. 1107-14.
63. Walshe, J.M., *Cause of death in Wilson disease.* Mov Disord, 2007. **22**(15): p. 2216-20.
64. Hlubocka, Z., et al., *Cardiac involvement in Wilson disease.* J Inherit Metab Dis, 2002. **25**(4): p. 269-77.
65. Kuan, P., *Cardiac Wilson's disease.* Chest, 1987. **91**(4): p. 579-83.
66. Ferenci, P., et al., *Diagnosis and phenotypic classification of Wilson disease.* Liver Int, 2003. **23**(3): p. 139-42.
67. Gollan, J.L. and T.J. Gollan, *Wilson disease in 1998: genetic, diagnostic and therapeutic aspects.* J Hepatol, 1998. **28 Suppl 1**: p. 28-36.
68. Merle, U., et al., *Clinical presentation, diagnosis and long-term outcome of Wilson's disease: a cohort study.* Gut, 2007. **56**(1): p. 115-20.
69. Stremmel, W., et al., *Wilson disease: clinical presentation, treatment, and survival.* Ann Intern Med, 1991. **115**(9): p. 720-6.
70. Mikol, J., et al., *Extensive cortico-subcortical lesions in Wilson's disease: clinico-pathological study of two cases.* Acta Neuropathol, 2005. **110**(5): p. 451-8.
71. Yang, X., et al., *Prospective evaluation of the diagnostic accuracy of hepatic copper content, as determined using the entire core of a liver biopsy sample.* Hepatology, 2015. **62**(6): p. 1731-41.
72. Halliwell, B. and J.M. Gutteridge, *Role of free radicals and catalytic metal ions in human disease: an overview.* Methods Enzymol, 1990. **186**: p. 1-85.
73. Gunther, M.R., et al., *Hydroxyl radical formation from cuprous ion and hydrogen peroxide: a spin-trapping study.* Arch Biochem Biophys, 1995. **316**(1): p. 515-22.

74. Huster, D., *Structural and metabolic changes in Atp7b-/- mouse liver and potential for new interventions in Wilson's disease.* Ann N Y Acad Sci, 2014. **1315**: p. 37-44.
75. Nair, J., et al., *Lipid peroxidation-induced etheno-DNA adducts in the liver of patients with the genetic metal storage disorders Wilson's disease and primary hemochromatosis.* Cancer Epidemiol Biomarkers Prev, 1998. **7**(5): p. 435-40.
76. Summer, K.H. and J. Eisenburg, *Low content of hepatic reduced glutathione in patients with Wilson's disease.* Biochem Med, 1985. **34**(1): p. 107-11.
77. Wu, J., et al., *The LEC rat has a deletion in the copper transporting ATPase gene homologous to the Wilson disease gene.* Nat Genet, 1994. **7**(4): p. 541-5.
78. Yamada, T., et al., *Elevation of the level of lipid peroxidation associated with hepatic injury in LEC mutant rat.* Res Commun Chem Pathol Pharmacol, 1992. **77**(1): p. 121-4.
79. Yasuda, J., et al., *Reactive oxygen species modify oligosaccharides of glycoproteins in vivo: a study of a spontaneous acute hepatitis model rat (LEC rat).* Biochem Biophys Res Commun, 2006. **342**(1): p. 127-34.
80. Yamamoto, H., et al., *Mechanism of enhanced lipid peroxidation in the liver of Long-Evans cinnamon (LEC) rats.* Arch Toxicol, 1999. **73**(8-9): p. 457-64.
81. Boulard, M., K.G. Blume, and E. Beutler, *The effect of copper on red cell enzyme activities.* J Clin Invest, 1972. **51**(2): p. 459-61.
82. Letelier, M.E., et al., *Possible mechanisms underlying copper-induced damage in biological membranes leading to cellular toxicity.* Chem Biol Interact, 2005. **151**(2): p. 71-82.
83. Vasic, V., et al., *Prevention and recovery of CuSO4-induced inhibition of Na+/K+ -ATPase and Mg2+ -ATPase in rat brain synaptosomes by EDTA.* Toxicol Lett, 1999. **110**(1-2): p. 95-104.
84. Zischka, H., et al., *Liver mitochondrial membrane crosslinking and destruction in a rat model of Wilson disease.* J Clin Invest, 2011. **121**(4): p. 1508-18.
85. Lichtmannegger, J., et al., *Methanobactin reverses acute liver failure in a rat model of Wilson disease.* J Clin Invest, 2016. **126**(7): p. 2721-35.
86. Sokol, R.J., et al., *Oxidant injury to hepatic mitochondria in patients with Wilson's disease and Bedlington terriers with copper toxicosis.* Gastroenterology, 1994. **107**(6): p. 1788-98.
87. Zischka, H. and S. Borchard, *Mitochondrial Copper Toxicity with a Focus on Wilson Disease*, in *Clinical and Translational Perspectives on WILSON DISEASE*, N. Kerkar and E.A. Roberts, Editors. 2018, Elsevier Science.
88. Roberts, E.A., B.H. Robinson, and S. Yang, *Mitochondrial structure and function in the untreated Jackson toxic milk (tx-j) mouse, a model for Wilson disease.* Mol Genet Metab, 2008. **93**(1): p. 54-65.
89. Einer, C., et al., *A High-Calorie Diet Aggravates Mitochondrial Dysfunction and Triggers Severe Liver Damage in Wilson Disease Rats.* Cell Mol Gastroenterol Hepatol, 2019. **7**(3): p. 571-596.
90. Sternlieb, I., et al., *An array of mitochondrial alterations in the hepatocytes of Long-Evans Cinnamon rats.* Hepatology, 1995. **22**(6): p. 1782-7.
91. Sternlieb, I., *Mitochondrial and fatty changes in hepatocytes of patients with Wilson's disease.* Gastroenterology, 1968. **55**(3): p. 354-67.
92. Sternlieb, I. and G. Feldmann, *Effects of anticopper therapy on hepatocellular mitochondria in patients with Wilson's disease: an ultrastructural and stereological study.* Gastroenterology, 1976. **71**(3): p. 457-61.
93. Shawky, R.M., et al., *Mitochondrial alterations in children with chronic liver disease.* Egyptian Journal of Medical Human Genetics, 2010. **11**(2): p. 143-151.
94. Sauer, S.W., et al., *Severe dysfunction of respiratory chain and cholesterol metabolism in Atp7b(-/-) mice as a model for Wilson disease.* Biochim Biophys Acta, 2011. **1812**(12): p. 1607-15.

95. Gu, M., et al., *Oxidative-phosphorylation defects in liver of patients with Wilson's disease.* Lancet, 2000. **356**(9228): p. 469-74.
96. Davies, K.M., et al., *Localization of copper and copper transporters in the human brain.* Metallomics, 2013. **5**(1): p. 43-51.
97. Telianidis, J., et al., *Role of the P-Type ATPases, ATP7A and ATP7B in brain copper homeostasis.* Front Aging Neurosci, 2013. **5**: p. 44.
98. Scheinberg, I.H. and I. Sternlieb, *Wilson's disease*. Major problems in internal medicine. 1984, Philadelphia: Saunders. xii, 171 p., 2 leaves of plates.
99. Horoupian, D.S., I. Sternlieb, and I.H. Scheinberg, *Neuropathological findings in penicillamine-treated patients with Wilson's disease.* Clin Neuropathol, 1988. **7**(2): p. 62-7.
100. Faa, G., et al., *Brain copper, iron, magnesium, zinc, calcium, sulfur and phosphorus storage in Wilson's disease.* J Trace Elem Med Biol, 2001. **15**(2-3): p. 155-60.
101. Litwin, T., et al., *Brain metal accumulation in Wilson's disease.* J Neurol Sci, 2013. **329**(1-2): p. 55-8.
102. Prashanth, L.K., et al., *Wilson's disease: diagnostic errors and clinical implications.* J Neurol Neurosurg Psychiatry, 2004. **75**(6): p. 907-9.
103. Muller, S.M., et al., *Effects of arsenolipids on in vitro blood-brain barrier model.* Arch Toxicol, 2018. **92**(2): p. 823-832.
104. Walshe, J.M., *Wilson's disease. The presenting symptoms.* Arch Dis Child, 1962. **37**: p. 253-6.
105. Aggarwal, A., et al., *A novel Global Assessment Scale for Wilson's Disease (GAS for WD).* Mov Disord, 2009. **24**(4): p. 509-18.
106. Dastur, D.K., D.K. Manghani, and N.H. Wadia, *Wilson's disease in India. I. Geographic, genetic, and clinical aspects in 16 families.* Neurology, 1968. **18**(1 Pt 1): p. 21-31.
107. Oder, W., et al., *Neurological and neuropsychiatric spectrum of Wilson's disease: a prospective study of 45 cases.* J Neurol, 1991. **238**(5): p. 281-7.
108. Dusek, P., et al., *The neurotoxicity of iron, copper and manganese in Parkinson's and Wilson's diseases.* J Trace Elem Med Biol, 2015. **31**: p. 193-203.
109. Poujois, A., et al., *Exchangeable copper: a reflection of the neurological severity in Wilson's disease.* Eur J Neurol, 2017. **24**(1): p. 154-160.
110. Stuerenburg, H.J., *CSF copper concentrations, blood-brain barrier function, and coeruloplasmin synthesis during the treatment of Wilson's disease.* J Neural Transm (Vienna), 2000. **107**(3): p. 321-9.
111. Vergun, O., K.E. Dineley, and I.J. Reynolds, *4.7 Ion Transport and Energy Metabolism*, in *Handbook of Neurochemistry and Molecular Neurobiology: Brain Energetics. Integration of Molecular and Cellular Processes*, A. Lajtha, G.E. Gibson, and G.A. Dienel, Editors. 2007, Springer US: Boston, MA. p. 429-465.
112. Vogel, F.S. and J.W. Evans, *Morphologic alterations produced by copper in neural tissues with consideration of the role of the metal in the pathogenesis of Wilson's disease.* J Exp Med, 1961. **113**: p. 997-1004.
113. Vogel, F.S. and L. Kemper, *In vitro acceleration of respiratory activity of neural tissues by copper.* Lab Invest, 1961. **10**: p. 883-91.
114. Vogel, F.S. and L. Kemper, *Biochemical reactions of copper within neural mitochondria, with consideration of the role of the metal in the pathogenesis of Wilson's disease.* Lab Invest, 1963. **12**: p. 171-9.
115. Hayashi, M., et al., *Accumulation of copper induces DNA strand breaks in brain cells of Long-Evans Cinnamon (LEC) rats, an animal model for human Wilson Disease.* Exp Anim, 2006. **55**(5): p. 419-26.
116. Terwel, D., et al., *Neuroinflammatory and behavioural changes in the Atp7B mutant mouse model of Wilson's disease.* J Neurochem, 2011. **118**(1): p. 105-12.

117. Ono, S., D.J. Koropatnick, and M.G. Cherian, *Regional brain distribution of metallothionein, zinc and copper in toxic milk mutant and transgenic mice.* Toxicology, 1997. **124**(1): p. 1-10.
118. Przybylkowski, A., et al., *Neurochemical and behavioral characteristics of toxic milk mice: an animal model of Wilson's disease.* Neurochem Res, 2013. **38**(10): p. 2037-45.
119. EASL, *EASL Clinical Practice Guidelines: Wilson's disease.* J Hepatol, 2012. **56**(3): p. 671-85.
120. Roberts, E.A., M.L. Schilsky, and D. American Association for Study of Liver, *Diagnosis and treatment of Wilson disease: an update.* Hepatology, 2008. **47**(6): p. 2089-111.
121. Hoogenraad, T.U., et al., *Oral zinc in Wilson's disease.* Lancet, 1978. **2**(8102): p. 1262.
122. Yuzbasiyan-Gurkan, V., et al., *Treatment of Wilson's disease with zinc: X. Intestinal metallothionein induction.* J Lab Clin Med, 1992. **120**(3): p. 380-6.
123. Sturniolo, G.C., et al., *Zinc therapy increases duodenal concentrations of metallothionein and iron in Wilson's disease patients.* Am J Gastroenterol, 1999. **94**(2): p. 334-8.
124. Brewer, G.J., et al., *The treatment of Wilson's disease with zinc. IV. Efficacy monitoring using urine and plasma copper.* Proc Soc Exp Biol Med, 1987. **184**(4): p. 446-55.
125. Czlonkowska, A., J. Gajda, and M. Rodo, *Effects of long-term treatment in Wilson's disease with D-penicillamine and zinc sulphate.* J Neurol, 1996. **243**(3): p. 269-73.
126. Wiggelinkhuizen, M., et al., *Systematic review: clinical efficacy of chelator agents and zinc in the initial treatment of Wilson disease.* Aliment Pharmacol Ther, 2009. **29**(9): p. 947-58.
127. Walshe, J.M., *Treatment of Wilson's disease with penicillamine.* Lancet, 1960. **1**(7117): p. 188-92.
128. Weiss, K.H., et al., *Efficacy and safety of oral chelators in treatment of patients with Wilson disease.* Clin Gastroenterol Hepatol, 2013. **11**(8): p. 1028-35 e1-2.
129. Walshe, J.M., *Penicillamine, a new oral therapy for Wilson's disease.* Am J Med, 1956. **21**(4): p. 487-95.
130. Scheinberg, I.H. and I. Sternlieb, *The long term management of hepatolenticular degeneration (Wilson's disease).* Am J Med, 1960. **29**: p. 316-33.
131. Czlonkowska, A., et al., *D-penicillamine versus zinc sulfate as first-line therapy for Wilson's disease.* Eur J Neurol, 2014. **21**(4): p. 599-606.
132. Davison, A.M., et al., *Effect of penicillamine on the kidney.* Proc R Soc Med, 1977. **70 Suppl 3**: p. 109-13.
133. Hall, C.L., et al., *Natural course of penicillamine nephropathy: a long term study of 33 patients.* Br Med J (Clin Res Ed), 1988. **296**(6629): p. 1083-6.
134. Brewer, G.J. and F.K. Askari, *Wilson's disease: clinical management and therapy.* J Hepatol, 2005. **42 Suppl**(1): p. S13-21.
135. Kalita, J., et al., *Worsening of Wilson disease following penicillamine therapy.* Eur Neurol, 2014. **71**(3-4): p. 126-31.
136. Litwin, T., et al., *Early neurological worsening in patients with Wilson's disease.* J Neurol Sci, 2015. **355**(1-2): p. 162-7.
137. Chen, D.B., et al., *Penicillamine increases free copper and enhances oxidative stress in the brain of toxic milk mice.* PLoS One, 2012. **7**(5): p. e37709.
138. Brewer, G.J., et al., *Treatment of Wilson disease with ammonium tetrathiomolybdate: IV. Comparison of tetrathiomolybdate and trientine in a double-blind study of treatment of the neurologic presentation of Wilson disease.* Arch Neurol, 2006. **63**(4): p. 521-7.
139. Walshe, J.M., *Management of penicillamine nephropathy in Wilson's disease: a new chelating agent.* Lancet, 1969. **2**(7635): p. 1401-2.
140. Siegemund, R., et al., *Mode of action of triethylenetetramine dihydrochloride on copper metabolism in Wilson's disease.* Acta Neurol Scand, 1991. **83**(6): p. 364-6.
141. Gibbs, K. and J.M. Walshe, *Liver copper concentration in Wilson's disease: effect of treatment with 'anti-copper' agents.* J Gastroenterol Hepatol, 1990. **5**(4): p. 420-4.

142. Iseki, K., et al., *Comparison of disposition behavior and de-coppering effect of triethylenetetramine in animal model for Wilson's disease (Long-Evans Cinnamon rat) with normal Wistar rat.* Biopharm Drug Dispos, 1992. **13**(4): p. 273-83.
143. Walshe, J.M., *Tetrathiomolybdate (MoS4) as an'anti-copper'agent in man.* IN:" Orphan Drugs and Orphan Diseases, 1986: p. 76-85.
144. Ogra, Y. and K.T. Suzuki, *Removal and efflux of copper from Cu-metallothionein as Cu/tetrathiomolybdate complex in LEC rats.* Res Commun Mol Pathol Pharmacol, 1995. **88**(2): p. 196-204.
145. Weiss, K.H., et al., *Bis-choline tetrathiomolybdate in patients with Wilson's disease: an open-label, multicentre, phase 2 study.* Lancet Gastroenterol Hepatol, 2017. **2**(12): p. 869-876.
146. Weiss, K.H., et al., *WTX101 - an investigational drug for the treatment of Wilson disease.* Expert Opin Investig Drugs, 2018. **27**(6): p. 561-567.
147. Eghtesad, B., et al., *Liver transplantation for Wilson's disease: a single-center experience.* Liver Transpl Surg, 1999. **5**(6): p. 467-74.
148. Emre, S., et al., *Orthotopic liver transplantation for Wilson's disease: a single-center experience.* Transplantation, 2001. **72**(7): p. 1232-6.
149. Guillaud, O., et al., *Long term results of liver transplantation for Wilson's disease: experience in France.* J Hepatol, 2014. **60**(3): p. 579-89.
150. Schilsky, M.L., I.H. Scheinberg, and I. Sternlieb, *Liver transplantation for Wilson's disease: indications and outcome.* Hepatology, 1994. **19**(3): p. 583-7.
151. Weiss, K.H., et al., *Outcome and development of symptoms after orthotopic liver transplantation for Wilson disease.* Clin Transplant, 2013. **27**(6): p. 914-22.
152. Ohya, Y., et al., *Re-evaluation of the indications for liver transplantation in Wilson's disease based on the outcomes of patients referred to a transplant center.* Pediatr Transplant, 2013. **17**(4): p. 369-73.
153. Rodriguez-Castro, K.I., F.J. Hevia-Urrutia, and G.C. Sturniolo, *Wilson's disease: A review of what we have learned.* World J Hepatol, 2015. **7**(29): p. 2859-70.
154. Schilsky, M.L., *Liver transplantation for Wilson's disease.* Ann N Y Acad Sci, 2014. **1315**: p. 45-9.
155. Sutcliffe, R.P., et al., *Liver transplantation for Wilson's disease: long-term results and quality-of-life assessment.* Transplantation, 2003. **75**(7): p. 1003-6.
156. Medici, V., et al., *Liver transplantation for Wilson's disease: The burden of neurological and psychiatric disorders.* Liver Transpl, 2005. **11**(9): p. 1056-63.
157. Yagci, M.A., et al., *Influence of Liver Transplantation on Neuropsychiatric Manifestations of Wilson Disease.* Transplant Proc, 2015. **47**(5): p. 1469-73.
158. Groth, C.G., et al., *Metabolic effects of hepatic replacement in Wilson's disease.* Transplant Proc, 1973. **5**(1): p. 829-33.
159. Ahmed, S., J. Deng, and J. Borjigin, *A new strain of rat for functional analysis of PINA.* Brain Res Mol Brain Res, 2005. **137**(1-2): p. 63-9.
160. Aden, D.P., et al., *Controlled synthesis of HBsAg in a differentiated human liver carcinoma-derived cell line.* Nature, 1979. **282**(5739): p. 615-6.
161. Ponten, J. and E.H. Macintyre, *Long term culture of normal and neoplastic human glia.* Acta Pathol Microbiol Scand, 1968. **74**(4): p. 465-86.
162. Ross, R.A., B.A. Spengler, and J.L. Biedler, *Coordinate morphological and biochemical interconversion of human neuroblastoma cells.* J Natl Cancer Inst, 1983. **71**(4): p. 741-7.
163. Edgell, C.J., C.C. McDonald, and J.B. Graham, *Permanent cell line expressing human factor VIII-related antigen established by hybridization.* Proc Natl Acad Sci U S A, 1983. **80**(12): p. 3734-7.
164. Das, A., N.L. Banik, and S.K. Ray, *Retinoids induced astrocytic differentiation with down regulation of telomerase activity and enhanced sensitivity to taxol for apoptosis in human glioblastoma T98G and U87MG cells.* J Neurooncol, 2008. **87**(1): p. 9-22.

165. Encinas, M., et al., *Sequential treatment of SH-SY5Y cells with retinoic acid and brain-derived neurotrophic factor gives rise to fully differentiated, neurotrophic factor-dependent, human neuron-like cells.* J Neurochem, 2000. **75**(3): p. 991-1003.
166. Knopfel, M. and M. Solioz, *Characterization of a cytochrome b(558) ferric/cupric reductase from rabbit duodenal brush border membranes.* Biochem Biophys Res Commun, 2002. **291**(2): p. 220-5.
167. Ciriolo, M.R., et al., *Reconstitution of Cu,Zn-superoxide dismutase by the Cu(I).glutathione complex.* J Biol Chem, 1990. **265**(19): p. 11030-4.
168. Brose, J., et al., *Redox sulfur chemistry of the copper chaperone Atox1 is regulated by the enzyme glutaredoxin 1, the reduction potential of the glutathione couple GSSG/2GSH and the availability of Cu(I).* Metallomics, 2014. **6**(4): p. 793-808.
169. Speisky, H., et al., *Generation of superoxide radicals by copper-glutathione complexes: redox-consequences associated with their interaction with reduced glutathione.* Bioorg Med Chem, 2009. **17**(5): p. 1803-10.
170. Lai, J.C. and J.P. Blass, *Neurotoxic effects of copper: inhibition of glycolysis and glycolytic enzymes.* Neurochem Res, 1984. **9**(12): p. 1699-710.
171. Hoppe-Tichy, T., et al., *[Manufacturing and stability of copper-histidine solution for treatment of Menkes' Kinky Hair Syndrome].* Pharmazie, 2005. **60**(3): p. 205-7.
172. Repetto, G., A. del Peso, and J.L. Zurita, *Neutral red uptake assay for the estimation of cell viability/cytotoxicity.* Nat Protoc, 2008. **3**(7): p. 1125-31.
173. Strober, W., *Trypan Blue Exclusion Test of Cell Viability.* Curr Protoc Immunol, 2015. **111**: p. A3 B 1-3.
174. Schmitt, S., et al., *A semi-automated method for isolating functionally intact mitochondria from cultured cells and tissue biopsies.* Analytical Biochemistry, 2013. **443**(1): p. 66-74.
175. Schulz, S., et al., *A protocol for the parallel isolation of intact mitochondria from rat liver, kidney, heart, and brain.* Methods Mol Biol, 2015. **1295**: p. 75-86.
176. Zhou, M., et al., *A stable nonfluorescent derivative of resorufin for the fluorometric determination of trace hydrogen peroxide: applications in detecting the activity of phagocyte NADPH oxidase and other oxidases.* Anal Biochem, 1997. **253**(2): p. 162-8.
177. Zamzami, N., D. Metivier, and G. Kroemer, *Quantitation of mitochondrial transmembrane potential in cells and in isolated mitochondria.* Methods Enzymol, 2000. **322**: p. 208-13.
178. Bernardi, P., et al., *Modulation of the mitochondrial permeability transition pore. Effect of protons and divalent cations.* J Biol Chem, 1992. **267**(5): p. 2934-9.
179. Schulz, S., et al., *Progressive stages of mitochondrial destruction caused by cell toxic bile salts.* Biochim Biophys Acta, 2013. **1828**(9): p. 2121-33.
180. Rahman, I., A. Kode, and S.K. Biswas, *Assay for quantitative determination of glutathione and glutathione disulfide levels using enzymatic recycling method.* Nat Protoc, 2006. **1**(6): p. 3159-65.
181. Ellman, G. and H. Lysko, *A precise method for the determination of whole blood and plasma sulfhydryl groups.* Anal Biochem, 1979. **93**(1): p. 98-102.
182. Pesta, D. and E. Gnaiger, *High-resolution respirometry: OXPHOS protocols for human cells and permeabilized fibers from small biopsies of human muscle.* Methods Mol Biol, 2012. **810**: p. 25-58.
183. Spinazzi, M., et al., *Assessment of mitochondrial respiratory chain enzymatic activities on tissues and cultured cells.* Nat Protoc, 2012. **7**(6): p. 1235-46.
184. Schulz, T.J., et al., *Induction of oxidative metabolism by mitochondrial frataxin inhibits cancer growth: Otto Warburg revisited.* J Biol Chem, 2006. **281**(2): p. 977-81.

185. Franke, H., H.J. Galla, and C.T. Beuckmann, *An improved low-permeability in vitro-model of the blood-brain barrier: transport studies on retinoids, sucrose, haloperidol, caffeine and mannitol.* Brain Res, 1999. **818**(1): p. 65-71.
186. Bornhorst, J., et al., *Impact of manganese on and transfer across blood-brain and blood-cerebrospinal fluid barrier in vitro.* J Biol Chem, 2012. **287**(21): p. 17140-51.
187. Marschall, T.A., et al., *Differing cytotoxicity and bioavailability of selenite, methylselenocysteine, selenomethionine, selenosugar 1 and trimethylselenonium ion and their underlying metabolic transformations in human cells.* Mol Nutr Food Res, 2016. **60**(12): p. 2622-2632.
188. Meyer, S., et al., *In vitro toxicological characterisation of three arsenic-containing hydrocarbons.* Metallomics, 2014. **6**(5): p. 1023-33.
189. Towbin, H., T. Staehelin, and J. Gordon, *Electrophoretic transfer of proteins from polyacrylamide gels to nitrocellulose sheets: procedure and some applications.* Proceedings of the National Academy of Sciences of the United States of America, 1979. **76**(9): p. 4350-4354.
190. Mizzen, C.A., et al., *Sensitive detection of metallothioneins-1, -2 and -3 in tissue homogenates by immunoblotting: a method for enhanced membrane transfer and retention.* J Biochem Biophys Methods, 1996. **32**(2): p. 77-83.
191. Elbashir, A., *A New Spectrophotometric Method for Determination of Penicillamine in Pharmaceutical Formulation Using 1, 2-naphthoquine-4-sulfonate (NQS)*. Vol. 01. 2013.
192. Krug, M., et al., *XDSAPP: a graphical user interface for the convenient processing of diffraction data using XDS.* Journal of Applied Crystallography, 2012. **45**: p. 568-572.
193. Kabsch, W., *Xds.* Acta Crystallogr D Biol Crystallogr, 2010. **66**(Pt 2): p. 125-32.
194. Evans, P., *Scaling and assessment of data quality.* Acta Crystallogr D Biol Crystallogr, 2006. **62**(Pt 1): p. 72-82.
195. McCoy, A.J., *Acknowledging Errors: Advanced Molecular Replacement with Phaser.* Methods Mol Biol, 2017. **1607**: p. 421-453.
196. Bujacz, A., *Structures of bovine, equine and leporine serum albumin.* Acta Crystallogr D Biol Crystallogr, 2012. **68**(Pt 10): p. 1278-89.
197. Emsley, P., et al., *Features and development of Coot.* Acta Crystallographica Section D-Biological Crystallography, 2010. **66**: p. 486-501.
198. Bradford, M.M., *A rapid and sensitive method for the quantitation of microgram quantities of protein utilizing the principle of protein-dye binding.* Anal Biochem, 1976. **72**: p. 248-54.
199. Schulz, S., et al., *The Parallel Testing of Isolated Rat Liver and Kidney Mitochondria Reveals a Calcium-Dependent Sensitivity to Diclofenac and Ibuprofen*, in *Mitochondrial Dysfunction Caused by Drugs and Environmental Toxicants*, Y. Will and J.A. Dykens, Editors. 2018, John Wiley & Sons, Inc.
200. Hunter, D.R. and R.A. Haworth, *The Ca2+-induced membrane transition in mitochondria. I. The protective mechanisms.* Arch Biochem Biophys, 1979. **195**(2): p. 453-9.
201. Borchard, S., et al., *The exceptional sensitivity of brain mitochondria to copper.* Toxicology in Vitro, 2018. **51**: p. 11-22.
202. Vogt, A., *Kupfer und silber aufgespeichert in auge, leber, milz und nieren als symptom der pseudosklerose*. Klin. Mbl. Augenheilk. Vol. 83. 1929. 417-419.
203. Rumpel, A., *Über das Wesen und die Bedeutung der Leberveränderungen und der Pigmentierungen bei den damit verbundenen Fällen von Pseudosklerose, zugleich ein Beitrag zur Lehre von der Pseudosklerose (Westphal-Strümpell).* Deutsche Zeitschrift für Nervenheilkunde, 1913. **49**(1): p. 54-73.
204. Sternlieb, I., *Fraternal concordance of types of abnormal hepatocellular mitochondria in Wilson's disease.* Hepatology, 1992. **16**(3): p. 728-32.

205. Chutkow, J.G., *Evidence for uptake of nonceruloplasminic copper in the brain: effect of ionic copper and amino acids.* Proc Soc Exp Biol Med, 1978. **158**(1): p. 113-6.
206. Nagasaka, H., et al., *Relationship between oxidative stress and antioxidant systems in the liver of patients with Wilson disease: hepatic manifestation in Wilson disease as a consequence of augmented oxidative stress.* Pediatr Res, 2006. **60**(4): p. 472-7.
207. Mari, M., et al., *Mitochondrial glutathione: features, regulation and role in disease.* Biochim Biophys Acta, 2013. **1830**(5): p. 3317-28.
208. Shipley, M.M., C.A. Mangold, and M.L. Szpara, *Differentiation of the SH-SY5Y Human Neuroblastoma Cell Line.* J Vis Exp, 2016(108): p. 53193.
209. Xing, F., et al., *The Anti-Warburg Effect Elicited by the cAMP-PGC1alpha Pathway Drives Differentiation of Glioblastoma Cells into Astrocytes.* Cell Rep, 2017. **18**(2): p. 468-481.
210. Tapia, L., et al., *Metallothionein is crucial for safe intracellular copper storage and cell survival at normal and supra-physiological exposure levels.* Biochem J, 2004. **378**(Pt 2): p. 617-24.
211. Riha, M., et al., *Novel method for rapid copper chelation assessment confirmed low affinity of D-penicillamine for copper in comparison with trientine and 8-hydroxyquinolines.* J Inorg Biochem, 2013. **123**: p. 80-7.
212. Smirnova, J., et al., *Copper(I)-binding properties of de-coppering drugs for the treatment of Wilson disease. alpha-Lipoic acid as a potential anti-copper agent.* Sci Rep, 2018. **8**(1): p. 1463.
213. Kojimahara, N., et al., *Defective copper binding to apo-ceruloplasmin in a rat model and patients with Wilson's disease.* Liver, 1995. **15**(3): p. 135-42.
214. Eom, J.E., et al., *Development of an albumin copper binding (ACuB) assay to detect ischemia modified albumin.* Anal Sci, 2014. **30**(10): p. 985-90.
215. Zgirski, A. and E. Frieden, *Binding of Cu(II) to non-prosthetic sites in ceruloplasmin and bovine serum albumin.* J Inorg Biochem, 1990. **39**(2): p. 137-48.
216. Greene, C., N. Hanley, and M. Campbell, *Claudin-5: gatekeeper of neurological function.* Fluids Barriers CNS, 2019. **16**(1): p. 3.
217. Fanning, A.S., et al., *The tight junction protein ZO-1 establishes a link between the transmembrane protein occludin and the actin cytoskeleton.* J Biol Chem, 1998. **273**(45): p. 29745-53.
218. Yurkova, I.L., et al., *Fragmentation of mitochondrial cardiolipin by copper ions in the Atp7b-/- mouse model of Wilson's disease.* Chem Phys Lipids, 2011. **164**(5): p. 393-400.
219. Verheul, F.E., et al., *The reactivity of thiol groups in bovine heart cytochrome c oxidase towards 5,5'-dithiobis(2-nitrobenzoic acid).* Biochim Biophys Acta, 1982. **681**(1): p. 118-29.
220. Danielson, S.R., et al., *Quantitative mapping of reversible mitochondrial Complex I cysteine oxidation in a Parkinson disease mouse model.* J Biol Chem, 2011. **286**(9): p. 7601-8.
221. Hill, B.G., et al., *Methods for the determination and quantification of the reactive thiol proteome.* Free Radic Biol Med, 2009. **47**(6): p. 675-83.
222. Kotlyar, A.B. and A.D. Vinogradov, *Slow active/inactive transition of the mitochondrial NADH-ubiquinone reductase.* Biochim Biophys Acta, 1990. **1019**(2): p. 151-8.
223. Vinogradov, A.D., *Catalytic properties of the mitochondrial NADH-ubiquinone oxidoreductase (complex I) and the pseudo-reversible active/inactive enzyme transition.* Biochim Biophys Acta, 1998. **1364**(2): p. 169-85.
224. Galkin, A., et al., *Identification of the mitochondrial ND3 subunit as a structural component involved in the active/deactive enzyme transition of respiratory complex I.* J Biol Chem, 2008. **283**(30): p. 20907-13.
225. Sternlieb, I., *Electron microscopy of mitochondria and peroxisomes of human hepatocytes.* Prog Liver Dis, 1979. **6**: p. 81-104.

226. Kobayashi, T., et al., *Calcium-induced mitochondrial swelling and cytochrome c release in the brain: its biochemical characteristics and implication in ischemic neuronal injury.* Brain Res, 2003. **960**(1-2): p. 62-70.
227. Kristian, T., et al., *Characteristics of the calcium-triggered mitochondrial permeability transition in nonsynaptic brain mitochondria: effect of cyclosporin A and ubiquinone O.* J Neurochem, 2000. **74**(5): p. 1999-2009.
228. Zischka, H., et al., *Electrophoretic analysis of the mitochondrial outer membrane rupture induced by permeability transition.* Anal Chem, 2008. **80**(13): p. 5051-8.
229. Nicholls, D.G. and S.J. Ferguson, *Bioenergetics 2*, ed. D.G. Nicholls and S.J. Ferguson. 1992: Academic Press. 255.
230. Hosseini, M.J., et al., *Toxicity of copper on isolated liver mitochondria: impairment at complexes I, II, and IV leads to increased ROS production.* Cell Biochem Biophys, 2014. **70**(1): p. 367-81.
231. Korshunov, S.S., V.P. Skulachev, and A.A. Starkov, *High protonic potential actuates a mechanism of production of reactive oxygen species in mitochondria.* FEBS Lett, 1997. **416**(1): p. 15-8.
232. Murphy, M.P., *How mitochondria produce reactive oxygen species.* Biochem J, 2009. **417**(1): p. 1-13.
233. Nakamura, M. and I. Yamazaki, *One-electron transfer reactions in biochemical systems. VI. Changes in electron transfer mechanism of lipoamide dehydrogenase by modification of sulfhydryl groups.* Biochim Biophys Acta, 1972. **267**(2): p. 249-57.
234. Davies, M.J., *Protein oxidation and peroxidation.* Biochem J, 2016. **473**(7): p. 805-25.
235. Mirzaei, H. and F. Regnier, *Creation of allotypic active sites during oxidative stress.* J Proteome Res, 2006. **5**(9): p. 2159-68.
236. Rebrin, I. and R.S. Sohal, *Comparison of thiol redox state of mitochondria and homogenates of various tissues between two strains of mice with different longevities.* Exp Gerontol, 2004. **39**(10): p. 1513-9.
237. Requejo, R., et al., *Cysteine residues exposed on protein surfaces are the dominant intramitochondrial thiol and may protect against oxidative damage.* FEBS J, 2010. **277**(6): p. 1465-80.
238. Stanger, B.Z., *Cellular homeostasis and repair in the mammalian liver.* Annu Rev Physiol, 2015. **77**: p. 179-200.
239. Arciello, M., G. Rotilio, and L. Rossi, *Copper-dependent toxicity in SH-SY5Y neuroblastoma cells involves mitochondrial damage.* Biochem Biophys Res Commun, 2005. **327**(2): p. 454-9.
240. Aschner, M., *The functional significance of brain metallothioneins.* FASEB J, 1996. **10**(10): p. 1129-36.
241. Thirumoorthy, N., et al., *A review of metallothionein isoforms and their role in pathophysiology.* World J Surg Oncol, 2011. **9**: p. 54.
242. West, A.K., et al., *Metallothionein in the central nervous system: Roles in protection, regeneration and cognition.* Neurotoxicology, 2008. **29**(3): p. 489-503.
243. Walshe, J.M. and M. Yealland, *Wilson's disease: the problem of delayed diagnosis.* J Neurol Neurosurg Psychiatry, 1992. **55**(8): p. 692-6.
244. Walshe, J.M., *The pattern of urinary copper excretion and its response to treatment in patients with Wilson's disease.* QJM, 2011. **104**(9): p. 775-8.
245. Butler, M., et al., *Pharmacokinetics of reduced D-penicillamine in patients with rheumatoid arthritis.* Arthritis Rheum, 1982. **25**(1): p. 111-6.
246. Laurie, S.H. and D.M. Prime, *The formation and nature of the mixed valence copper-D-penicillamine-chloride cluster in aqueous solution and its relevance to the treatment of Wilson's disease.* J Inorg Biochem, 1979. **11**(3): p. 229-39.

247. Quagraine, E.K. and R.S. Reid, *UV/visible spectrophotometric studies of the interactions of thiomolybdates, copper(II) and other ligands.* J Inorg Biochem, 2001. **85**(1): p. 53-60.
248. McArdle, H.J., et al., *The effect of D-penicillamine on metallothionein mRNA levels and copper distribution in mouse hepatocytes.* Chem Biol Interact, 1990. **75**(3): p. 315-24.
249. Doll, D.N., et al., *Mitochondrial crisis in cerebrovascular endothelial cells opens the blood-brain barrier.* Stroke, 2015. **46**(6): p. 1681-9.
250. Grab, D.J., et al., *Borrelia burgdorferi, host-derived proteases, and the blood-brain barrier.* Infect Immun, 2005. **73**(2): p. 1014-22.
251. Oldendorf, W.H., M.E. Cornford, and W.J. Brown, *The large apparent work capability of the blood-brain barrier: a study of the mitochondrial content of capillary endothelial cells in brain and other tissues of the rat.* Ann Neurol, 1977. **1**(5): p. 409-17.
252. Weerapana, E., et al., *Quantitative reactivity profiling predicts functional cysteines in proteomes.* Nature, 2010. **468**(7325): p. 790-5.
253. Bulteau, A.L., et al., *Reversible redox-dependent modulation of mitochondrial aconitase and proteolytic activity during in vivo cardiac ischemia/reperfusion.* Proc Natl Acad Sci U S A, 2005. **102**(17): p. 5987-91.
254. Modis, Y. and R.K. Wierenga, *A biosynthetic thiolase in complex with a reaction intermediate: the crystal structure provides new insights into the catalytic mechanism.* Structure, 1999. **7**(10): p. 1279-90.
255. Drose, S., U. Brandt, and I. Wittig, *Mitochondrial respiratory chain complexes as sources and targets of thiol-based redox-regulation.* Biochim Biophys Acta, 2014. **1844**(8): p. 1344-54.
256. Galkin, A., et al., *Lack of oxygen deactivates mitochondrial complex I: implications for ischemic injury?* J Biol Chem, 2009. **284**(52): p. 36055-61.
257. Gorenkova, N., et al., *Conformational change of mitochondrial complex I increases ROS sensitivity during ischemia.* Antioxid Redox Signal, 2013. **19**(13): p. 1459-68.
258. Efremov, R.G. and L.A. Sazanov, *Structure of the membrane domain of respiratory complex I.* Nature, 2011. **476**(7361): p. 414-20.
259. Cobine, P.A., et al., *Mitochondrial matrix copper complex used in metallation of cytochrome oxidase and superoxide dismutase.* J Biol Chem, 2006. **281**(48): p. 36552-9.

7 APPENDIX

7.1 Supplementary data

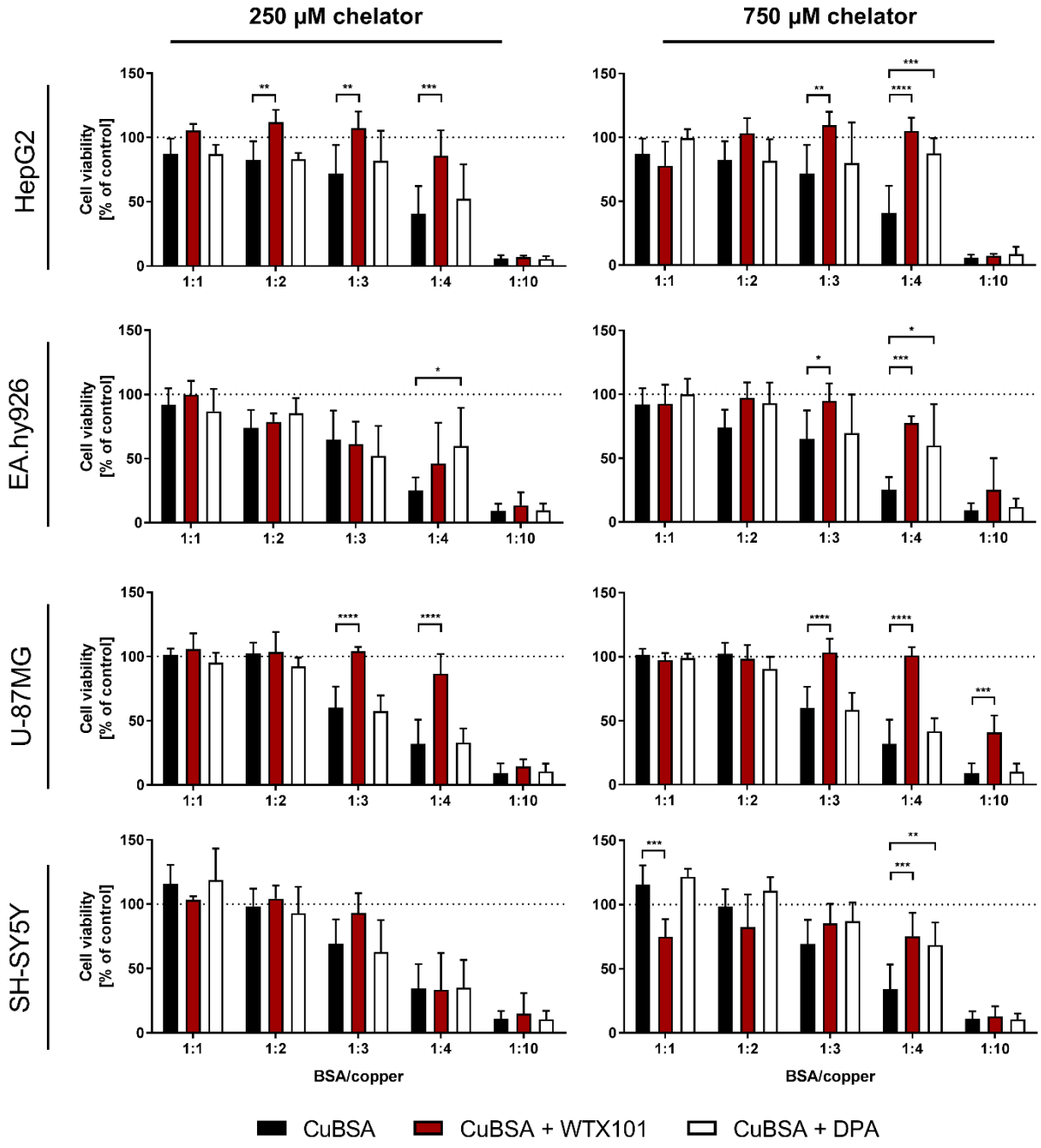

Figure S1. WTX101 protects EA.hy926 and U-87MG cells from copper toxicity (Neutral red assay).

All investigated cell lines show a dose-dependent decrease in cell viability under 24 h treatment with 250 µM BSA and increasing amounts of copper ranging from 250 to 2500 µM. In the presence of 750 µM DPA, this cytotoxic effect is not significantly diminished compared to BSA and copper alone. In contrast, the presence of 750 µM WTX101 protects mainly HepG2, EA.hy926 and U-87MG cells from cell death (N = 3 – 5, n = 6 - 10).

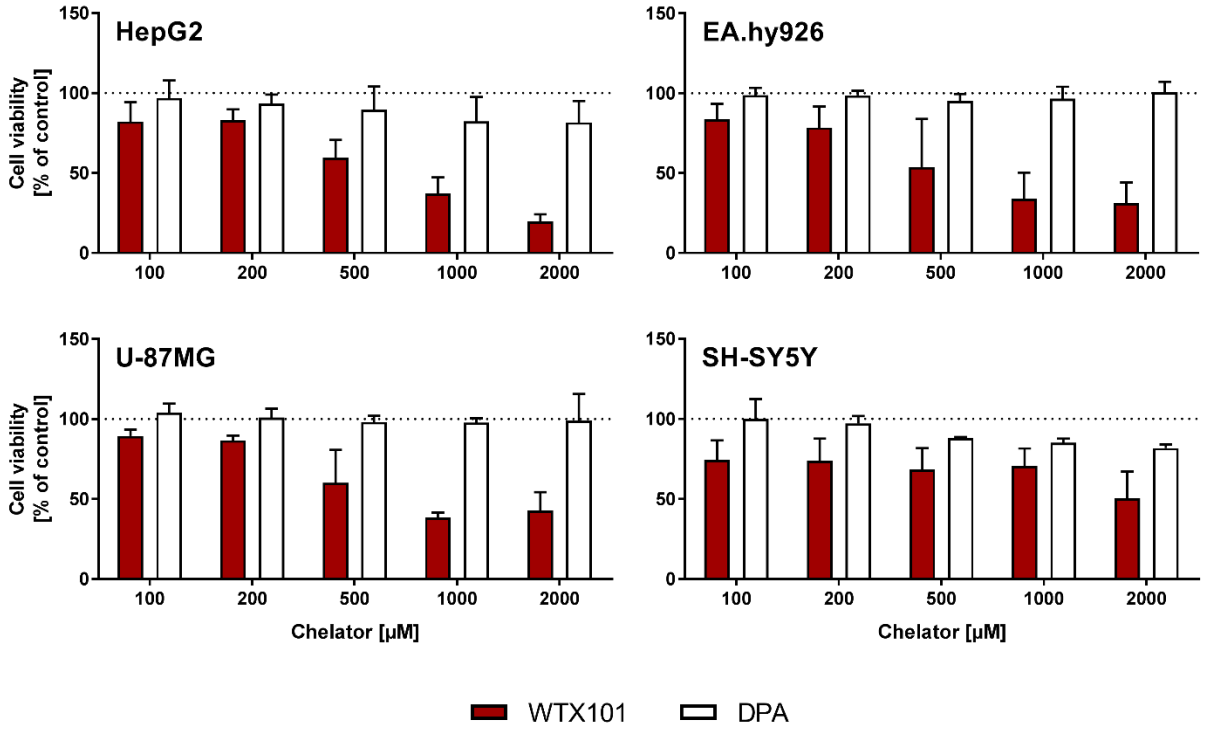

Figure S2. Cell toxicity of the copper chelators WTX101 and DPA determined by the CellTiterGlo® assay.

HepG2, EA.hy926, U-87MG and SH-SY5Y cells were treated with the respective chelator for 24 h. WTX101 exhibits the highest cell toxicity, whereas DPA is non-toxic over the tested concentration range (N = 3, n = 6).

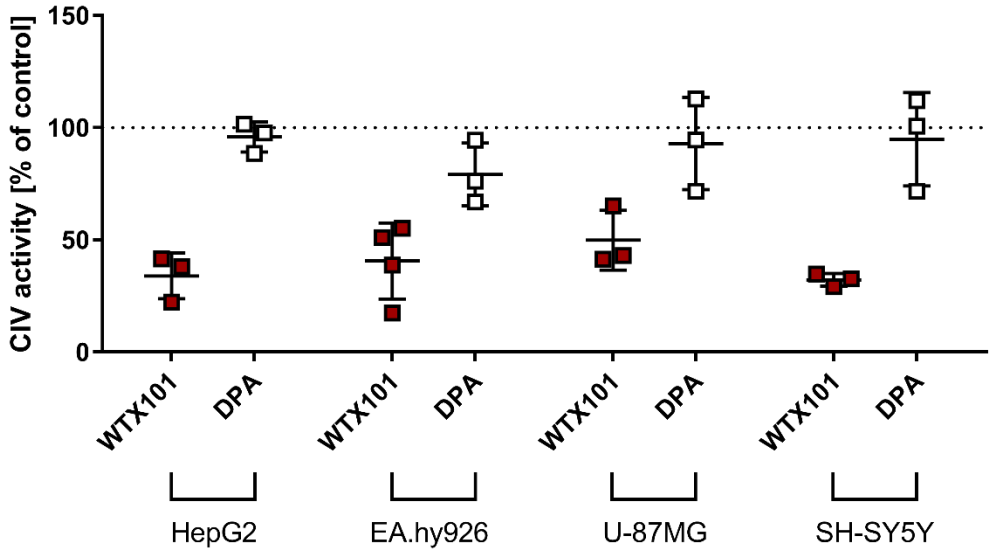

Figure S3. WTX101 leads to cellular toxicity by de-coppering of mitochondrial complex IV.

Cells were treated with 200 µM WTX101 or DPA for 24 h. WTX101 leads to a reduced complex IV activity in all investigated cell lines, whereas DPA has no effect on complex IV activity (N = 3, n = 6).

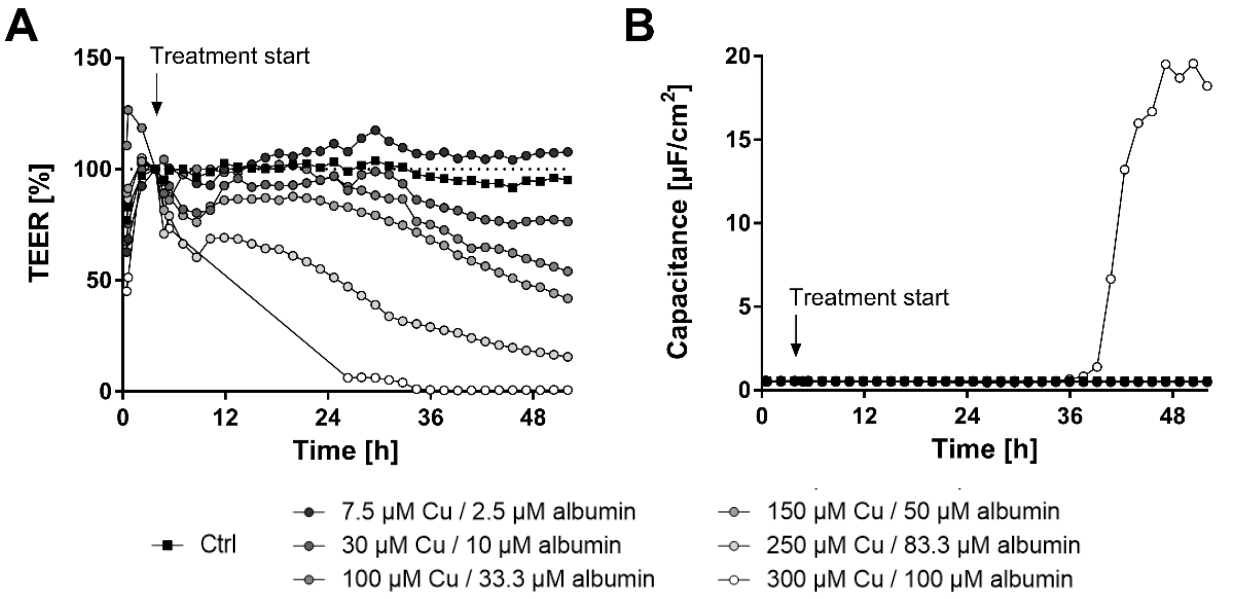

Figure S4. Dose-dependent decrease of the TEER upon copper challenges on PBCECs.

(A) Increasing concentrations of BSA-bound copper lead to decreasing transepithelial electrical resistance (TEER) values in primary porcine brain capillary endothelial cells (PBCECs) (N = 1, n = 2). (B) Concomitant measurement of the capacitance reveals stable capacitance values up to 250 µM copper (plus 83.3 µM BSA) for 48 h. Only at the highest copper concentration (100 µM BSA/300 µM copper), capacitance values increase strongly at 36 h of treatment (N = 1, n = 2).

7.2 Abbreviations

BSA	Bovine serum albumin
CCCP	Carbonyl cyanide m-chlorophenyl hydrazine
DPA	D-penicillamine
DTNB	5,5'-dithiobis-(2-nitrobenzoic acid)
EPR	Electron paramagnetic resonance
ETS	Electron transport system
FCCP	Carbonyl cyanide-p-(trifluoromethoxy)phenylhydrazone
GSH	Glutathione
IMM	Inner mitochondrial membrane
IMS	Mitochondrial intermembrane space
KCN	Potassium cyanide
MMP, $\Delta\psi_m$	Mitochondrial membrane potential
NEM	N-ethylmaleimide
$OD_{540\ nm}$	Optical density at 540 nm
OMM	Outer mitochondrial membrane
PBCEC	Porcine brain capillary endothelial cells
RCR	Respiratory control ratio
Rh123	Rhodamine 123
ROS	Reactive oxygen species
ROX	Residual oxygen consumption
TEER	Transepithelial electrical resistance
WD	Wilson disease
WTX101	Bis-choline tetrathiomolybdate

7.3 List of figures

7.4 List of tables

List of publications

First or last author:

1. **S. Borchard**, F. Bork, T. Rieder, C. Eberhagen, B. Popper, J. Lichtmannegger, S. Schmitt, J. Adamski, M. Klingenspor, K.-H. Weiss, H. Zischka. The exceptional sensitivity of brain mitochondria to copper. Toxicol in Vitro. (2018) 51:11-22.
2. S. Schulz*, **S. Borchard***, T. Rieder, C. Eberhagen, B. Popper, J. Lichtmannegger. S. Schmitt, H. Zischka. The Parallel Testing of Isolated Rat Liver and Kidney Mitochondria Reveals a Calcium-Dependent Sensitivity to Diclofenac and Ibuprofen. In: Will Y, Dykens JA, editors. Mitochondrial Dysfunction Caused by Drugs and Environmental Toxicants. John Wiley & Sons, Inc.; 2018. (* both authors share first authorship)
3. **S. Borchard**, F. Bork, T. Rieder, C. Eberhagen, H. Zischka. Free thiols are major targets of copper toxicity in brain mitochondria. Meeting abstract (P1.032) at Cell Symposium: Multifaceted Mitochondria 2018, San Diego, CA, USA.
4. H. Zischka, **S. Borchard**. Mitochondrial Copper Toxicity with a Focus on Wilson Disease. In: Kerkar N, Roberts EA, editors. Clinical and Translational Perspectives on WILSON DISEASE. Elsevier Science (2018).
5. **S. Borchard**, S. Raschke, K.M. Zak, C. Eberhagen, C. Einer, E. Weber, J. Lichtmannegger, A. Wieser, T. Rieder, G.M. Popowicz, J. Adamski, M. Klingenspor, T. Schwerdtle, T. Plitz, H. Zischka. The high-affinity chelator WTX101 prevents copper-induced blood-brain barrier damage. *Manuscript submitted*

Co-author:

1. C. Giorgi, S. Marchi, I.C.M. Simoes, Z. Ren, G. Morciano, M. Perrone, P. Patalas-Kraqczyk, **S. Borchard**, P. Jedrak, K. Pierzynowska, J. Szymanski, D.Q. Wang, P. Portincasa, G. Wegrzyn, H. Zischka, P. Dobrzyn, M. Bonora, J. Duszynski, A. Rimessi, A. Karkucinska-Wieckowska, A. Dobrzyn, G. Szabadkai, B. Zavan, P.J. Oliveir, V.A. Sardao, P. Pinton, M.R. Wieckowski. Mitochondria and Reactive Oxygen Species in Aging and Age-Related Diseases. Int Rev Cell Mol Biol. (2018) 340:209-344.
2. E.V. Polishchuk, A. Merola, J. Lichtmannegger, A. Romano, A. Indrieri, E.Y. Ilyechova, M. Concilli, R. Del Cegli, R. Crispino, M. Mariniello, R. Petruzzelli, G. Ranucci, R. Iorio, F. Pietrocola, C. Einer, **S. Borchard**, A. Zibert, H.H. Schmidt, E. Di Schiavi, L.V. Puchkova, B. Franco, G. Kroemer, H. Zischka, R.S. Polishchuk. Autophagy operates as a pro-survival mechanism in Wilson disease. Gastroenterology. (2019) 156(4):1173-1189.
3. C. Einer*, C. Leitzinger*, J. Lichtmannegger, C. Eberhagen, T. Rieder, **S. Borchard**, R. Wimmer, G. Denk, B. Popper, F. Neff, E.V. Polishchuk, R.S. Polishchuk, S.M. Hauck, C. von Toerne, U. Karst, J.C. Müller, B.S. Baral, A.A. DiSpirito, A.E. Kremer, J. Semrau, K.H. Weiss, S. Hohenester, H. Zischka. A high-calorie diet aggravates mitochondrial dysfunction and triggers severe liver damage in Wilson disease rats. Cell Mol Gastroenterol Hepatol. (2019) 7(3):571-596.
   (* both authors share first authorship)

4. C. Einer, S. Hohenester, R. Wimmer, L. Wottke, R. Artmann, S. Schulz, C. Gosmann, A. Simmons, C. Leitzinger, C. Eberhagen, **S. Borchard**, S. Schmitt, S.M. Hauck, C. von Toerne, M. Jastroch, E. Walheim, C. Rust, A.L. Gerbes, B. Popper, D. Mayr, M. Schnurr, A.M. Vollmar, G. Denk, H. Zischka. Mitochondrial adaptation in steatotic mice. Mitochondrion. (2018) 40:1-12.

5. C. Einer, S. Hohenester, R. Wimmer, L. Wottke, R. Artmann, S. Schulz, C. Gosmann, A. Simmons, C. Leitzinger, C. Eberhagen, **S. Borchard**, S. Schmitt, S.M. Hauck, C. von Toerne, M. Jastroch, E. Walheim, C. Rust, A.L. Gerbes, B. Popper, D. Mayr, M. Schnurr, A.M. Vollmar, G. Denk, H. Zischka. Data on chow, liver tissue and mitochondrial fatty acid compositions as well as mitochondrial proteome changes after feeding mice a western diet for 6-24 weeks. Data Brief. (2017) 15:163-9.

6. S. Hohenester, C. Einer, C. Leitzinger, G. Denk, **S. Borchard**, K.H. Weiss, H. Zischka. Steatose der Leber beschleunigt die Manifestation des M. Wilson im Tiermodell durch synergistische mitochondriale Schädigung. Z Gastroenterol. (2018) 56(08): KV 229.

7. V. Subramanian, **S. Borchard**, O. Azimzadeh, W. Sievert, J. Merl-Pham, M. Mancuso, E. Pasquali, G. Multhoff, B. Popper, H. Zischka, M.J. Atkinson, S. Tapio. PPAR alpha Is Necessary for Radiation-Induced Activation of Noncanonical TGF beta Signaling in the Heart. J Proteome Res. (2018) 17(4):1677-89.

8. E. Gnaiger, E. Aasander Frostner, N. Abdul Karim, N.A. Abumrad, D. Acuna-Castroviejo, R.C. Adiele, et al. Mitochondrial respiratory states and rates. MitoFit Preprint Arch, 2019 doi:10.26124/mitofit:190001.v6.

9. M. Mulazzani*, M. Huber*, **S. Borchard**, S. Langer, B. Angele, E. Schuh, E. Meinl, M. Dreyling, T. Birnbaum, A. Straube, U. Koedel, L. von Baumgarten. APRIL and BAFF: novel biomarkers for central nervous system lymphoma. J Hematol Oncol. (2019) 12(1):102.
(* both authors share first authorship)

Proof of figures and tables taken from published articles

Figure 1 and Figure 4

Adapted from Wu, F., et al., Wilson's disease: a comprehensive review of the molecular mechanisms. Int J Mol Sci, 2015. 16(3): p. 6419-31.

Figure 2

Taken from Giorgi, C., et al., Mitochondria and Reactive Oxygen Species in Aging and Age-Related Diseases. Int Rev Cell Mol Biol, 2018. 340: p. 209-344 with kind permission.

License number: 4654781360163

Figure 3

Taken from Correa, T.D., et al., Time course of blood lactate levels, inflammation, and mitochondrial function in experimental sepsis. Crit Care, 2017. 21(1): p. 105.

Figure 5

Taken from Zischka, H. and Borchard, S., Mitochondrial Copper Toxicity with a Focus on Wilson Disease, in Clinical and Translational Perspectives on WILSON DISEASE, N. Kerkar and E.A. Roberts, Editors. 2018, Elsevier Science with kind permission.

License number: 4654781206034

Figures 9 - 15 and 17 - 20, Tables 5 and 6

In parts taken and adapted from Borchard, S, et al., The exceptional sensitivity of brain mitochondria to copper. Toxicol in Vitro., 2018. 51:11-22.

Acknowledgements

My main thanks and gratitude belong to Prof. Hans Zischka who gave me the opportunity to do my PhD in his group. I am deeply grateful for his guidance and continuous support throughout my thesis. Thanks for giving me such an interesting topic and the opportunity to get insights into so many different aspects of scientific work.

I would also like to thank Prof. Jerzy Adamski and Prof. Martin Klingenspor for their insightful comments and discussions during the thesis committee meetings. Thank you for examining this work.

Special thanks to all members of the research group: Sabine for supporting me throughout this thesis with challenging questions and fruitful discussions, Carola for her encouraging help on electron microscopy, Lichti for sharing his experiences and knowledge with me, Tamara for her support on mitochondrial isolations, Claudia, Adriana, Judith and Yaschar for their support and discussions. Finally, thanks to Francesca for experimentally supporting this thesis as Bachelor student. It was a pleasure to work with all of you.

Thanks to all cooperation partners: Peter Grill for metal determination, Dr. Bastian Popper for his support on electron microscopy, Prof. Tanja Schwerdtle and Stefanie Raschke for their scientific and experimental support on the *in vitro* blood-brain barrier system and the possibility to stay in their laboratory, Dr. Krzysztof M. Zak and Dr. Grzegorz M. Popowicz for their crystallization work and Dr. Albrecht Wieser for his scientific and technical help on electron paramagnetic resonance measurements. Special thanks to Dr. Thomas Plitz for exciting discussions.

The whole team of Oroboros Instruments GmbH, Innsbruck, Austria is thanked for the possibility to stay in their research laboratory. Thanks for the fruitful discussions and scientific support.

Finally, I would like to thank my parents and my sister for their support and endless patience. Special thanks to Flo, you motivated me every single day. Your love, support and encouragements during the tough times of this thesis are unaffordable.

This work is dedicated to my grandma.